

**GLOBAL SOURCES AND DISTRIBUTION OF ATMOSPHERIC
METHYL CHLORIDE**

A Dissertation
Presented to
The Academic Faculty

By

Yasuko Yoshida

In Partial Fulfillment
Of the Requirements for the Degree
Doctor of Philosophy in the School of Earth and Atmospheric Sciences

Georgia Institute of Technology

August 2006

Global Sources and Distribution of Atmospheric Methyl Chloride

Approved by:

Dr. Yuhang Wang, Advisor
School of Earth and Atmospheric
Sciences
Georgia Institute of Technology

Dr. Robert Dickinson
School of Earth and Atmospheric
Sciences
Georgia Institute of Technology

Dr. Athanasios Nenes
School of Earth and Atmospheric
Sciences
Georgia Institute of Technology

Dr. Armistead Russell
School of Civil and Environmental
Engineering
Georgia Institute of Technology

Dr. David Tan
School of Earth and Atmospheric
Sciences
Georgia Institute of Technology

Date Approved: June 16, 2006

To Ben and Ikuko

ACKNOWLEDGEMENTS

I would like to express my sincere appreciation to my faculty advisor, Dr. Yuhang Wang, for his direction, guidance and support throughout my PhD study. I would also like to thank my thesis committee members, Dr. Robert Dickinson, Dr. Athanasios Nenes, Dr. Armistead Russell, and Dr. David Tan, for their assistance.

I thank Dr. David Erickson and Dr. Jose L. Hernandez for providing the UWM-COADS data and helpful comments. I also thank Dr. Donald Blake for his suggestions. Special thanks go to Dr. Derek Cunnold for providing us the AGAGE data. I am grateful to CMDL and Dr. Geoff Dutton for providing us their unpublished data. I am also indebted to Dr. Daniel Jacob and Dr. Colette Heald for their help. I would like to thank Dr. Louis Giglio for his helpful suggestions.

I am very thankful to my colleagues, Dr. Tao Zeng, Changsub Shim, Yunsoo Choi, Dr. Wei Liu, Xueyuan Deng, and Chun Zhao, who always encouraged and helped me in my research.

Finally, my deep appreciation goes to my family, especially my sister and brother in law, Ikuko and Ben Silber, whose tremendous and perpetual encouragement and support enabled me to complete my study.

TABLE OF CONTENTS

| | |
|--|-----|
| ACKNOWLEDGEMENTS | iv |
| LIST OF TABLES | x |
| LIST OF FIGURES | xi |
| SUMMARY | xiv |
| CHAPTER I BIOGEOCHEMICAL CYCLES OF GLOBAL CHLORINE: AN OVERVIEW | 1 |
| 1.1 Introduction | 1 |
| 1.2 Global chlorine storage | 4 |
| 1.2.1 Chlorine storage in hydrosphere | 4 |
| 1.2.2 Chlorine storage in atmosphere | 7 |
| 1.2.2.1 The troposphere | 7 |
| 1.2.2.2 The stratosphere | 8 |
| 1.2.3 Chlorine storage in soil | 8 |
| 1.2.4 Chlorine storage in biomass | 9 |
| 1.3 Global chlorine fluxes | 10 |
| 1.3.1 Mantle to troposphere | 10 |
| 1.3.2 Ocean to troposphere | 11 |
| 1.3.2.1 Seasalt aerosol and volatile inorganic Cl | 11 |
| 1.3.2.2 Organic Cl gases | 11 |
| 1.3.3 Vegetation to the atmosphere | 12 |
| 1.3.3.1 Biogenic emissions | 12 |
| 1.3.3.2 Biomass burning | 13 |

| | |
|---|----|
| 1.3.4 Industrial and combustion sources | 13 |
| 1.3.5 Deposition to surface | 14 |
| 1.3.5.1 Deposition to the oceans | 14 |
| 1.3.5.2 Deposition to the land | 15 |
| 1.3.6 Transport between troposphere and stratosphere | 16 |
| 1.3.7 Freshwater to the oceans | 16 |
| 1.3.8 Crust to freshwater | 16 |
| 1.3.9 Soil to freshwater | 17 |
| 1.3.10 Oceans to crust | 17 |
| 1.3.11 Soil to the atmosphere | 17 |
| 1.3.12 Vegetation to soil | 18 |
| 1.3.13 Soil to vegetation | 18 |
| 1.3.14 Formation and mineralization of Cl _{org} in soil | 19 |
| 1.4 Summary and conclusions | 19 |
| CHAPTER II A THREE-DIMENSIONAL GLOBAL MODEL STUDY OF ATMOSPHERIC METHYL CHLORIDE BUDGET AND DISTRIBUTIONS | 23 |
| 2.1 Introduction | 23 |
| 2.2 Model description | 25 |
| 2.3 Sources of CH ₃ Cl | 26 |
| 2.3.1 Biomass burning | 26 |
| 2.3.2 Oceanic emissions | 27 |
| 2.3.3 Incineration/industrial emissions | 29 |
| 2.3.4 Salt marshes and wetlands | 29 |

| | |
|--|----|
| 2.3.5 Biogenic emissions | 30 |
| 2.4 Sinks of CH ₃ Cl | 31 |
| 2.4.1 Reaction with OH | 31 |
| 2.4.2 Soil sink | 34 |
| 2.5 Results | 36 |
| 2.5.1 Global distribution of atmospheric CH ₃ Cl near the surface | 39 |
| 2.5.1.1 Seasonal variation | 39 |
| 2.5.1.2. Latitudinal variation | 42 |
| 2.5.2. Vertical profiles of atmospheric CH ₃ Cl | 45 |
| 2.5.2.1 Tropical Pacific (PEM-Tropics A and B) | 45 |
| 2.5.2.2 Tropical Pacific and Southern Oceans (ACE 1) | 47 |
| 2.5.2.3 Tropical Atlantic (TRACE-A) | 48 |
| 2.5.2.4 Indian Ocean (INDOEX) | 49 |
| 2.5.2.5 Western Pacific (PEM-West A and B, TRACE-P) | 49 |
| 2.5.2.6 North America (TOPSE) | 51 |
| 2.5.3 Latitude-altitude distribution of atmospheric CH ₃ Cl | 51 |
| 2.6 Conclusions | 56 |
| CHAPTER III INVERSE MODELING OF THE GLOBAL METHYL CHLORIDE SOURCES | 59 |
| 3.1 Introduction | 59 |
| 3.2 Methods | 62 |
| 3.2.1 Observations | 62 |
| 3.2.2 Forward Model | 62 |
| 3.2.2.1 Model description | 62 |

| | |
|--|----|
| 3.2.2.2 Sources and sinks of CH ₃ Cl | 65 |
| 3.2.3 Inverse Model | 68 |
| 3.2.3.1 Inversion methods | 68 |
| 3.2.3.2 Selection of the state vector | 69 |
| 3.2.3.3 Error estimation | 70 |
| 3.3 Results | 74 |
| 3.3.1 Sensitivity to state vector size | 74 |
| 3.3.1.1 Monthly flux | 74 |
| 3.3.1.2 Evaluation with surface measurements | 77 |
| 3.3.1.3 Evaluation with aircraft measurements | 80 |
| 3.3.2 Sensitivity to surface and aircraft data sets | 85 |
| 3.4 Discussion | 87 |
| 3.5 Conclusions | 88 |
| CHAPTER IV UNCERTAINTIES IN USING SATELLITE FIRE COUNTS FOR BIOMASS BURNING EMISSIONS IN THE SOUTHEAST UNITED STATES | 91 |
| 4.1 Introduction | 91 |
| 4.2 Data and Methods | 92 |
| 4.2.1 Burned area inventory | 92 |
| 4.2.2 Fire count data | 95 |
| 4.2.3 Leaf area index (LAI) data | 96 |
| 4.2.4 Cloud fraction data | 96 |
| 4.3. Results | 97 |
| 4.3.1 Correlations between VISTAS burned area and MODIS fire count | 97 |

| | |
|-----------------------------|-----|
| 4.3.2 Effect of cloud cover | 105 |
| 4.3.3 Effect of LAI | 106 |
| 4.4 Discussion | 108 |
| 4.5 Conclusions | 114 |
| REFERENCES | 116 |

LIST OF TABLES

| | | |
|-----------|---|-----|
| Table 1.1 | Chemical structure and names of 21 examples of naturally-produced chlorinated organic compounds [<i>Öberg</i> , 2002]. | 2 |
| Table 1.2 | Contributions of halocarbons to total organic chlorine in the troposphere [<i>Montzka et al.</i> , 2003]. | 4 |
| Table 1.3 | Chlorine content of earth's reservoirs. | 5 |
| Table 1.4 | Estimated natural chlorine flux between reservoirs [<i>Graedel and Keene</i> , 1995]. | 11 |
| Table 2.1 | Estimated global budget of CH ₃ Cl. | 33 |
| Table 2.2 | Atmospheric measurements of CH ₃ Cl. | 38 |
| Table 3.1 | Atmospheric measurements of CH ₃ Cl. | 63 |
| Table 3.2 | CH ₃ Cl sources and sinks and their uncertainties. | 66 |
| Table 3.3 | Model parameters in the state vector. | 71 |
| Table 4.1 | Fire data provided by state agencies by fire type. | 93 |
| Table 4.2 | Annual total of VISTAS burned area and MODIS fire count. | 98 |
| Table 4.3 | Correlations between the MODIS fire counts and cloud fractions at daily basis. | 106 |

LIST OF FIGURES

| | | |
|------------|--|----|
| Figure 1.1 | The earth's major chlorine reservoirs and natural processes of transferring chlorine among the reservoirs [Winterton, 2002]. | 6 |
| Figure 1.2 | The chlorine budget and cycle for the planetary reservoirs. The units for the budget and flux are Tg and Tg yr ⁻¹ , respectively. The difference between inflow and outflow is shown as Δ (Tg yr ⁻¹). Red, blue and black numbers indicate organic, inorganic, and total chlorine, respectively. For references, please see the text. | 22 |
| Figure 2.1 | Latitudinal distributions of observed and simulated CH ₃ Cl at the surface sites. Broken line indicates data by <i>Khalil and Rasmussen</i> [1999] (the data were lowered by 8.3% to account for a calibration difference). The thick black solid line links the CMDL (Diamonds) and AGAGE data (asterisks). Thin vertical lines indicate the standard deviations; the end symbols are minus signs, diamonds, and asterisks for K&R, CMDL, and AGAGE data, respectively. Emission inventories for OC-2 (Table 2.1) are used. Model results are shown with the standard OH concentrations and two perturbation cases, in which the NH and SH hemispheric OH concentrations are either increased or decreased by 10% (see text for more details). | 35 |
| Figure 2.2 | Latitudinal distribution of the known sources and sinks of CH ₃ Cl. For the legend, "e-" and "s-" denote emission and sink, respectively and characters OC, BB, IN, BG, SM, WT, TT, SL denote ocean, biomass burning, incineration/industrial, biogenic, salt marshes, wetlands, the total of all emissions, and soil, respectively. | 37 |
| Figure 2.3 | Simulated surface mixing ratio of CH ₃ Cl for January and July. | 37 |
| Figure 2.4 | Surface measurement sites (indicated by symbols) and aircraft observation regions used in this study. | 40 |
| Figure 2.5 | Seasonal variations of observed and simulated CH ₃ Cl at the surface sites. Broken lines indicate data by <i>Khalil and Rasmussen</i> [1999], black solid lines indicate CMDL data (G. Dutton, personal communications, 2004), and dotted-broken lines indicate AGAGE data [Simmonds <i>et al.</i> , 2004]. The K&R data were lowered by 8.3% to account for a calibration difference. Model results are shown in color. The orange dotted lines are the reference run with the OH reaction rate constant by <i>DeMore et al.</i> [1997]. The purple | |

| | | |
|------------|---|----|
| | dotted lines are the reference run with the OH rate constant by <i>Sander et al.</i> [2003]. The green lines are the OC-1 run. The blue lines are the OC-2 run. These 4 simulations used meteorological data for September 1996 – August 1997. The red solid lines are the mean of 6-year simulations with oceanic sink calculated as in the OC-2 run. The vertical lines represent the standard deviations. | 41 |
| Figure 2.6 | Latitudinal distributions of observed and simulated CH ₃ Cl at the surface sites. Line symbols are the same as Figure 2.5. | 43 |
| Figure 2.7 | Vertical profiles of CH ₃ Cl averaged over the aircraft observation regions shown in Figure 2.4. For the TOPSE experiment, monthly mean values from February to May are calculated. Please see the text for abbreviation for each project region. Thin solid lines indicate the medians of observations, crosses indicate the means of observations, and thin horizontal lines indicate the observed standard deviations. Diamonds indicate the means of the six model runs. For model results, contributions from each source as well as all sources are shown. OC, BB, IN, BG, SM, WT, and TT denote ocean, biomass burning, incineration/industrial, biogenic, salt marshes, wetlands, and total, respectively. | 46 |
| Figure 2.8 | Observed and simulated latitude-altitude distributions for selected aircraft observation regions shown in Figure 2.4. For TRACE-P and TOPSE, the western/eastern and the northern/southern regions are combined, respectively. Abbreviations are the same as used in Figure 2.7 Only grid boxes with > 10 observation points are shown. | 52 |
| Figure 2.9 | Same as Figure 2.8 but for the relative difference computed as (model-observation)/model. | 53 |
| Figure 3.1 | Surface measurement sites (indicated by symbols) and aircraft observation regions. The measurements are listed in Table 3.1. | 64 |
| Figure 3.2 | Singular vectors of the prewhitened Jacobian matrix \mathbf{K} for the 16 parameter case. “bg”, “bb”, “oc” and “sl” denote biogenic, biomass burning, ocean and soil, respectively. Spring, summer, fall and winter are denoted by “sp”, “sm”, “fl”, and “wn”, respectively. | 72 |
| Figure 3.3 | A priori and a posteriori monthly sources and sinks for the three cases with different model parameters (Table 3.3). | 75 |

| | | |
|-------------|---|-----|
| Figure 3.4 | Seasonal variations of observed and simulated CH ₃ Cl at the surface sites. The vertical bars show the standard deviations of the measurements. | 78 |
| Figure 3.5 | Latitudinal distributions of observed and simulated CH ₃ Cl at the surface sites. The vertical bars show the standard deviations of the measurements. | 79 |
| Figure 3.6 | A priori and a posteriori relative biases computed as (model-observation)/observation with respect to aircraft observations as a function of latitude and latitude for regions shown in Figure 3.1. | 81 |
| Figure 3.7 | A priori and a posteriori monthly sources and sinks using the measurements from surface sites, aircraft, and both. | 86 |
| Figure 4.1 | Trend of VISTAS fire. | 94 |
| Figure 4.2 | Seasonal variations of VISTAS burned areas and MODIS fire counts. Four different fire types in VISTAS are shown in color. | 99 |
| Figure 4.3 | County-level monthly total of VISTAS burned area as a function of MODIS fire count. | 100 |
| Figure 4.4 | State-level monthly total of VISTAS burned area as a function of MODIS fire count. | 101 |
| Figure 4.5 | State-level total VISTAS burned area as a function of MODIS fire count for each month. | 102 |
| Figure 4.6 | State-level monthly total VISTAS burned area as a function of MODIS fire count for different VISTAS fire types. | 104 |
| Figure 4.7 | State-level monthly total MODIS fire counts as a function of monthly mean LAI. | 107 |
| Figure 4.8 | Surface observation sites used in the CMAQ simulation evaluation [Zeng <i>et al.</i> , 2006]. | 109 |
| Figure 4.9 | CMAQ simulation results compared with observations for OC [Zeng <i>et al.</i> , 2006]. | 110 |
| Figure 4.10 | CMAQ simulation results compared with observations for EC [Zeng <i>et al.</i> , 2006]. | 111 |
| Figure 4.11 | Probability of fire detection of MODIS for temperate deciduous forest in daytime [Giglio <i>et al.</i> , 2003]. | 113 |

SUMMARY

Global simulations of atmospheric methyl chloride (CH_3Cl) are conducted using the GEOS-Chem model in order to understand better its sources and sinks. Though CH_3Cl is one of the most abundant organic chlorine species in the stratosphere, not much is known about its sources and the budget remains unbalanced. In addition to the known sources (1.5 Tg yr^{-1}) from ocean, biomass burning, incineration/industry, salt marshes, and wetlands, a hypothetical aseasonal biogenic source of 2.9 Tg yr^{-1} is added in order to match needed emissions. Observations from 7 surface sites and 8 aircraft field experiments are used to evaluate the model simulations. The model results with a priori emissions and sinks reproduce CH_3Cl observations at northern mid and high latitudes reasonably well. However, the seasonal variation of CH_3Cl at southern mid and high latitudes is severely overestimated. Simulated vertical profiles show disagreements in the vicinities of major sources, principally reflecting the uncertainties in the estimated distributions of our added pseudo-biogenic and the biomass burning sources.

Inverse modeling is then applied using Bayesian least-squares method in order to obtain optimal source distributions of CH_3Cl on the basis of the surface and aircraft observations and the model results. Up to 39 parameters describing the continental/hemispheric and seasonal dependence of the major sources of CH_3Cl are used in the inversion. We find that the available surface and aircraft observations cannot constrain all the parameters, resulting in relatively large uncertainties in the inversion results. By examining the degrees of freedom in the inversion Jacobian matrix, we choose a reduced set of parameters that can be constrained by the observations while providing

valuable information on the sources and sinks. In particular, we resolve the seasonal dependence of the biogenic and biomass burning sources for each hemisphere. The in situ aircraft measurements are found to provide better constraints on the emission sources than surface measurements. The a posteriori emissions result in better agreement with the observations particularly at southern high latitudes. The a posteriori biogenic and biomass burning sources decrease by 13 and 11% to 2500 and 545 Gg yr⁻¹, respectively, while the a posteriori net ocean source increases by about a factor of 2 to 761 Gg yr⁻¹. The decrease in biomass burning emissions is largely due to the reduction in the emissions in seasons other than spring in the northern hemisphere. The inversion results indicate that the biogenic source has a clear winter minimum in both hemispheres, likely reflecting the decrease of biogenic activity during that season.

In the last section, we conducted a study of the relationships between satellite fire count and burned area using data from the Moderate Resolution Imaging Spectroradiometer (MODIS) and a burned area inventory from the Visibility Improvement – State and Tribal Association of the Southeast (VISTAS). We compare seasonal trend of these two data sets and discuss the uncertainties of the satellite fire count data for estimating biomass burning emissions. Effects of cloud cover and tree canopy on fire detection of MODIS are also investigated using cloud cover and leaf area index (LAI) data from MODIS. Among the four types of fire reported in the VISTAS inventory including wildfires, prescribed (managed) fire, agricultural burning and land clearing of debris, prescribed burning is the most significant, and its effects on air quality have been shown in model simulations. In the ten VISTAS states in the southeastern U.S., only Florida

shows clear correlations between the fire counts and burned area data. For Alabama and Georgia, there are significant discrepancies between the two data sets; spring peaks in the VISTAS inventory and summer peaks in the MODIS fire count data. MODIS fire detections could be affected by cloud over in some states in some months. Stronger negative correlation between the fire counts and the cloud cover are observed during spring and summer in Alabama, Florida, and Georgia. There is no clear evidence found that shows LAI affects the fire detections. One possible reason for the discrepancy in early spring in Alabama and Georgia is that the temperature of prescribed burning could be too low to be detected by MODIS. The summer discrepancy could be due to the false detection of MODIS, which tends to occur on hot and dry surfaces.

CHAPTER I

BIOGEOCHEMICAL CYCLES OF GLOBAL CHLORINE: AN OVERVIEW

1.1 Introduction

Chlorine is the 18th most abundant element on the earth. However, our current knowledge of this species, especially about its biogeochemical cycles, is very limited [Graedel and Keene, 1996]. It was once believed that chlorine was not involved in biological processes because chlorinated organic compounds were xenobiotic, and that it existed in the environment mainly in ionic form, such as chloride (Cl^-). However, studies in the last several decades have revealed that approximately 2000 chlorinated species are produced through natural enzymatic, thermal, and other processes in the atmosphere, the ocean, and the soil [Gribble, 1992; Öberg, 2002]. Öberg [2002] stated that previous belief that chlorinated organic compounds were generally xenobiotic stemmed from a large number of anthropogenic chlorinated organic species found to be environmentally toxic and hazardous. Table 1.1 shows 21 examples of naturally-produced chlorinated compounds [Öberg, 2002]. The gas phase chlorine containing species consists of two categories: the fully halogenated organics, which are unreactive in the troposphere, and the reactive chlorine compounds [Graedel and Keene, 1995]. The major reactive chlorinated organic gases in the troposphere include methyl chloride (CH_3Cl), methyl chloroform (CH_3CCl_3), perchloroethylene ($\text{CCl}_2=\text{CCl}_2$), methylene chloride (CH_2Cl_2), and chloroform (CHCl_3) (Table 1.2).

Table 1.1 Chemical structure and names of 21 examples of naturally-produced chlorinated organic compounds [Öberg, 2002].

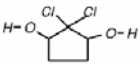
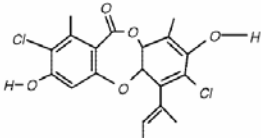
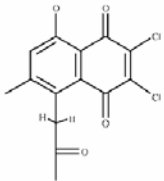
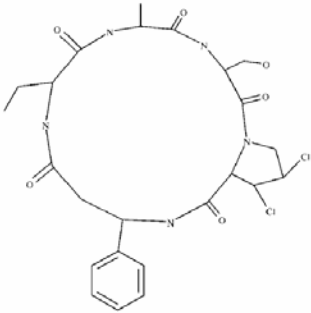
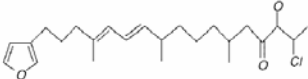
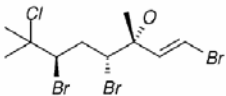
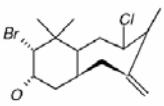
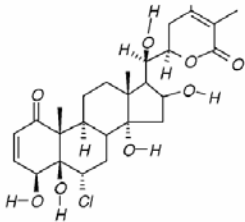
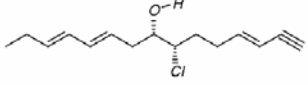
| Structure | Trivial name | Reference |
|---|---------------------------|-------------------------|
|  | Caldariomycin | Clutterbuck et al. 1937 |
|  | Nornidulin | Bracken 1954 |
|  | Mollisin | Miller 1961 |
|  | Islanditoxin | Miller 1961 |
|  | Konakhin | N'Diaye et al. 1991 |
|  | (Chlorinated monoterpene) | Faulkner 1977 |
|  | Elatol | Sims et al. 1974 |
|  | Physalolactone | Ray et al. 1978 |
|  | Prerogioloxepane | Guella et al. 1992 |

Table 1.1 (continued).

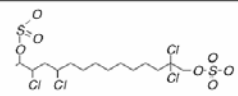
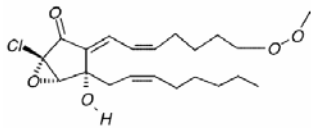
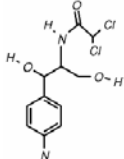
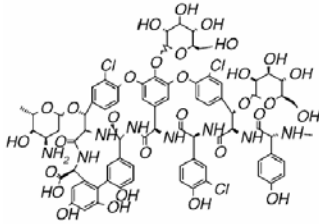
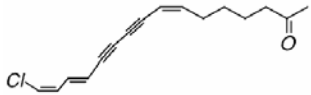
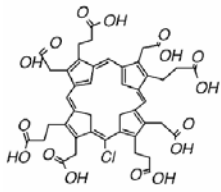
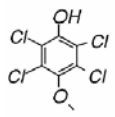
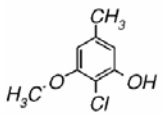
| Structure | Trivial name | Reference |
|---|--|----------------------------|
|  | (A chlorosulfolipid) | Haines 1973 |
|  | (An epoxy prostanoid/ a prostaglandin) | Iguchi et al. 1987 |
|  | Chloroamphenicol (chloromycetin) | Gottlieb et al. 1948 |
|  | Chloropolysporin C | Takatsu et al. 1987 |
|  | (A chloroacetylene) | Walker and Faulkner 1981 |
|  | (A chlorinated porphyrin) | Lin et al. 1993 |
|  | Drosophilin | Anchel 1952 |
|  | (Volatile phenolic compound) | Gavin et al. 1978 |
| CH ₃ Cl | Chloromethane (methylchloride) | Harper 1985 |
| CH ₂ Cl ₂ | Dichloromethane | Blackman et al. 1992 |
| CHCl ₃ | Chloroform | Pyysalo 1976 |
| CCl ₄ | Carbontetrachloride | McConnell and Fenical 1977 |

Table 1.2 Contributions of halocarbons to total organic chlorine in the troposphere [Montzka et al., 2003].

| | Cl _{org} [pptv Cl] |
|----------------------------------|-----------------------------|
| Aggregate CFCs | 2156 |
| CH ₃ Cl | 550 |
| CCl ₄ | 384 |
| Aggregate HCFCs | 182 |
| CH ₃ CCl ₃ | 139 |
| Short-lived gases ^a | 100 |
| Halon-1211 | 4 |
| Total Cl _{org} | 3516 |

^a Gases such as CH₂Cl₂, CHCl₃, and C₂Cl₄.

The oceans are a major source of Cl⁻ [Graedel and Keene, 1996]. The geochemical cycle of Cl⁻ is driven by both physical forces such as wind, water and fire, and chemical forces such as chemical weathering and ion exchange. Where the air is dry and evapo-transpiration exceeds wet deposition, Cl⁻ is transferred from soil to the air. The biogeochemical cycle of chlorine as a whole, which involves the formation, degradation and cycling of inorganic and organic chlorine compounds, is not very well understood [Öberg, 2002; Öberg, 2003]. In this chapter, we outline the global chlorine cycle, focusing on fate and transport of chlorine in the hydrosphere, atmosphere, biosphere and pedosphere, and then estimate the global budget of chlorine.

1.2 Global chlorine storage

1.2.1 Chlorine storage in the hydrosphere

Table 1.3 and Figure 1.1 show the chlorine (Cl⁻) content of earth's major reservoirs and exchanges among them [Graedel and Keene, 1996; Winterton, 2000]. Graedel and Keene [1996] estimated that the earth's crust contains 60×10^9 Tg (tera gram = 10^{12} gram) of chlorine. Because of their aqueous solubility, inorganic chloride

salts dissolve into the hydrosphere including the oceans (97% of the hydrosphere), ice sheets and glaciers (2%), ground water (0.7%), lakes (0.01%), soil (0.005%), and rivers (0.0001%) as a consequence of the chemical and physical weathering of igneous, sedimentary and metamorphic rocks. Assuming the volume of sea water of $1.36 \times 10^8 \text{ km}^3$ and the average Cl^- concentration of 19.354 g kg^{-1} , the chlorine content of the ocean is calculated as $26 \times 10^9 \text{ Tg Cl}^-$ [Graedel and Keene, 1996; Winterton, 2000].

Table 1.3 Chlorine content of earth's reservoirs.

| Reservoir | Chlorine content [Tg] |
|--------------|-----------------------|
| Mantle | 22×10^{12} |
| Crust | 60×10^9 |
| Oceans | 26×10^9 |
| Pedosphere | 24×10^3 |
| Freshwater | 320×10^3 |
| Cryosphere | 0.5×10^{-3} |
| Troposphere | 5.3 |
| Stratosphere | 0.4 |

The total volume of the global surface waters in lakes and rivers accounts for $1 \times 10^5 \text{ km}^3$, and the water contained in soil is about an equivalent amount [Graedel and Keene, 1996]. Assuming an average dissolved chlorine concentration of 5.8 mg L^{-1} , Graedel and Keene [1996] estimated the chlorine content in surface waters as 580 Tg. The groundwater has a typical chlorine concentration of 40 mg L^{-1} , which yields the reservoir content of $320 \times 10^3 \text{ Tg}$ [Graedel and Keene, 1996].

Graedel and Keene [1996] calculated the global cryospheric chlorine content using the volume of ice on the planet of 29 km^3 and average chlorine concentration of $5 \times 10^{-7} \text{ mol Cl L}^{-1}$. They estimated a total of $0.5 \times 10^{-3} \text{ Tg}$.

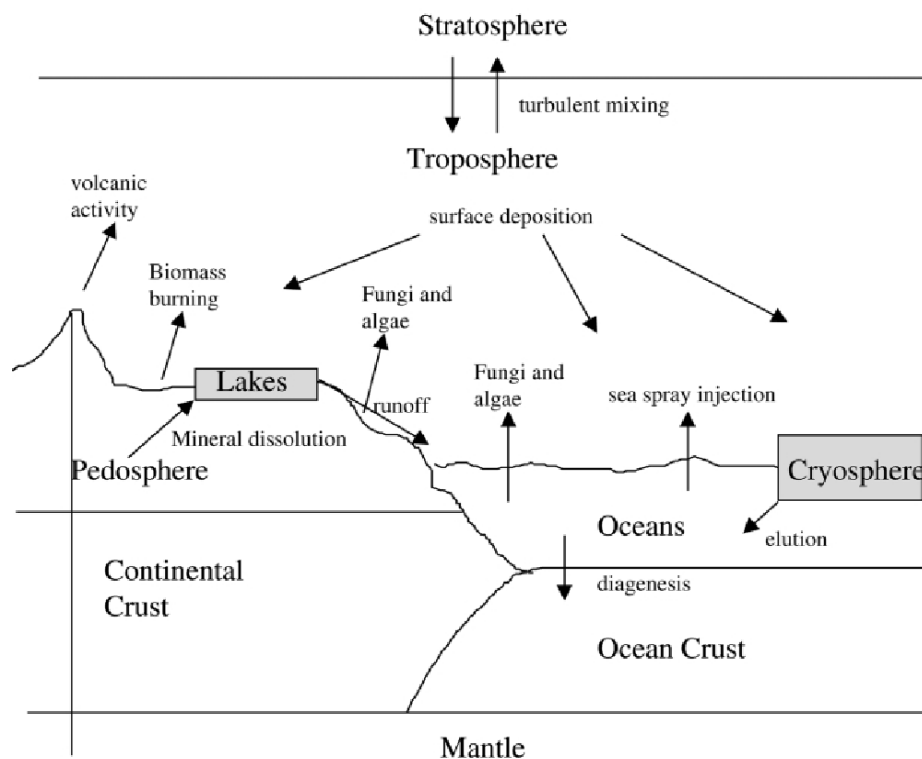
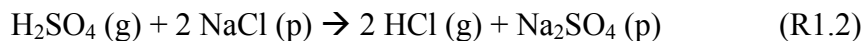
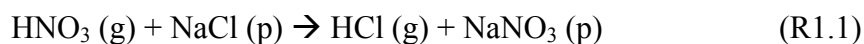


Figure 1.1 The earth's major chlorine reservoirs and natural processes of transferring chlorine among the reservoirs [Winterton, 2002].

1.2.2 Chlorine storage in the atmosphere

1.2.2.1 The troposphere

The most abundant natural chlorine containing gases in the atmosphere are hydrogen chloride (HCl) and methyl chloride (CH₃Cl) [Graedel and Keene, 1996]. The main sources of atmospheric HCl are anthropogenic emissions from coal burning and waste combustion, and biomass burning, and natural source such as volcanoes and seasalt aerosol. Near the surface of remote ocean regions, 100–300 pptv HCl is commonly measured, though the concentrations are higher over coastal urban areas, suggesting that seasalt may be the dominant source of HCl via acid displacement processes;



where g and p refer to species present in the gaseous and particulate phases, respectively [Winterton, 2000]. Assuming the average HCl concentration of 200 pptv in the boundary layer, Graedel and Keene [1996] estimated a tropospheric reservoir of about 0.2 Tg Cl.

The HCl concentrations change with altitude, which reflects its sources and the removal rate by chemical reactions and rainout. Above the boundary layer, the concentration decreases to ≤ 100 pptv [Graedel and Keene, 1996]. Graedel and Keene [1996] calculated the HCl content for the free troposphere at about 0.4 Tg Cl.

Using a mean atmospheric CH₃Cl concentration of 620 pptv, Graedel and Keene [1996] estimated a reservoir content for the troposphere of about 3.7 Tg Cl. More recent observation places the global means closer to 550 pptv [Montzka *et al.*, 2003], which yields tropospheric burden of ~ 2.9 Tg. Table 1.2 shows total organic chlorine (Cl_{org}) contained in long-lived halocarbons in the troposphere from both natural and

anthropogenic sources. Aggregate CFCs account for more than 60% of the total organic chlorine. Using total mass of global air of 5.2×10^{18} kg, the total mass of Cl_{org} in the troposphere is calculated as 17.9 Tg.

In the marine boundary layer, a considerable amount of chlorine is injected into the atmosphere as seasalt aerosol [Winterton, 2000]. With typical concentrations of 100 nmol m^{-3} measured from ships, Graedel and Keene [1996] calculated the chlorine burden in seasalt particles in the lower troposphere to be between 1 and 1.5 Tg Cl.

1.2.2.2 The stratosphere

The average concentration of total chlorine in the stratosphere was measured at 3.53 ± 0.10 ppbv [Zander *et al.*, 1996]. Assuming chlorine level derived from natural source (*i.e.* CH_3Cl) as about 0.7 ppbv, the stratospheric reservoir content of natural Cl is calculated as about 0.4 Tg [Graedel and Keene, 1996].

1.2.3 Chlorine storage in soil

Many scientists agree that Cl_{org} is ubiquitous in soil. The soil organic matter contains 0.01–0.5% of Cl_{org} , which is as common as phosphorous. Asplund *et al.* [1989] suggested that the Cl_{org} content in soil might be related to the amount of the organic matter, based on the observations that the chlorine-to-carbon ratio varies significantly less than the Cl_{org} concentration does. Combining global carbon storage data in soil with the chlorine-to-carbon ratios, Öberg [2003] estimated the total storage of Cl_{org} in the pedosphere to be 3350 Tg; because the calculation is based on soil samples from only 6

global sites, and assuming the median chlorine-to-carbon ratio is valid as an average estimate of chlorine-to-carbon ratio in the world soil, the uncertainty could be very large.

Based on the analyses of the measurements mentioned above, *Öberg* [2003] calculated the average concentration of Cl^- in soil in the world to be about 50–140 g $\text{Cl}^- \text{ m}^{-2}$. That estimate is within the same range of magnitude of the value of 200 $\text{Cl}^- \text{ m}^{-2}$ given by *Graedel and Keene* [1996]. Assuming that the mean soil density is 1 g cm^{-3} and the average concentration of Cl^- in soil is 100 $\mu\text{g g}^{-1}$ following *Graedel and Keene* [1996], *Öberg* [2003] estimated the global total Cl^- in the soil as $24 \times 10^3 \text{ Tg}$.

1.2.4 Chlorine storage in biomass

Though plant tissue contains organically bound chlorine, few studies have quantified those compounds in plants. It is known that the Cl_{org} concentration varies among plants and by the types of tissue within a plant. Because of the scarcity of the data, it is very difficult to estimate the Cl_{org} content of various types of plants and their tissues [*Öberg*, 2003]. *Öberg* [2003] used a $\text{Cl}_{\text{org}}/\text{C}$ ratio of 0.1 mg $\text{Cl}_{\text{org}} \text{ g}^{-1} \text{ C}$ and area and mean plant biomass of the major ecosystems in the world by *Houghton* [1995], and calculated the global storage of Cl_{org} in vegetation as 56 Tg.

Cl^- can be found in all organisms, and it participates in fundamental biological processes such as photosynthesis [*Öberg*, 2003]. The concentrations of Cl^- in plant tissues are very diverse, from 0.03 mg g^{-1} (w/w) in tissues of severely deficient plant to a few percent in plant in salt marshes [*Page*, 1982]. *Lobert et al.* [1999] estimated Cl^- content of various types of biomass, such as woody tissues on average contain 109 $\mu\text{g Cl}^- \text{ g}^{-1}$ and 254 $\mu\text{g Cl}^- \text{ g}^{-1}$ in temperate and tropical regions, respectively. Leaves in temperate and

tropical forests contain $389 \mu\text{g Cl}^- \text{g}^{-1}$ and $873 \mu\text{g Cl}^- \text{g}^{-1}$, respectively. Savannah grass on average contains $1022 \mu\text{g Cl}^- \text{g}^{-1}$. Combining these Cl^- content estimates and the global biomass distribution information by *Houghton* [1995], *Öberg* [2003] computed the global storage of Cl^- in vegetation to be 615 Tg.

1.3 Global chlorine fluxes

1.3.1 Mantle to troposphere

Volcanic eruptions are significant sources of HCl. The bulk of volcanic chlorine is thought to be due to seawater entering magma chambers and being emitted with other gases and particles during eruptions. Some of the volcanic chlorine may be directly extracted from chlorine in the mantle [*Graedel and Keene*, 1995]. *Symonds et al.*, [1988] estimated a rough range of the source rate of volcanic HCl as $0.4 - 11 \text{ Tg Cl yr}^{-1}$. *Graedel and Keene* [1995] arbitrarily assigned an average of 2 Tg Cl yr^{-1} to extraction from the mantle reservoir and the rest to ocean-troposphere transport. Table 1.4 shows the inter-reservoir fluxes of natural chlorine estimated by *Graedel and Keene* [1995]. Because of substantial clouds and rain generated by volcanic eruptions and high solubility of HCl, most of the chlorine is quickly deposited on the surface. Though many other chlorine-containing gases are emitted from volcanoes, their fluxes are small [*Graedel and Keene*, 1995].

Table 1.4 Estimated natural chlorine flux between reservoirs [*Graedel and Keene, 1995*].

| Inter-reservoir transfer | | Flux [Tg Cl yr ⁻¹] |
|-----------------------------|--|--------------------------------|
| Mantle to troposphere | | 2 |
| Pedosphere to troposphere | <i>Mineral aerosol</i> | 15 |
| | <i>Biomass burning</i> | 3 |
| | <i>Bioproducted</i> | 0.5 |
| Crust to freshwater | | 175 |
| Pedosphere to freshwater | <i>Precipitation passthrough</i> | 34 |
| | <i>Evaporate beds</i> | 11 |
| Freshwater to oceans | | 220 |
| Oceans to troposphere | <i>Seasalt injection</i> | 6000 |
| | <i>HCl from seasalt (a proportion of seasalt injection flux)</i> | 25 |
| | <i>Magma intrusion</i> | 4 |
| | <i>Bioproducted</i> | 2 |
| | <i>Oceans</i> | 5990 |
| Troposphere to surface | <i>Pedosphere</i> | 34 |
| | <i>Cryosphere</i> | 6 |
| | | |
| Troposphere to stratosphere | | 0.03 |
| Stratosphere to troposphere | | 0.03 |
| Oceans to crust | | 17 |

1.3.2 Ocean to troposphere

1.3.2.1 Seasalt aerosol and volatile inorganic Cl

It is believed that significant amounts of salts are lost from the ocean to the atmosphere in the form of seasalt aerosol formed by turbulent wind and associated wave action at the sea surface, and its re-deposition over the continents. Runoff from rivers to the ocean then must include some re-deposited chloride in addition to the chloride due to weathering [*Winterton, 2000*]. *Graedel and Keene* [1995] estimated that about 6×10^3 Tg yr⁻¹ of seasalt aerosol is injected into the marine boundary layer, in which the HCl produced from reactions involving naturally derived acids and seasalt aerosol would be about 25 Tg Cl yr⁻¹.

1.3.2.2 Organic Cl gases

The oceans are important natural sources of organochlorine compounds. Studies have shown that although chlorinated products may be formed directly, chemical exchange between biogenically produced brominated and iodinated materials and chloride ion is also possible [Winterton, 2000]. Up until a decade ago, CH₃Cl was believed to originate mostly from the ocean. For example, Graedel and Keene [1995] calculated the CH₃Cl flux of 2 Tg yr⁻¹ based on measured atmospheric CH₃Cl concentrations and its reaction rate with OH. However, recent direct measurements of CH₃Cl in sea water suggest that the contribution of CH₃Cl from this source is much lower and the net flux is estimated to be 0.3–0.4 Tg yr⁻¹ [Moore, 2000]. Our results of 3-D model simulation of global CH₃Cl (Chapters 2 and 3) support the observation results.

There is evidence showing *in situ* production of other chlorinated compounds [Graedel and Keene, 1995; Winterton, 2000]. The Reactive Chlorine Emission Inventory (RCEI) study, which is part of the Global Emissions Inventory Activity (GEIA) conducted under the auspices of the International Global Atmospheric Chemistry (IGAC) project, provided the global annual oceanic net emission rate of the most abundant gases such as CH₃Cl, chloroform (CHCl₃), dichloromethane (CH₂Cl₂), perchloroethylene (C₂Cl₄), and trichloroethylene (C₂HCl₃). The total emission of these gases is 980 Gg yr⁻¹ [Khalil *et al.*, 1999].

1.3.3 Vegetation to the atmosphere

1.3.3.1 Biogenic emissions

Vegetation might be an important source of atmospheric chlorine-containing gases such as CH₃Cl, although its full extent has not been established. Several

experimental studies have shown evidence of the biogenic CH_3Cl emissions. *Watling and Harper* [1998] calculated emission of CH_3Cl from wood-rotting fungi to be 114 Gg Cl yr^{-1} . *Yokouchi et al.* [2002] estimated an annual flux of 640 Gg Cl yr^{-1} from tropical plants. For other chlorinated compounds such as CH_2Cl_2 , C_2Cl_4 , and CHCl_3 , budget analyses suggests that industrial emissions are the major sources [*Khalil et al.*, 1999].

1.3.3.2 Biomass burning

Biomass burning is a major source of many atmospheric trace gases [*Lobert et al.*, 1999]. About 90% of today's biomass burning is human-induced and only a small percentage is due to natural phenomena such as lightning and lava outflow [*Öberg*, 2003]. As a part of the RCEI activity mentioned above, *Lobert et al.* [1999] calculated emissions of reactive chlorine containing compounds from biomass burning. The estimated global emissions in the inventory are 640 Gg Cl yr^{-1} for CH_3Cl , 49 Gg Cl yr^{-1} for CH_2Cl_2 , 1.8 Gg Cl yr^{-1} for CHCl_3 , and 13 Gg Cl yr^{-1} for CH_3CCl_3 , which gives a total emission of 7.0 Tg Cl yr^{-1} . In addition, *Lobert et al.* [1999] estimated the sum of volatile inorganic and particulate chlorine to be 6.35 Tg Cl yr^{-1} .

1.3.4 Industrial and combustion sources

The incineration of municipal and industrial wastes is known to produce HCl and CH_3Cl . Fossil fuels also contain chlorine, although the chlorine content of oil-based fuels is negligible, but in the case of coal combustion, the emission levels are significant [*Graedel and Keene*, 1995; *McCulloch et al.*, 1999a]. According to the RCEI inventory [*McCulloch et al.*, 1999a], the HCl emitted in 1990 includes 4.6 Tg Cl from fossil fuel

and 2 Tg Cl from waste burning. Emissions of CH₃Cl associated with combustions are calculated to be 75 Gg Cl yr⁻¹ from fossil fuels, 32 Gg Cl yr⁻¹ from waste combustion, and 7 Gg Cl yr⁻¹ from industrial activities [McCulloch *et al.*, 1999a].

Other chlorinated hydrocarbons such as trichloroethene (C₂HCl₃), tetrachloroethene (C₂Cl₄), and dichloromethane (CH₂Cl₂) are widely used in industrial and commercial processes. These chemicals are also byproducts of gasoline and coal combustion [McCulloch *et al.*, 1999b]. McCulloch *et al.* [1999b] estimated the annual emissions of C₂HCl₃, C₂Cl₄, and CH₂Cl₂ to be 195 Gg, 313 Gg, and 487 Gg as chlorine, respectively.

1.3.5 Deposition to surface

1.3.5.1 Deposition to the oceans

Deposition to the surface is the principal sink for HCl and seasalt particles [Graedel and Keene, 1995]. The flux of chlorine from the troposphere to the oceans is relatively large compared to the other fluxes [Graedel and Keene, 1996]. Atmospheric HCl concentrations are inversely correlated with relative humidity, presumably because the high solubility of HCl increases the loss of HCl to wet surfaces at high humidity. Since there is no observed long-term increase in the organic and inorganic chlorine in the troposphere [Montzka *et al.*, 2003], we calculated the oceanic sink of tropospheric Cl⁻ to be 5986 Tg yr⁻¹ assuming the tropospheric chlorine budget is balanced.

For non-HCl reactive chlorine gases, their oceanic sink could be negligible because of very low aqueous solubilities except CH₃Cl [Graedel and Keene, 1995]. The RCEI inventory suggests an annual oceanic sink of CH₃Cl to be 105 Gg Cl yr⁻¹ [Khalil *et*

al., 1999]. *Graedel and Keene* [1995] calculated the oceanic sink of inorganic chlorine containing species as 5855 yr^{-1} .

1.3.5.2 Deposition to the land

Most of the larger aerosol particles are deposited back to the ocean, or washed out of the atmosphere in marine precipitation, whose average chlorine concentration is 100–200 $\mu\text{mol Cl}^{-} \text{L}^{-1}$. Some particles small enough to be transported over land undergo processes of dry deposition or rainout [Winterton, 2000]. The dry deposition is rather difficult to determine, whereas the wet deposition can be easily measured. Assuming a median Cl^{-} concentration of $0.1 \text{ mg Cl}^{-} \text{L}^{-1}$, an annual rainfall of $110 \times 10^3 \text{ km}^3 \text{ yr}^{-1}$ over the land, and twice as high dry deposition, *Öberg* [2003] calculated an annual global deposition rate to be 33 Tg Cl yr^{-1} . This is consistent with the $34 \text{ Tg Cl}^{-} \text{ yr}^{-1}$ estimated by *Graedel and Keene* [1996] and *Winterton* [2000]. Deposition to the cryosphere is calculated to be $6 \text{ Tg Cl}^{-} \text{ yr}^{-1}$ [*Graedel and Keene*, 1996].

Wet deposition also contains organically bound chlorine. The Cl_{org} in precipitation could originate from natural sources such as marine aerosols, volcanic eruptions and other terrestrial sources as well as photochemical production in the atmosphere [*Öberg*, 2003]. The concentration of Cl_{org} in precipitation varies from a few to $\sim 30 \mu\text{g L}^{-1}$. Assuming an average concentration of $10 \mu\text{g L}^{-1}$, *Öberg* [2003] estimated the deposition rate of Cl_{org} over high precipitation regions ($> 2000 \text{ mm yr}^{-1}$) to be about 0.02 g m^{-2} . Investigating deposition patterns at a spruce forest in Northwest Denmark, *Öberg* [2003] concluded that dry deposition is not a major sink of Cl_{org} . Assuming the global annual rainfall over the world land area as $110 \times 10^3 \text{ km}^3 \text{ yr}^{-1}$ and a median

concentration of $10 \mu\text{g Cl}_{\text{org}} \text{L}^{-1}$, a total deposition rate to the land surface is calculated as 1.1 Tg yr^{-1} .

1.3.6 Transport between troposphere and stratosphere

Chlorine-containing compounds emitted to the troposphere with a sufficiently long lifetime could be transported into the stratosphere. Using results of an atmospheric transport and chemistry model and measurements of atmospheric concentration of chlorinated gases, *Graedel and Keene* [1995] estimated the flux from troposphere to stratosphere as 0.3 Tg yr^{-1} . We estimate Cl flux from the stratosphere to the troposphere to be 0.3 Tg yr^{-1} .

1.3.7 Freshwater to the oceans

Assuming about $38 \times 10^3 \text{ km}^3$ of an average annual flux of river water to the oceans, that of groundwater to the oceans about $2.2 \times 10^3 \text{ km}^3 \text{ yr}^{-1}$, and a typical riverine chlorine concentration of $7 \text{ mg Cl}^{-} \text{L}^{-1}$, *Graedel and Keene* [1996] calculated Cl flux from river to the oceans to be 220 Tg yr^{-1} .

1.3.8 Crust to freshwater

Most riverine chlorine is not of atmospheric origin. About 80% of it originates from weathering of chlorine-containing minerals and rocks, and from thermal and mineral springs in volcanic areas [*Graedel and Keene*, 1996]. *Graedel and Keene* [1996] estimated 175 Tg yr^{-1} is attributable to weathering of the earth's crust.

1.3.9 Soil to freshwater

The loss of organic chlorine by leaching is not very well understood. Only a few studies of Cl_{org} in soil leachates have been conducted. Assuming an average carbon concentration of 50 mg L^{-1} in soil leachates around the world and an average chlorine-to-carbon ratio of $2 \text{ mg Cl}_{\text{org}} \text{ g}^{-1} \text{ C}$, the global flux is calculated as 4.7 Tg yr^{-1} [Öberg, 2003].

The movement of Cl^- is closely related to the movement of water. The chloride ion is negatively charged; in the soil matrix, it is repelled by the solid structures and easily transported through the soil by the movement of water. This flux is thought to be equivalent for the wet and dry deposition, assuming soil acts neither as a sink nor a source of Cl^- [Öberg, 2003]. There is a loss of Cl^- from evaporite beds into freshwater, though the amount is unknown [Graedel and Keene, 1996]. Assuming a steady state for total chlorine in the soil, the loss of Cl^- to freshwater is calculated as 6 Tg yr^{-1} .

1.3.10 Oceans to crust

Graedel and Keene [1996] estimated the flux of oceanic Cl to the earth's crust via diagenetic flow as 17 Tg yr^{-1} .

1.3.11 Soil to the atmosphere

There are several studies that show terrestrial soils as a source of chlorinated gases [Khalil *et al.*, 1999]. Rhew *et al.* [2000] estimated an annual global release of $120 \text{ Gg Cl yr}^{-1}$ of CH_3Cl from salt marshes and Varner *et al.* [1999] calculated a global CH_3Cl flux from wetlands to be 34 Gg Cl yr^{-1} .

For other gases, *Khalil et al.* [1999] estimated the global CHCl_3 emission from soils as $200 \text{ Gg Cl yr}^{-1}$.

1.3.12 Vegetation to soil

A large amount of biomass, including stem wood, branches, leaves and roots, is delivered to the soil as dead organic matter. Since the plant tissue contains organic chlorine, plant litter appears to contain organic chlorine [Öberg, 2003]. Assuming that all of the net primary productivity (NPP) enters the terrestrial system as detritus and that the detritus contains $0.1 \text{ mg Cl}_{\text{org}} \text{ g}^{-1}$ organic matter (d.w.), Öberg [2003] calculated the flux from vegetation to soil to be $5.5 \text{ Tg Cl}_{\text{org}} \text{ yr}^{-1}$.

A study in a forest in northwestern Denmark shows that the Cl_{org} concentration in the throughfall, which is rainfall passing through the plant canopy, is considerably higher than that in the precipitation. Higher concentrations were observed in the samples placed closer to the tree. The strong correlation between the Cl_{org} and organic carbon in the throughfall also indicate that the increased Cl_{org} originate from internal sources in the forest [Öberg, 2003]. Öberg [2003] assume that the transport from vegetation to soil via throughfall to be half as large as that of via litterfall and estimated an annual flux of $2.25 \text{ Tg Cl}_{\text{org}}$.

1.3.13 Soil to vegetation

Based on the flux estimates calculated above and an assumption that the chlorine budget of vegetation is balanced, the chlorine flux from soil to vegetation is calculated as 22 Tg yr^{-1} .

1.3.14 Formation and mineralization of Cl_{org} in soil

It has been revealed that formation and mineralization of Cl_{org} take place in soil [Öberg, 2003 and references therein]. In the process of formation of Cl_{org} , soil acts as a sink of Cl^- and as a source in mineralization of Cl_{org} . There are numerous soil organisms that transform Cl^- to Cl_{org} , and there is strong evidence that biotic processes drive the degradation of Cl_{org} [Gribble, 1996; Öberg, 2003]. Though abiotic processes also could be involved in the chlorine cycle, these mechanisms are poorly understood [Öberg, 2003].

Several field studies were conducted to measure the amounts of Cl_{org} and Cl^- in litters, which suggest that the formation of Cl_{org} (consumption of Cl^-) is larger than the mineralization of Cl_{org} (release of Cl^-) under general circumstances. However, the net formation of Cl_{org} decreases where nitrogen fertilizer are used, and increases where the pH of soil is high. Also, the studies indicate that the net formation is seasonal, i.e. a maximum during fall and a minimum in early summer in Scandinavian soil. Since the net formation/mineralization of chlorine is strongly influenced by environmental variables and the rates of these two processes cannot yet be separated, it is difficult to estimate the rate of formation/mineralization of Cl_{org} in soil on a global basis [Öberg, 2003].

1.4 Summary and conclusions

Figure 1.2 summarizes the budget and cycles for global chlorine. The mantle holds the largest content, but only a small portion of which is transferred to the other reservoir (i.e. atmosphere) through volcanic eruptions. The chlorine content of the crust is smaller than that of the mantle by a factor of about 20. The only outflow of crustal chlorine is due to weathering. The oceans have the third highest chlorine content on the

planet, which is accessible and is actively involved in the global cycling of chlorine. The cryosphere holds less chlorine relative to all the other reservoirs, whereas freshwater seems to play an important role in transporting large amounts of Cl^- to the oceans [Graedel and Keene, 1996]. The troposphere is a small reservoir, but it interacts with many other reservoirs such as the oceans, the soil, the vegetation, the cryosphere, the mantle, and the stratosphere. The chlorine contents of soils and vegetation are the fifth and sixth largest among the reservoirs, respectively, and about 90% of the burden is inorganic chlorine. Even though the reservoir contents discussed here are rough estimates, the differences among the reservoirs are large enough to establish the order of the reservoirs [Graedel and Keene, 1996].

The relative importance of the fluxes is also depicted in Figure 1.2. The seasalt production over the sea surface is a significant source of Cl^- . The oceanic sink of tropospheric Cl^- is the dominant, followed by wet and dry deposition to the land surface, which is about factor of 50 smaller than the oceanic sink. The flux estimate of biogenically-produced chlorinated compounds might be underestimated because significant amounts of source are still missing for CH_3Cl , which is one of the most abundant organochlorine compounds in the atmosphere, though several model studies [Lee-Taylor *et al.*, 2001; Yoshida *et al.*, 2004; Yoshida *et al.*, 2006] suggest that more than 2 Tg yr^{-1} of CH_3Cl could be emitted from tropical plants.

Among the nine reservoirs shown in the figure, four are out of balance: the freshwater, the oceans, the crust and the mantle. There is evidence that the internal chlorine cycle takes place in the pedosphere involving uptake and release of chloride and also uptake of organic chlorine compounds by organisms, formation of organic chlorine

species by soil organisms and plants, mineralization of organic chlorine compounds and transport of both organic and inorganic chlorine compounds with detritus from the plant system to the soil, though most of this internal cycle have not been quantified.

Though the ranking of the chlorine contents in the reservoirs and the fluxes among them are well estimated, the individual quantities could have moderate to high uncertainties. In order to understand the chlorine budget and cycles better, we need improved mass balance for chlorine input and output from the oceans, soils, and the atmosphere. Also, further studies of the biogeochemistry and biogeochemistry of chlorine species, and investigation of origin and concentration of chlorine in precipitation, ground water, and soil leachates would be helpful.

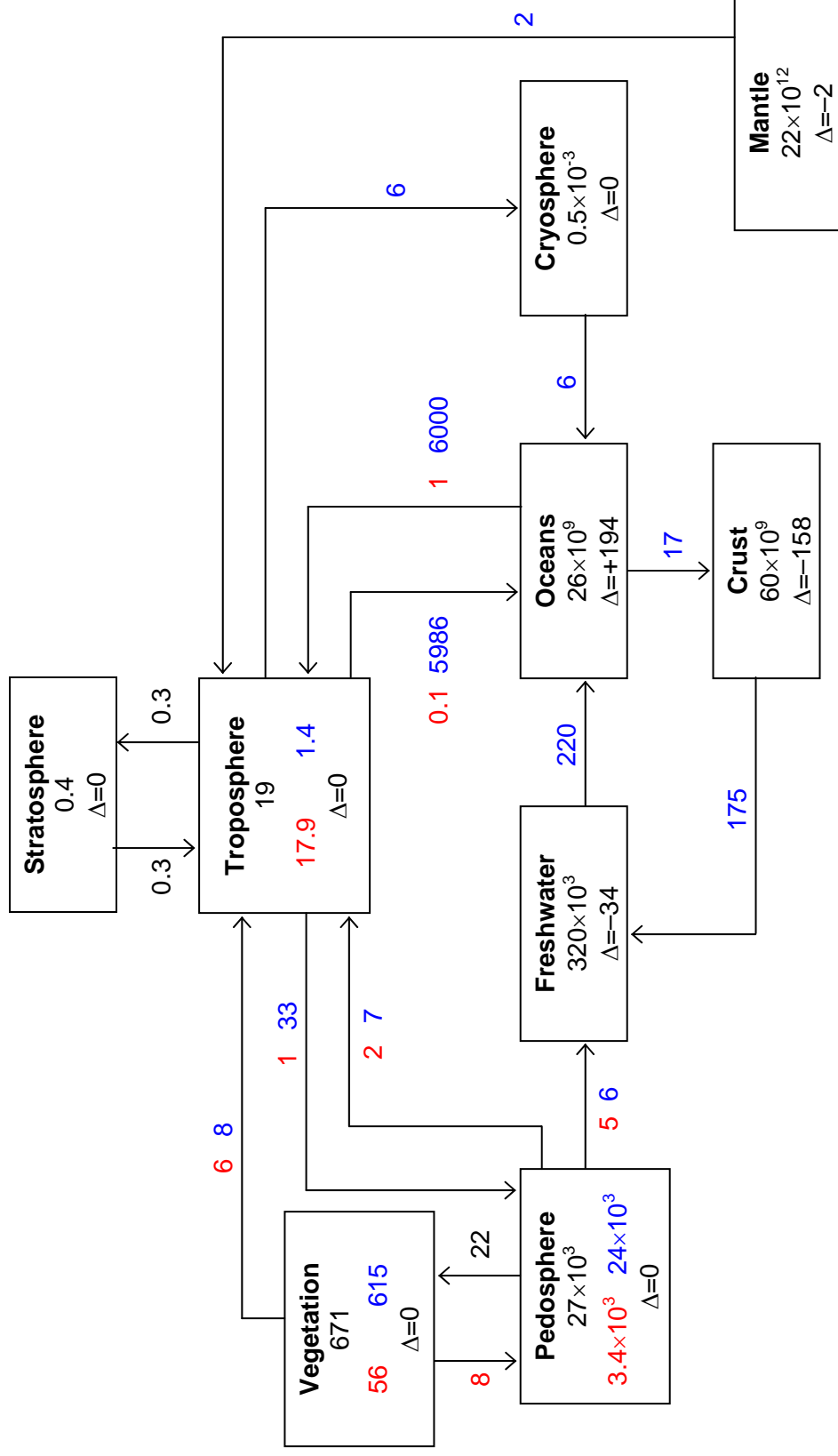


Figure 1.2 The chlorine budget and cycle for the planetary reservoirs. The units for the budget and flux are Tg and Tg yr^{-1} , respectively. The difference between inflow and outflow is shown as Δ (Tg yr^{-1}). Red, blue and black numbers indicate organic, inorganic, and total chlorine, respectively. For references, please see the text.

CHAPTER II

A THREE-DIMENSIONAL GLOBAL MODEL STUDY OF ATMOSPHERIC METHYL CHLORIDE BUDGET AND DISTRIBUTIONS

2.1 Introduction

Methyl chloride (CH_3Cl) is one of the most abundant chlorine-containing gas in the atmosphere; it is a major contributor to stratospheric chlorine. The global average mixing ratio of CH_3Cl in the troposphere is measured at about 550 ± 30 parts per trillion per volume (pptv) [Montzka *et al.*, 2003]. It is believed that CH_3Cl originates in large part from natural sources [Khalil *et al.*, 1999]. According to the emission data provided in the Reactive Chlorine Emissions Inventory (RCEI) conducted under the International Global Atmospheric Chemistry (IGAC) Global Emissions Inventory Activity (GEIA) project, the estimated emissions from known sources such as biomass burning, oceans, incineration/industrial sources are 910 (650–1,120), 650 (40–950), and 162 (30–294) Gg (giga gram = 10^9 gram) yr^{-1} , respectively [Keene *et al.*, 1999; Khalil *et al.*, 1999; Lobert *et al.*, 1999; McCulloch *et al.*, 1999]. Emission from certain wood-rotting fungi is estimated at 156 (35–385) Gg yr^{-1} , though no global distribution is currently available [Watling and Harper, 1998; Khalil *et al.*, 1999; Lee-Taylor *et al.*, 2001]. In addition, Rhew *et al.* [2000] estimated annual global release of 170 (65–440) Gg of CH_3Cl from salt marshes and Varner *et al.* [1999] calculated a global flux of 48 Gg yr^{-1} from wetlands.

The major removal process of CH_3Cl in the atmosphere is due to oxidation by OH radicals, which accounts for 3.5 (2.8–4.6) Tg (tera gram = 10^{12} gram) loss per year

[Koppmann *et al.*, 1993]. It is estimated that about 285 Gg of tropospheric CH₃Cl is transported to the stratosphere and lost there by photo dissociation and OH oxidation. Although the ocean is a net source globally, it is a significant net local sink in high-latitude regions. The RCEI estimate for the oceanic sink over the net uptake regions is 150 Gg yr⁻¹ [Moore *et al.*, 1996; Khalil *et al.*, 1999; Keene *et al.*, 1999]. Soils are recognized as an additional sink, and Keene *et al.* [1999] estimated it could be as much as 256 Gg yr⁻¹, but the uncertainty is quite high [Lee-Taylor *et al.*, 2001; Rhew *et al.* 2001]. The CH₃Cl budget based on the current “best guess” estimates given above leaves a substantial deficit for sources by ~1.8 Tg yr⁻¹. This imbalance might be explained by one or some combination of the following: (1) the emission from one or more sources is underestimated; (2) the CH₃Cl loss by reaction with OH is overestimated; (3) there exists some significant unidentified source(s) of CH₃Cl [Keene *et al.*, 1999].

The overall uncertainties in CH₃Cl emissions from known sources are relatively large and the estimated OH sink has significant uncertainties that come in part from the uncertainties in the temperature dependence of the OH + CH₃Cl reaction rate constant [Keene *et al.*, 1999; Lee-Taylor *et al.*, 2001]. After examining the results of a series of model runs using different OH reaction rates, Lee-Taylor *et al.* [2001] concluded that the budget imbalance is not due to assumption (2) above. Their model results with identified emissions showed a significant inter-hemispheric gradient, which was not observed. In order to remove the gradient, some unidentified source must exist at high latitudes in the southern hemisphere such as oceanic emissions, which might be unrealistic considering oceanic observation results. Therefore, they concluded that the budget discrepancy likely comes from a land-based missing source [Lee-Taylor *et al.*, 2001].

Yokouchi *et al.* [2000] reported that enhanced mixing ratios of CH₃Cl were correlated with α -pinene, a short-lived species emitted by vegetation, in air masses over subtropical Okinawa Island. Strong emissions of CH₃Cl from tropical plants were observed by Yokouchi *et al.* [2002] and they suggested that tropical forests could be the major source. However, emission fluxes and the detailed emission mechanisms from terrestrial vegetation are unknown [Keene *et al.*, 1999; Yokouchi *et al.*, 2000; Yokouchi *et al.*, 2002].

Very few global 3-D simulations of CH₃Cl have been conducted. Lee-Taylor *et al.* [2001] presented a 3-D model study for CH₃Cl distributions, but they evaluated their results using only surface observations and did not interpret the results in terms of contributions of each source to the observed concentrations and seasonal variations. In this paper we present more comprehensive modeling and analyses of CH₃Cl on the basis of surface and aircraft observations using the global GEOS-Chem model.

2.2 Model description

The model used in this study is the GEOS-Chem (version 5.02) global 3-D chemical transport model of tropospheric chemistry driven by assimilated meteorological fields from the Goddard Earth Observing System (GEOS) of the NASA Global Modeling and Assimilation Office (GMAO) (<http://www-as.harvard.edu/chemistry/trop/geos/>) [Bey *et al.*, 2001]. We use a horizontal resolution of 4° latitude \times 5° longitude. The vertical layers vary by different model simulation years. In order to compare to atmospheric field experiments, we simulated the CH₃Cl distributions using 7 different meteorological fields for the years of 1991, 1992, 1994, 1995, August 1996 – September

1997, 2000, and 2001. For simulation years before December 1995, the model has 20 vertical levels, for December 1995, 1996 and 1997, 26 levels, and for 2000 and 2001, 48 levels. To calculate the chemical loss of CH_3Cl , the tropospheric OH field was taken from the GEOS-Chem full-chemistry simulation by *Martin et al.* [2003] and the stratospheric OH field taken from a 2-D stratosphere/mesosphere model was used [Schneider et al., 2000]. The tropospheric OH field yields a global mean methyl chloroform (CH_3CCl_3) lifetime of 5.6 years in good agreement with the observations [Spivakovsky et al., 2000; Prinn et al., 2001; Martin et al., 2003]. In this study, CH_3Cl emitted from different sources is transported as separate tracers. In this manner, contributions from each source to the spatial and temporal distributions of CH_3Cl can be evaluated in the model.

2.3 Sources of CH_3Cl

2.3.1 Biomass burning

Biomass burning is the largest known source of CH_3Cl . *Lobert et al.* [1999] estimated 910 (650–1120) Gg yr^{-1} emissions from this source in the RCEI inventory on a $1^\circ \times 1^\circ$ grid based on the emission ratios of CH_3Cl to CO and CO_2 . Hot spots of emission are located in the regions of Southeast Asia, India, tropical Africa and South America. No seasonality was given in the inventory; we first scaled their annual biomass burning CH_3Cl flux with seasonal biomass and biofuel burning CO emissions used in GEOS-Chem. The satellite observation-based biomass burning CO inventory was obtained from *Duncan et al.* [2003] except for the time period of February–April 2001, when the monthly inventory by *Heald et al.* [2003] is used. Model simulations using this inventory

show large overestimates over the western Pacific. *Lee-Taylor et al.* [2001] reduced the biomass burning source over Southeast Asia by 50% in the RCEI inventory. In our work, we apply a $\text{CH}_3\text{Cl}/\text{CO}$ molar emission ratio of 5.7×10^{-4} [*Lobert et al.*, 1999] to estimate a biomass burning CH_3Cl source of $611 \pm 38 \text{ Gg yr}^{-1}$. The range reflects the interannual variability of biomass burning CO by *Duncan et al.* [2003] and *Heald et al.* [2003]. The estimate used in our study is at the lower limit calculated by *Lobert et al.* [1999]. We found that a lower biomass burning source is in better agreement with the observations (section 2.5).

2.3.2 Oceanic emissions

The ocean is the second largest known source of CH_3Cl . In the RCEI inventory, *Khalil et al.* [1999] estimated an annual net oceanic emission of CH_3Cl of 655 Gg yr^{-1} using an empirical relationship between sea surface temperature (SST) and CH_3Cl saturation anomaly. Oceanic emissions are located mainly in the tropics and subtropics. At latitudes higher than 50° , the ocean is a net sink. The estimated uncertainties of the oceanic flux are a factor of 2 to 3, mainly due to measurement errors of several variables used in the transfer velocity calculation [*Khalil et al.*, 1999]. Based on the measured solubility of CH_3Cl in seawater at different temperatures, *Moore* [2000] estimated a net CH_3Cl flux of $300\text{--}400 \text{ Gg yr}^{-1}$ from the ocean including a global annual ocean uptake of $90\text{--}150 \text{ Gg}$. In this study, we recalculated the oceanic flux using the National Oceanic and Atmospheric Administration Climate Monitoring and Diagnostics Laboratory (NOAA-CMDL) empirical relationship between saturation and SST as by *Khalil et al.* [1999] with monthly climatological wind speed distributions. The wind data are taken

from the revised monthly mean summaries of the Comprehensive Ocean-Atmosphere Data Set (UWM-COADS) produced at University of Wisconsin-Milwaukee in collaboration with NOAA/National Oceanographic Data Center [*daSilva et al.*, 1994]. Sea surface temperature fields are the 10-year averages (1990–1999) of a global extended reconstructed SST (ERSST) produced by *Smith and Reynolds* [2003] based on the Comprehensive Ocean-Atmosphere Data Set (COADS). The sea-air interface transfer velocity of CH₃Cl (*k*) was calculated following *Wanninkhof* [1992]:

$$k \text{ (cm h}^{-1}\text{)} = 0.39 v^2 (S_c/660)^{-1/2} \quad (2.1)$$

$$S_c = 2385 [1 - 0.065 (\text{SST}) + 0.002043 (\text{SST})^2 - 2.6 \times 10^{-5} (\text{SST})^3] \quad (2.2)$$

where *v* is the long-term average wind speed (m s⁻¹) at 10m above sea level, *S_c* is the unitless Schmidt number of CH₃Cl, and SST is in °C [*Khalil and Rasmussen*, 1999; *Khalil et al.*, 1999].

In our model calculation, monthly mean sea ice coverage is applied to prevent CH₃Cl loss to the sea ice. The sea ice data are taken from the International Satellite Land-Surface Climatology Project (ISLSCP) Initiative II data archive [*Hall et al.*, 2003]. Our model result of the global annual oceanic flux is about 350 Gg yr⁻¹, which is 20% lower than the value estimated by a direct extrapolation of in situ observations (440 Gg yr⁻¹) by *Khalil et al.*, [1999] and 47 % lower than the 655 Gg yr⁻¹ in the RCEI inventory, but is in the same range given by *Moore* [2000]. A critical issue we found in the comparison of simulated and observed surface CH₃Cl concentrations is the ocean loss over the uptake region at southern high latitudes. Our estimate of 30 Gg yr⁻¹ is much lower than that in the RCEI inventory of 150 Gg yr⁻¹. Therefore, we use two inventories to account for the difference. The first inventory is as described above. In the second inventory, we

increased the sink over ocean uptake regions to 150 Gg yr^{-1} . The emissions over the net source regions are increased to $\sim 500 \text{ Gg yr}^{-1}$ (by $\sim 30\%$) in order to maintain the net ocean source of 350 Gg yr^{-1} .

2.3.3 Incineration/industrial emissions

It is known that CH_3Cl is released into the atmosphere from combustion of fossil fuels with high chlorine contents such as coal. Combustion of domestic and municipal waste containing chlorine also emits CH_3Cl . *McCulloch et al.* [1999] calculated the global emissions from fossil fuel combustion and waste incineration to be 75 ± 70 and $32 \pm 23 \text{ Gg Cl yr}^{-1}$, respectively. They also estimated a source of 7 Gg Cl yr^{-1} from other industrial sources. The total CH_3Cl emission from coal combustion, incineration and other industrial activities is then estimated as $162 (114 \pm 93) \text{ Gg yr}^{-1}$ in the RCEI inventory [*McCulloch et al.*, 1999]. In this study, we applied the non-seasonal RCEI emission inventory for this source.

2.3.4 Salt marshes and wetlands

Rhew et al. [2000] estimated the global CH_3Cl emissions from salt marshes as $170 (65\text{--}440) \text{ Gg yr}^{-1}$ based on field studies from two coastal salt marshes in California. We distribute the flux using a land cover database from the International Satellite Land Surface Climatology Project (ISLSCP) Initiative I data [*Sellers et al.*, 1995]. We confine the emissions to the growing season such as May to September at northern mid to high latitudes and November to March at southern mid to high latitudes.

The global CH₃Cl flux from freshwater wetlands was calculated by *Varner et al.* [1999] as 48 Gg yr⁻¹. In our model, the emissions are distributed using the ISLSCP Initiative I land cover data [*Sellers et al.*, 1995] and are limited to the growing season in the same manner as in the salt marsh emission calculation.

2.3.5 Biogenic emissions

Close correlations between enhanced concentrations of CH₃Cl and biogenic compound, α -pinene emitted by terrestrial plants have been observed [*Yokouchi et al.*, 2000]. *Yokouchi et al.* [2002] reported that some particular plant families in tropical forests (certain types of ferns and Dipterocarpaceae) emit a significant amount of CH₃Cl. They calculated that the emission from only Dipterocarpaceae species in Asian tropical forests could be 910 Gg yr⁻¹ by extrapolating emission rates obtained from CH₃Cl flux measurements in a glasshouse, although the uncertainty is very large. *Hamilton et al.* [2003] estimated a global annual CH₃Cl production of 75–2,500 Gg between 30°N and 30°S based on their CH₃Cl flux observation from senescent and dead leaves. *Lee-Taylor et al.* [2001] conducted model studies for CH₃Cl, assuming that terrestrial vegetation plays a significant role in CH₃Cl production. They concluded that the model most successfully reproduced the observed mixing ratios of CH₃Cl when they added 2,330–2,430 Gg yr⁻¹ of a hypothetical biogenic source combined with a 50% reduction of biomass-burning emissions from Southeast Asia in the RCEI biomass burning inventory.

In our study, 2,430–2,900 Gg yr⁻¹ is added as the biogenic source of CH₃Cl. We distributed the biogenic source to all vegetated areas between 30°N and 30°S. The land cover classification is based on the ISLSCP Initiative I data set [*DeFries and Townshend*,

1994]. The uniform distribution over all vegetated areas with the flat annual emission rate is based on model sensitivity analyses (the results are not shown) since currently the dependence of biogenic CH₃Cl emission on vegetation, temperature, and sunlight is unknown. The major constraint is the observed seasonal variation of CH₃Cl at northern mid and high latitudes. Biogenic emissions at mid and high latitudes in summer would lead to overestimates of CH₃Cl in those regions. Furthermore, scaling biogenic CH₃Cl emission to the seasonality of isoprene (e.g., *Lee-Taylor et al.*, [2001]) would also lead to a too small seasonal variation in comparison to the observations because the seasonality of isoprene emissions is opposite to the observed seasonality of CH₃Cl. Our calculated emissions between 30°S–30°N account for 93% of the global CH₃Cl source, which agrees with the estimates by *Khalil and Rasmussen* [1999], who suggested that 85% of the emission of CH₃Cl comes from tropical and subtropical regions based on their inverse modeling results with simplified box models for tropospheric transport and OH oxidation.

2.4 Sinks of CH₃Cl

2.4.1 Reaction with OH

The main sink of CH₃Cl in the atmosphere is oxidation by hydroxyl radicals:



In our model calculation, we used two different reaction rate constants for reaction (R2.1), k_{97} , and k_{03} , reported by *DeMore et al.* [1997] and *Sander et al.* [2003], respectively. The rate constant (k) is represented by the Arrhenius expression $k = A \exp(-E/RT)$, where values for A given by *DeMore et al.* [1997] and *Sander et al.* [2003] are 4.0×10^{-12} and $2.4 \times 10^{-12} \text{ cm}^3 \text{ s}^{-1}$, and for E/R , 1400 and 1250K, respectively. T is temperature (K). The

rate constant at 298K is $3.6 \times 10^{-14} \text{ cm}^3 \text{ s}^{-1}$ for both, and the uncertainty (at 298K) is 1.2 and 1.15, respectively. The k_{03} is higher than k_{97} by about 9% at $T=250\text{K}$. The calculated global losses of CH_3Cl with the “reference” emissions (Table 2.1) using k_{97} and k_{03} are 4.1 Tg yr^{-1} for both, which agree with literature values [Koppmann *et al.*, 1993; Khalil and Rasmussen, 1999]. The model results with the different k value are compared in section 2.5.1.

The OH field used is taken from the work by Martin *et al.* [2003]. The interhemispheric ratio of mass-weighted OH is 1.03; about 2.6% higher in the northern hemisphere (NH) than in the southern hemisphere (SH). Calculated annual mean global CH_3CCl_3 lifetime to loss by tropospheric OH is 5.6 years, which is consistent with estimates from observations by Spivakovsky *et al.* [2000] (5.7 ± 0.7 years) and Prinn *et al.* [2001] ($6.0 +1.0, -0.7$ years). However, the interhemispheric OH ratio calculated from CH_3CCl_3 measurements using the inverse method varies by study. For instance, the NH/SH ratio estimated by Prinn *et al.* [2001] and Krol and Lelieveld [2003] is 0.88 and 0.98, respectively. Krol and Lelieveld [2003] commented that the differences between their interhemispheric ratio and that given by Prinn *et al.* [2001] could be due to the model resolution difference. They also explained that their slightly higher OH concentrations in the SH than NH might be derived from model or emission errors. Nearly equal hemispheric mean OH was also reported by Spivakovsky *et al.* [2000].

Table 2.1 Estimated global budget of CH₃Cl.

| Unit: Gg yr ⁻¹ | | | | |
|---------------------------|--------------------|------------------|------------------|---------------------|
| Runs | Reference | OC-1 | OC-2 | Model mean |
| SOURCES (total) | (4,525) | (4,214) | (4,333) | (4,399 ± 43) |
| Ocean | 805 ^a | 380 | 499 | 508 ± 5 |
| Biomass burning | 910 ^b | 554 | 554 | 611 ± 38 |
| Incineration/industrial | 162 ^c | 162 ^c | 162 ^c | 162 ^c |
| Pseudo biogenic | 2,430 ^d | 2,900 | 2,900 | 2,900 |
| Salt marshes | 170 ^e | 170 ^e | 170 ^e | 170 ^e |
| Wetlands | 48 ^f | 48 ^f | 48 ^f | 48 ^f |
| SINKS (total) | (4,525) | (4,214) | (4,333) | (4,399 ± 43) |
| OH reaction | 4,124 | 3,926 | 3,930 | 3,994 ± 42 |
| Ocean | 145 ^a | 32 | 147 | 149 ± 1 |
| Soil | 256 ^g | 256 ^g | 256 ^g | 256 ^g |

^{a - g} Those values are taken from the following references: ^a *Khalil et al.* [1999], ^b *Lobert et al.* [1999], ^c *McCulloch et al.* [1999], ^d *Lee-Taylor et al.* [2001], ^e *Rhew et al.* [1999], ^f *Varner et al.* [1999], ^g *Khalil and Rasmussen* [1999] and *Keene et al.* [1999]. Other emissions and sinks are calculated as explained in the text.

In order to test the sensitivity of the CH₃Cl distribution to reaction with OH in our model, we conducted three test simulations using OH fields with different NH/SO₂ distribution, such as original OH field (the annual mean NH/SO₂ mass ratio is 1.03), OH increased and decreased by 10% (NH/SO₂ ratio of 1.26), and decreased and increased by 10% (NH/SO₂ ratio of 0.84), in the NH and SO₂, respectively. Figure 2.1 shows the resulting latitudinal CH₃Cl distributions with different OH distributions compared with observed concentrations. In these simulations, the reaction rate constant was taken from

Sander et al. [2003]. The result with the original OH concentrations gives almost symmetrical N-S distribution as observed while results with modified OH fields show clear N-S gradients. It is therefore clear that deviation from the current hemispheric mean OH ratio by $\pm 20\%$ could not reproduce the observed CH_3Cl distributions. The additional constraint on the interhemispheric mean OH ratio is valuable because the estimate is not as sensitive to model errors of the interhemispheric transport as that derived from CH_3CCl_3 , the source of which is located in the northern industrial regions.

2.4.2 Soil sink

The global soil sink of CH_3Cl is estimated to be 256 Gg yr^{-1} [*Keene et al.*, 1999; *Khalil and Rasmussen*, 1999]. No global distribution of the soil uptake rates is available. *Rhew et al.* [2001] found that there is a strong correlation in the measured uptake rates of CH_3Br and CH_3Cl in southern California shrubland ecosystems, and concluded there could be a similar mechanism of consumption for both compounds. In our model, we scaled the soil sink of CH_3Cl with that of methyl bromide (CH_3Br), whose global loss rates were estimated by *Shorter et al.* [1995], assuming that the soil uptake of CH_3Cl is proportional to CH_3Br . The soil type was defined using vegetation type data from the ISLSCP Initiative I data [*DeFries and Townshend*, 1994]. Seasonality was applied by assuming growing seasons of 365, 240, and 180 days in tropical, temperate, and boreal regions, respectively [*Shorter et al.*, 1995]. The calculated annual CH_3Cl loss to soil is, 69, 137, 16, and 34 Gg yr^{-1} for tropical forest/savanna, temperate forest/grassland, boreal forest, and cultivated land, respectively.

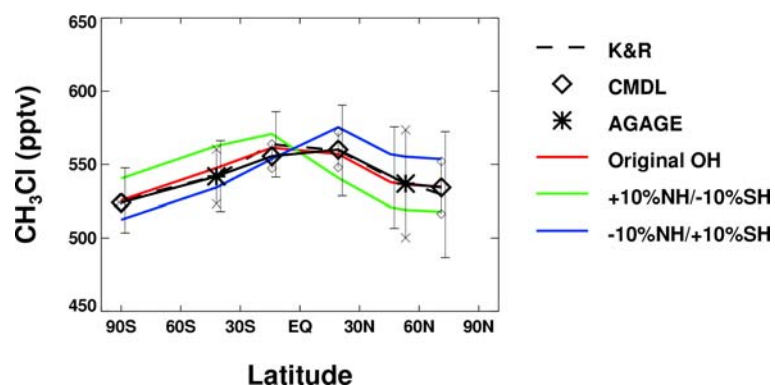


Figure 2.1 Latitudinal distributions of observed and simulated CH_3Cl at the surface sites. Broken line indicates data by *Khalil and Rasmussen* [1999] (the data were lowered by 8.3% to account for a calibration difference). The thick black solid line links the CMDL (Diamonds) and AGAGE data (asterisks). Thin vertical lines indicate the standard deviations; the end symbols are minus signs, diamonds, and asterisks for K&R, CMDL, and AGAGE data, respectively. Emission inventories for OC-2 (Table 2.1) are used. Model results are shown with the standard OH concentrations and two perturbation cases, in which the NH and SH hemispheric OH concentrations are either increased or decreased by 10% (see text for more details).

2.5 Results

We conducted several model runs with different input data: one of them employs the sources from existing emission inventories such as the RCEI inventories (for oceanic, biomass burning, incineration/industrial sources) and pseudo-biogenic emission of the literature value (i.e., *Lee-Taylor et al.* [2001]), which is referred to as the reference run. Run OC-1 includes the oceanic and biomass burning emissions calculated in our model (section 2.3). The oceanic sink in run OC-1 is about 80% smaller than that calculated by *Khalil et al.* [1999] and it resulted in higher average surface concentrations in the SH by about 10 pptv (~2%) than in the NH, which is not observed. In run OC-2, oceanic emissions and sinks are increased so that total oceanic sink over net uptake regions becomes the same as that given by RCEI [*Khalil et al.* 1999] and the net oceanic emissions are the same as in OC-1 run. The runs of reference, OC-1 and OC-2 are simulated with the same meteorological field of September 1996–August 1997. Figure 2.2 summarizes the latitudinal distribution of the annual-mean emissions and sinks (except the sink via OH oxidation) of CH₃Cl used in those runs. The average values of 7-year model runs (1991, 1992, 1994, 1995, Sep96–Aug97, 2000, 2001) are shown as “model mean”. The annual total of the emissions and sinks are listed in Table 2.1. Figure 2.3 shows simulated global surface CH₃Cl mixing ratio distributions for January and July. Higher concentrations are simulated over regions where major sources are located. The lower concentrations in the summer hemisphere are due in part to active OH oxidation.

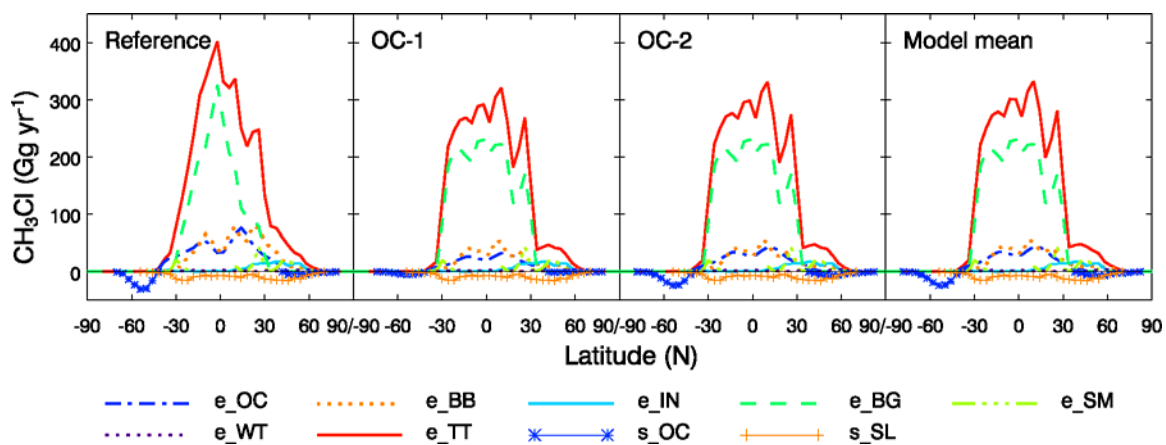


Figure 2.2 Latitudinal distribution of the known sources and sinks of CH_3Cl . For the legend, “e-” and “s-” denote emission and sink, respectively and characters OC, BB, IN, BG, SM, WT, TT, SL denote ocean, biomass burning, incineration/industrial, biogenic, salt marshes, wetlands, the total of all emissions, and soil, respectively.

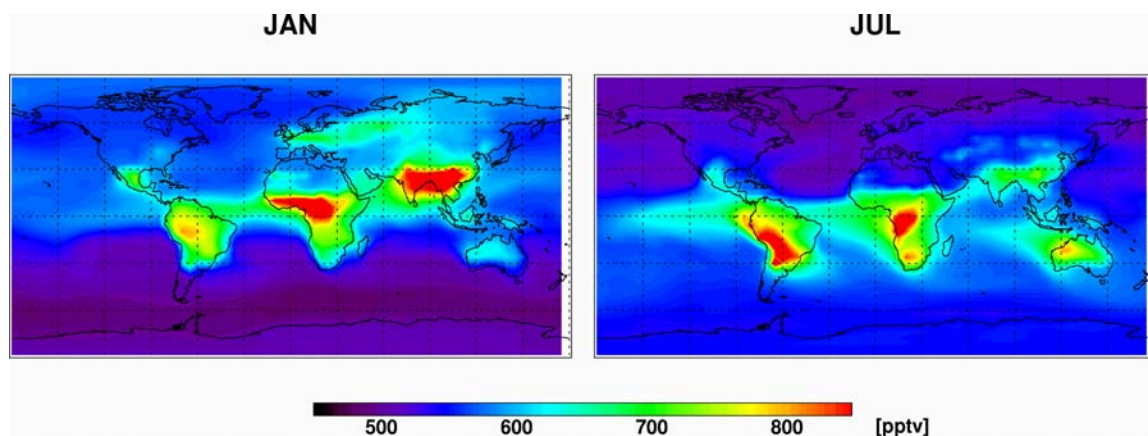


Figure 2.3 Simulated surface mixing ratio of CH_3Cl for January and July.

The model results are evaluated with surface and aircraft observations. Seven surface sites and 9 aircraft field experiments are included. Table 2.2 summarizes these observations used.

Table 2.2 Atmospheric measurements of CH₃Cl.

| | Region | Time period | Reference |
|--------------------------|---|--|--|
| <i>Surface stations</i> | | | |
| K & R | Alaska (71.2N, 156.5W) Oregon (45.5N, 124W) Hawaii (19.3N, 154.5W) Samoa (14.1S, 170.6W) Tasmania (42S, 145E) Antarctica (90S) | 1981-1997 | <i>Khalil and Rasmussen [1999]</i> |
| NOAA-CMDL | Alaska (71.3N, 156.6W) Hawaii (19.5N, 155.6W) Samoa (14.2S, 170.6W) Antarctica (90.0S, 102.0E) | Jan 1998-Mar 2002 Dec 1999-Feb 2002 Dec 1998-Feb 2003 Jan 2001-Nov 2003 | <i>G. Dutton, personal communication, 2004</i> |
| AGAGE | Ireland (53.2N, 9.5W) Tasmania (40.4S, 144.4E) | 1998-2001 | <i>Simmonds et al. [2004]</i> |
| <i>Aircraft missions</i> | | | |
| PEM-Tropics A | Tropical Pacific | Aug-Oct 1996 | <i>Blake et al. [1999a]</i> |
| PEM-Tropics B | Tropical Pacific | Mar-Apr 1999 | <i>Blake et al. [2001]</i> |
| ACE 1 | Pacific/Southern Ocean | Nov-Dec 1995 | <i>Blake et al. [1999b]</i> |
| TRACE-A | Tropical Atlantic | Sep-Oct 1992 | <i>Blake et al. [1996]</i> |
| INDOEX | Indian Ocean | Feb-Mar 1999 | <i>Scheeren et al. [2002]</i> |
| PEM-West A | Western Pacific | Sep-Oct 1991 | <i>Blake et al. [1997]</i> |
| PEM-West B | Western Pacific | Feb-Mar 1994 | <i>Blake et al. [1997]</i> |
| TRACE-P | Western Pacific | Feb-Apr 2001 | <i>Blake et al. [2003b]</i> |
| TOPSE | North America | Feb-May 2000 | <i>Blake et al. [2003a]</i> |

2.5.1 Global distribution of atmospheric CH₃Cl near the surface

2.5.1.1 Seasonal variation

Our model results are compared with three surface observation data sets measured at 7 surface stations. The locations of these 7 sites are shown in Figure 2.4. The observed and simulated seasonal variations of CH₃Cl at the stations are compared in Figure 2.5.

The data from *Khalil and Rasmussen* [1999] was lowered by 8.3% in all figures in order to adjust to the calibration difference [Montzka *et al.*, 2003]. We note that the CMDL data may have a systematic error up to 20 pptv due to losses of CH₃Cl in field deployed reference tanks (*G. Dutton*, personal communication, 2004). There are two observed data sets for Alaska, Hawaii, Samoa, Tasmania and Antarctica, and those two seasonal variations are similar except in Samoa, where the CMDL data show two peaks in February–March and in August, while a single peak in June–July was reported by *Khalil and Rasmussen* [1999].

The model results with a total emission of 4,500 Gg yr⁻¹ (“reference” in Table 2.1) with different OH reaction rate constants (k_{97} and k_{03} , section 2.4) are shown in Figure 2.5 as Ref-k97 and Ref-k03, respectively. The other model results shown as OC-1, OC-2, and model mean are calculated using k_{03} . The global annual mean surface concentration of Ref-k97 and Ref-k03 is 599 and 579 pptv, respectively, and the difference, about 3%, is solely due to the difference of the reaction rate constants. The reference run with k_{97} (Ref_k97) gives higher concentrations than the observations by 3–18% especially at the tropical and NH sites. Using the rate constant k_{03} , the run Ref-k03 overestimates the observations by up to 14% except for January–June at Tasmania and Antarctica sites. For these two sites, the OC-2 concentrations are close to the Ref-k03 concentrations except

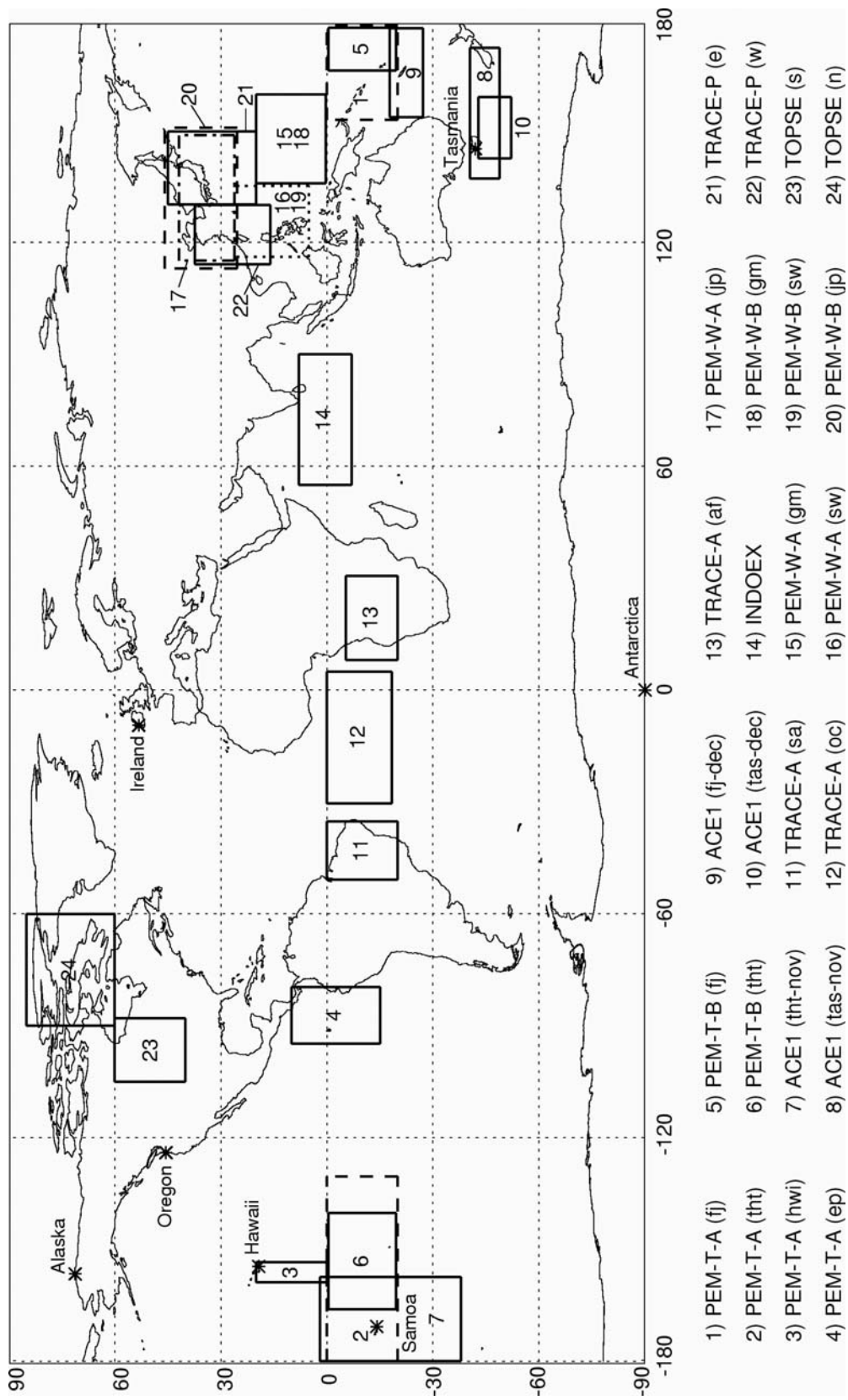


Figure 2.4 Surface measurement sites (indicated by symbols) and aircraft observation regions used in this study.

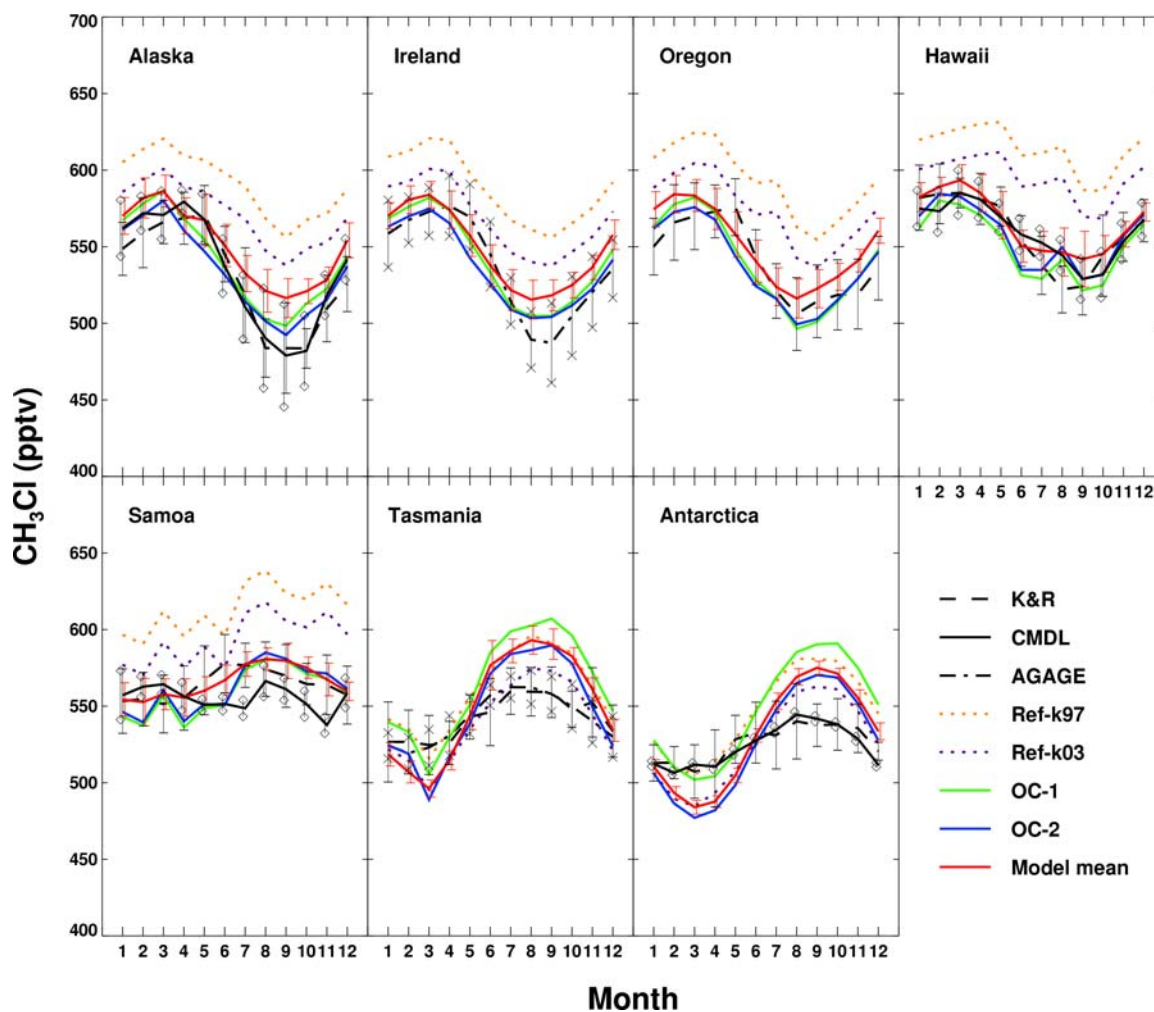


Figure 2.5 Seasonal variations of observed and simulated CH_3Cl at the surface sites. Broken lines indicate data by *Khalil and Rasmussen* [1999], black solid lines indicate CMDL data (*G. Dutton*, personal communications, 2004), and dotted-broken lines indicate AGAGE data [*Simmonds et al.*, 2004]. The K&R data were lowered by 8.3% to account for a calibration difference. Model results are shown in color. The orange dotted lines are the reference run with the OH reaction rate constant by *DeMore et al.* [1997]. The purple dotted lines are the reference run with the OH rate constant by *Sander et al.* [2003]. The green lines are the OC-1 run. The blue lines are the OC-2 run. These 4 simulations used meteorological data for September 1996 – August 1997. The red solid lines are the mean of 6-year simulations with oceanic sink calculated as in the OC-2 run. The vertical lines represent the standard deviations.

for June–October in Tasmania, where Ref-k03 gives lower concentrations by 3–4%. The overestimates of Ref-k03 indicate that the biomass burning emissions in the RCEI inventory might be overestimated. The wrong seasonality simulated in the Ref-k03 run is due to the scaling of the biogenic source to isoprene emissions, which peak in summer, when observed CH_3Cl shows a minimum.

OC-1 and OC-2 show little difference at all sites except for Tasmania and Antarctica, where the effect of the oceanic uptake of CH_3Cl is significant. OC-2 gives lower concentrations than OC-1 by about 2–5% in better agreement with the observations. The model results with our estimates of biomass burning and oceanic emissions with increased oceanic sink over the uptake regions (OC-2 and Model mean) reproduces the general features and the magnitudes of seasonal variations relatively well at northern high latitude stations (Alaska, Ireland and Oregon), such as maxima in spring to early summer and minima in late summer and fall. At the Hawaii site, the summer overestimate is largest in August in Ref-k97. The peak for the multi-year mean is not as large, but the summer overestimate is apparent, suggesting that the biogenic source upwind from Hawaii is overestimated. The amplitude of the seasonal cycle calculated by the model is too large compared to the observations at southern higher latitudes. The reasons will be discussed further in the next section.

2.5.1.2. Latitudinal variation

Figure 2.6 shows the annual and seasonal latitudinal distributions of CH_3Cl at the same 7 surface stations in Figure 2.4. The observed annual means of CH_3Cl show little interhemispheric gradient, while there are relatively clear seasonal gradients. Ref-k03

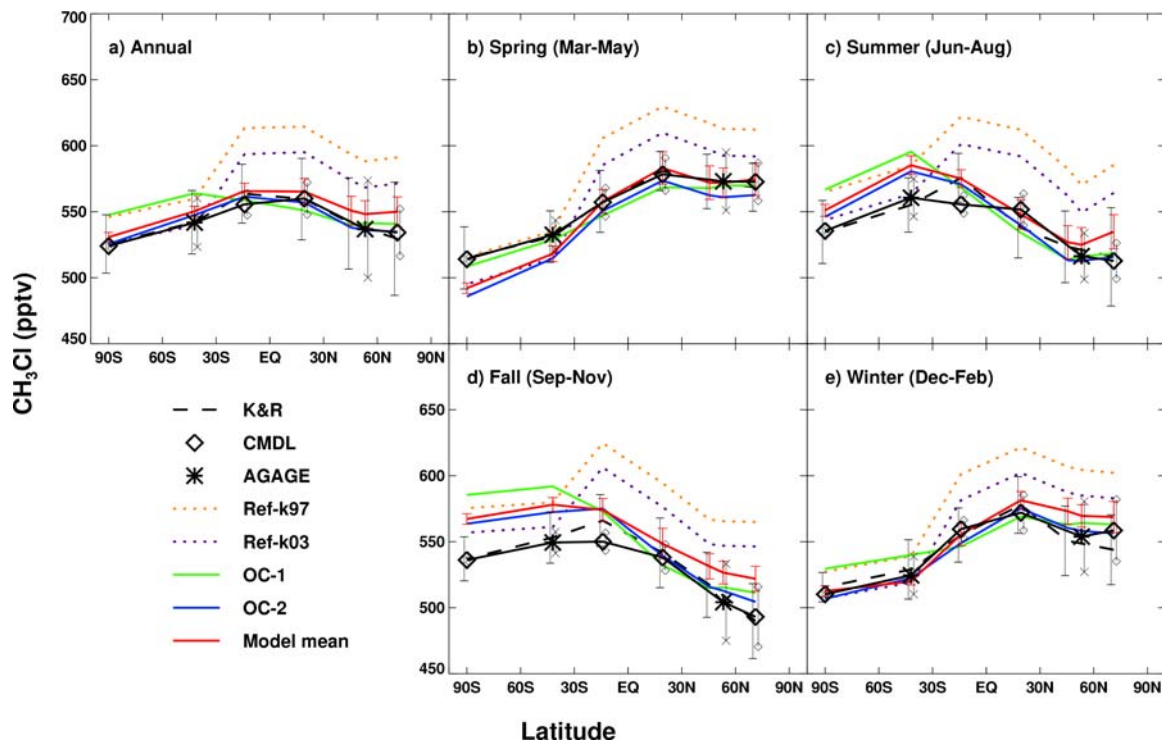


Figure 2.6 Latitudinal distributions of observed and simulated CH_3Cl at the surface sites. Line symbols are the same as Figure 2.5.

overestimates the observations in the tropics and northern higher latitudes. A possible reason for the higher concentrations in the NH for the run Ref-k03 is that the biomass burning emissions are biased towards the NH. The estimated NH/SH ratio of biomass burning emissions by *Lobert et al.* [1999] is about 2.2; whereas we calculated a ratio of 1.6 based on scaling to the biomass burning CO inventory [*Duncan et al.*, 2003]. *Lee-Taylor et al.* [2001] mentioned that they reduced the biomass burning CH₃Cl flux from southern and eastern Asia by half in order to reduce the interhemispheric gradient in their model results. The overestimates of Ref-k03 at low latitudes could be explained by the distribution of the isoprene-scaled biogenic emissions, which are biased toward equatorial regions (Figure 2.2).

The difference between OC-1 and OC-2 runs shows the effect of oceanic sink on surface concentrations. These two runs have almost the same net oceanic emissions, but OC-2 has more than four-times the oceanic sink over the net uptake regions than OC-1. Since the SH has more oceanic area than the NH, the concentrations of CH₃Cl are more sensitive to ocean uptake in the SH than the NH. The OC-1 run shows a south-north gradient while OC-2 shows a symmetrical distribution as observed (Figure 2.6-a). However, the simulated seasonal variations in OC-2 and for other years (“model mean”) are much higher than the observations. It largely reflects the small seasonal variation in the ocean uptake at southern high latitudes, which is $\pm 2 \text{ Gg yr}^{-1}$ as compared to $\pm 100 \text{ Gg yr}^{-1}$ driven by the seasonality of the OH chemistry. The physical parameterization is based on wind speed and SST [*Khalil et al.*, 1999]. *Khalil et al.* [1999] mentioned that this proxy calculation represented the flux for warm waters well, but not the uptake in cold waters. *Tokarczyk et al.* [2003] reported that the CH₃Cl degradation rate constants

have no clear SST dependence. Further investigation is needed to understand the mechanisms controlling the seasonality of ocean uptake.

2.5.2. Vertical profiles of atmospheric CH_3Cl

Figure 2.7 shows the vertical distributions of CH_3Cl from aircraft measurements and our model for regions shown in Figure 2.4. Model results are taken from simulations with assimilated meteorology for the same period as the observations except for PEM-Tropic B and INDOEX, for which the GMAO assimilated meteorological data for GEOS-Chem are unavailable. For these two missions, we use the average of 7-year runs for 1991, 1992, 1994, 1995, Sep1996–Aug1997, 2000 and 2001. The OC-2 oceanic sink of uptake regions is applied. The contribution for individual sources is shown. We discuss the results by geographical region.

2.5.2.1 Tropical Pacific (PEM-Tropics A and B)

The PEM-Tropics A took place over the remote South Pacific Ocean between August 24 and October 6, 1996. The observations of CH_3Cl show little variation with altitude except over the eastern Pacific region (ep) (Figures 2.7-1 – 2.7-4). Over this region, the observations show elevated concentrations at about 2–4 km, which reflects the easterly outflow of air masses from South America that were strongly influenced by biomass burning emissions [Blake *et al.*, 1999a]. The model closely reproduces the observations for Fiji (fj) although it overestimates for the eastern Pacific region (ep) especially near the surface, where concentrations are over-predicted due to biogenic CH_3Cl emissions from tropical rain forests in our model (Figure 2.7-4). For Hawaii (hwi),

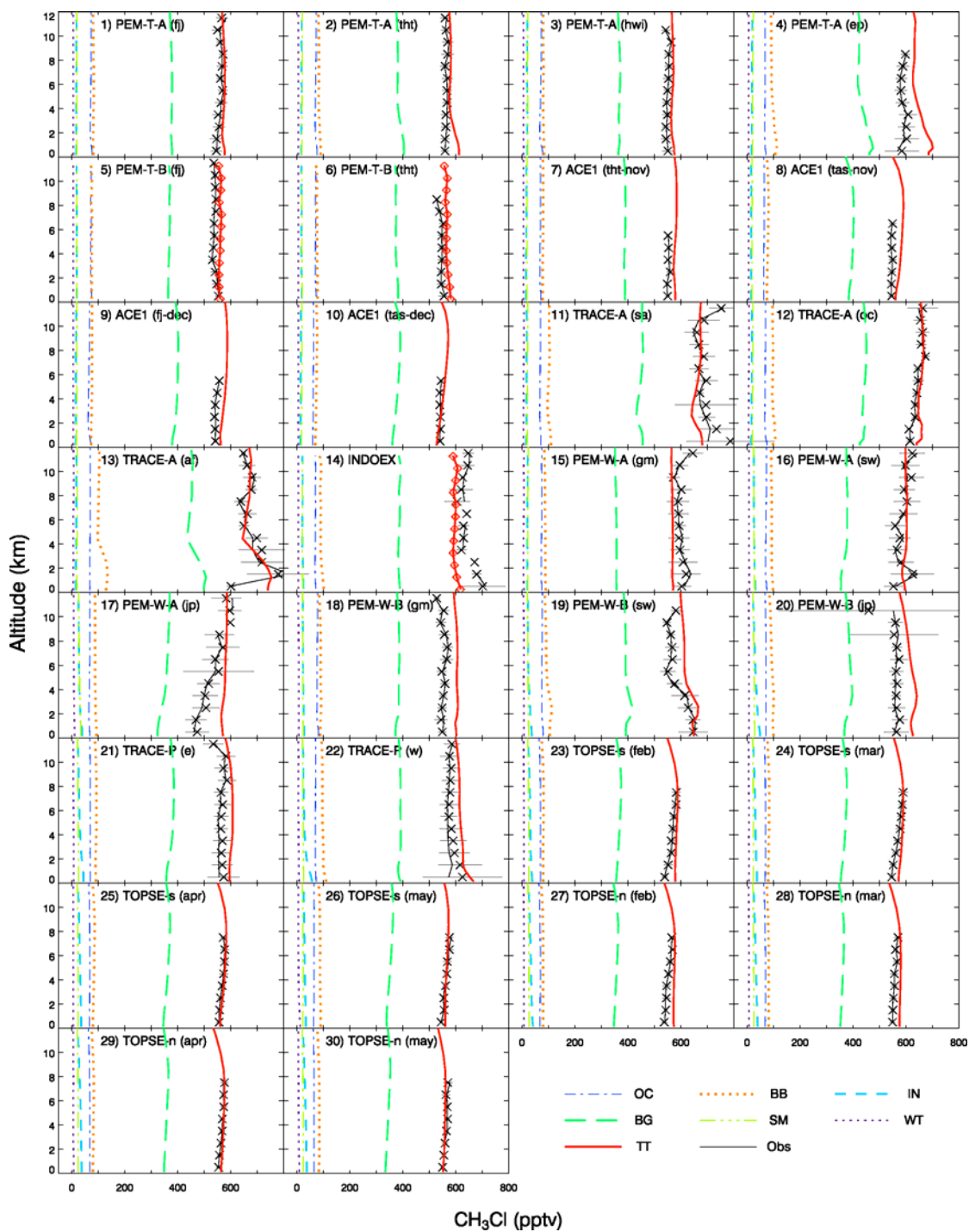


Figure 2.7 Vertical profiles of CH_3Cl averaged over the aircraft observation regions shown in Figure 2.4. For the TOPSE experiment, monthly mean values from February to May are calculated. Please see the text for abbreviation for each project region. Thin solid lines indicate the medians of observations, crosses indicate the means of observations, and thin horizontal lines indicate the observed standard deviations. Diamonds indicate the means of the six model runs. For model results, contributions from each source as well as all sources are shown. OC, BB, IN, BG, SM, WT, and TT denote ocean, biomass burning, incineration/industrial, biogenic, salt marshes, wetlands, and total, respectively.

the model concentrations are higher than the observations by ~30 pptv for all altitudes.

Measurements during the PEM-Tropics B mission were taken over the tropical Pacific in March and early April 1999. Observed and simulated values are compared for Fiji (fj) and Tahiti (tht) regions (Figure 2.7-5, 2.7-6). The model simulations generally show slight overestimates. *Blake et al.* [2001] reported that CH₃Cl concentrations observed in PEM-Tropics A were higher than observed in PEM-Tropics B south of 10°S because of significant biomass burning emissions during PEM-Tropics A in the tropical dry season. In Figures 2.7-1 – 2.7-6, however, this trend is not obvious in regional profiles because we average the concentrations over larger areas as shown in Figure 2.4. The latitude-altitude plots discussed in section 2.5.3 (Figures 2.8-1, 2.8-2, 2.8-5 and 2.8-6) show this trend.

2.5.2.2 Tropical Pacific and Southern Oceans (ACE 1)

The ACE 1 mission was conducted over the Pacific and Southern Oceans during November and December 1995. Slight positive vertical gradients of CH₃Cl were observed for samples taken over the four regions shown in Figure 2.4 (Figures 2.7-7 – 2.7-10). *Blake et al.* [1999b] explained the vertical trend could be derived from the long range transport of air containing high biomass burning CH₃Cl. Our model results overestimate the concentrations for all regions except the Tasmania-December region (tas-dec). Simulated CH₃Cl also shows greater vertical gradients for all regions except for the Tahiti-November region (tht-nov). The overestimates of the vertical gradient in the model are mainly due to our pseudo-biogenic CH₃Cl rather than biomass burning CH₃Cl.

2.5.2.3 Tropical Atlantic (TRACE-A)

The TRACE-A mission, in September–October 1992, focused on investigating the effects of biomass burning over the South Atlantic, South America, and southern Africa. The observed enhancements of CH_3Cl in the boundary layer (at 0–2 km) over Brazil/South America (sa) and southern Africa (af) (Figures 2.7-11 and 2.7-13) indicate the regional biomass burning effects [Blake *et al.*, 1996]. Over South America, another maximum was observed above 10 km. Analyzing samples collected at high altitude and the boundary layer, Blake *et al.* [1996] concluded that biomass burning over Brazil and frequent deep convection within and downwind of the fires could explain the enhanced concentrations in the upper troposphere. The model reproduces the maxima in the boundary layer observed over South America and southern Africa, while it underestimates the magnitudes. In addition to the biomass burning source suggested by Blake *et al.* [1996], our model indicates that our added biogenic source contributes significantly to the boundary layer enhancement (Figures 2.7-11 and 2.7-13). The biomass burning source of CH_3Cl is often deduced by the enhancement ratio of CH_3Cl to CO on the basis of field measurements. Our model results suggest that such deduced biomass burning source of CH_3Cl could be overestimated if the biogenic contribution to the observed CH_3Cl to CO enhancements ratios is not properly accounted for.

The model does not reproduce the observed high concentrations in the upper troposphere over South America (Figure 2.7-11). However, no such large enhancement is evident over the tropical South Atlantic (Figure 2.7-12) or Africa (Figure 2.7-13). The convective enhancement at 12 km may therefore reflect the biased sampling of specific convective plumes by the DC-8 aircraft, which would not be reflected in the simulated

monthly mean concentrations. Over the South Atlantic (oc) (Figure 2.7-12), the vertical profile of measured CH₃Cl concentrations shows slight increases with altitude and the model matches relatively well with the observations except at 0–2 km, where combined biogenic and biomass burning CH₃Cl concentrations result in a maximum that was not present in the observations.

2.5.2.4 Indian Ocean (INDOEX)

During the INDOEX campaign air samples were collected over the northern Indian Ocean in February–March 1999. Enhanced concentrations of CH₃Cl and other combustion tracers such as CO, hydrocarbons, and CH₃CN were observed in the outflow from India and Southeast Asia, indicating that extensive biofuel emissions in those areas contributed to the high CH₃Cl levels [Scheeren *et al.*, 2002]. The model underestimates the observations at all altitudes (Figure 2.7-14). Based on the INDOEX observations, Scheeren *et al.* [2002] reported a CH₃Cl/CO molar emission ratio of 1.74×10^{-3} for the biofuel emissions, which is about three times larger than that of 0.57×10^{-3} [Lobert *et al.*, 1999] used in our model. Increasing the biofuel CH₃Cl/CO molar ratio to 1.74×10^{-3} led to an increase of 50 pptv in India and Southeast Asia, resulting in a better agreement with the observations (not shown).

2.5.2.5 Western Pacific (PEM-West A and B, TRACE-P)

The PEM-West A mission was conducted in September and October 1991 over the western Pacific. During the PEM-West B mission, air samples were collected from February to March 1994. One major feature in the vertical profiles of CH₃Cl during

PEM-West A (Figure 2.7-15 – 2.7-17) is the enhanced concentrations observed at high altitude (above 10 km), which reflect transport of CH₃Cl by typhoons [*Blake et al.*, 1997; *Kondo et al.*, 1997; *Newell et al.*, 1996]. The model results show little vertical variation and did not reproduce those elevated concentrations. Higher CH₃Cl mixing ratios observed below 6 km during PEM-West B than PEM-West A in the southwest (sw) region (Figures 2.7-16 and 2.7-19) could be explained by stronger westerly outflow from the Asian continent in winter than in fall [*Blake et al.*, 1997; *Kondo et al.*, 1997]. During PEM-West B, little vertical variations were observed over Guam (gm) and Japan (jp) (Figures 2.7-18 and 2.7-20), reflecting small influence from the continental outflow while over the southwest (sw) region, CH₃Cl concentrations are higher at 0–5 km (Figure 2.7-19). Our model tends to overestimate the observations possibly as the result of its tendency to transport too much biogenic CH₃Cl from low latitudes. In the southwestern region, simulated concentrations show some enhancements at low altitude (~3 km), which are due to biogenic and biomass burning emissions (Figure 2.7-19).

The measurements during TRACE-P were obtained over the northwestern Pacific between February and April 2001. During this mission, a strong influence of Asian outflow was detected, which also characterized the main feature of the PEM-West B observations [*Jacob et al.*, 2003]. TRACE-P observations indicate significant effects of biomass burning emissions at high altitudes [*Liu et al.*, 2003; *Russo et al.*, 2003]. In the eastern region of TRACE-P (e), our model results show higher concentrations at middle altitudes than observed; the model bulge is largely attributed to the biogenic source (Figure 2.7-21). In the western region (w), both the model and observed (mean) values are higher in the boundary layer and decrease with altitude, reflecting higher

concentrations of incineration/industrial and biomass burning sources near the surface (Figure 2.7-22). The simulated CH_3Cl concentrations from the biosphere appear to be overestimated. We will examine the potential causes of the overestimates in the next section.

2.5.2.6 North America (TOPSE)

The TOPSE experiment was carried out during February to May 2000 at mid to high latitudes over North America. Figures 2.7-23 – 2.7-30 show monthly mean observed and simulated vertical profiles for northern and southern TOPSE regions in Figure 2.4. Slight positive vertical gradients were observed throughout the measurement period. The largest vertical gradients were observed at mid latitudes in February and March (Figures 2.7-23 and 2.7-24). Our model closely reproduces the observed concentrations in general. However, it does not reproduce the higher vertical gradients in February and March due to the overestimated emissions near the surface. The positive vertical gradients are largely attributed by the model to biogenic CH_3Cl transported from the tropics.

2.5.3 Latitude-altitude distribution of atmospheric CH_3Cl

Latitude-altitude cross sections of observed and simulated CH_3Cl concentrations for selected aircraft field experiments are compared in Figure 2.8. Figure 2.9 illustrates the relative difference between observed and simulated values. During PEM-Tropics A, a slight north-south gradient was observed over the Tahiti region; the concentrations south of 10°S are higher by about 20 pptv than in the northern section. Our model simulates the observations well for the southern section, where the difference is within $\pm 5\%$, but

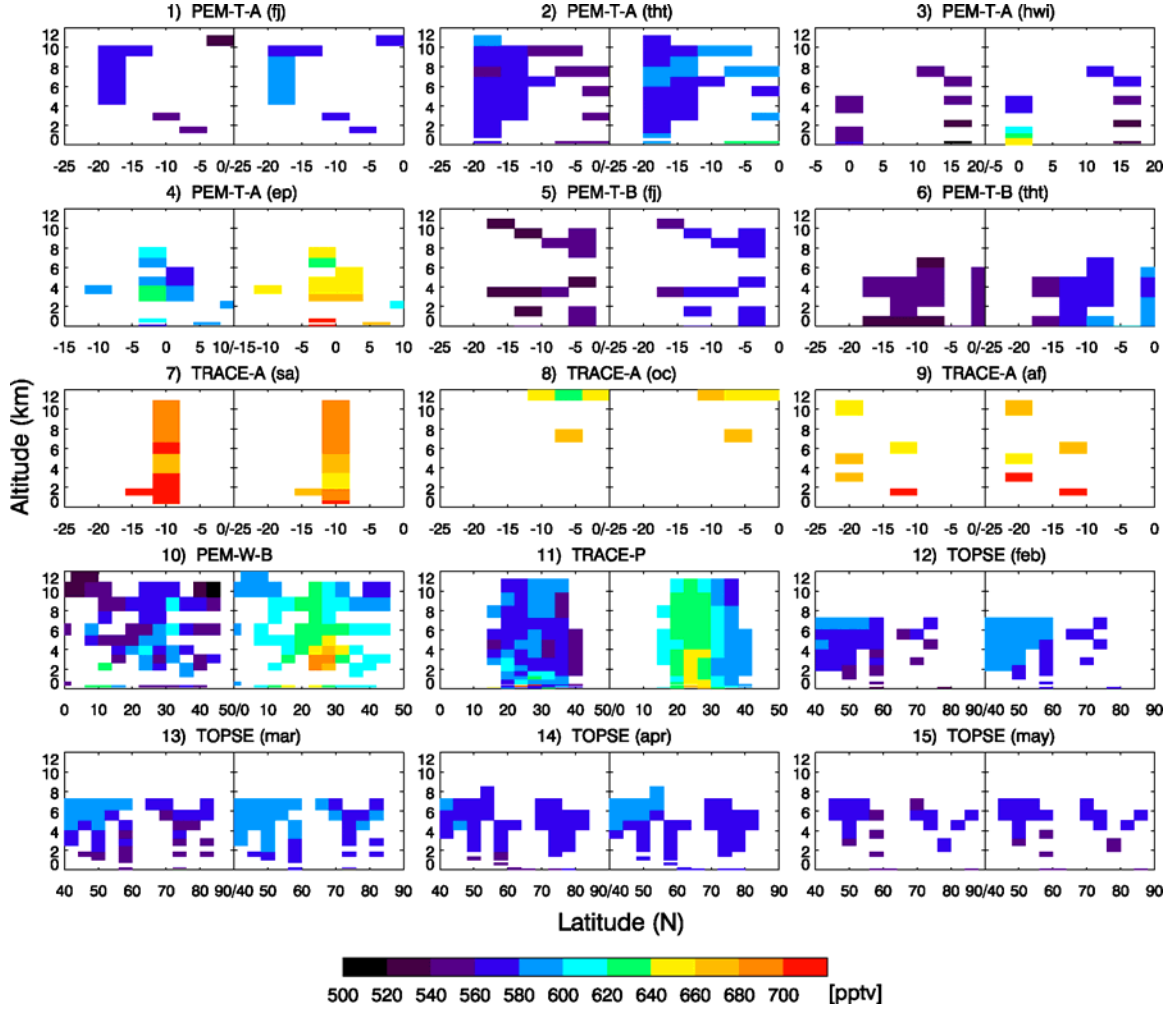


Figure 2.8 Observed and simulated latitude-altitude distributions for selected aircraft observation regions shown in Figure 2.4. For TRACE-P and TOPSE, the western/eastern and the northern/southern regions are combined, respectively. Abbreviations are the same as used in Figure 2.7 Only grid boxes with > 10 observation points are shown.

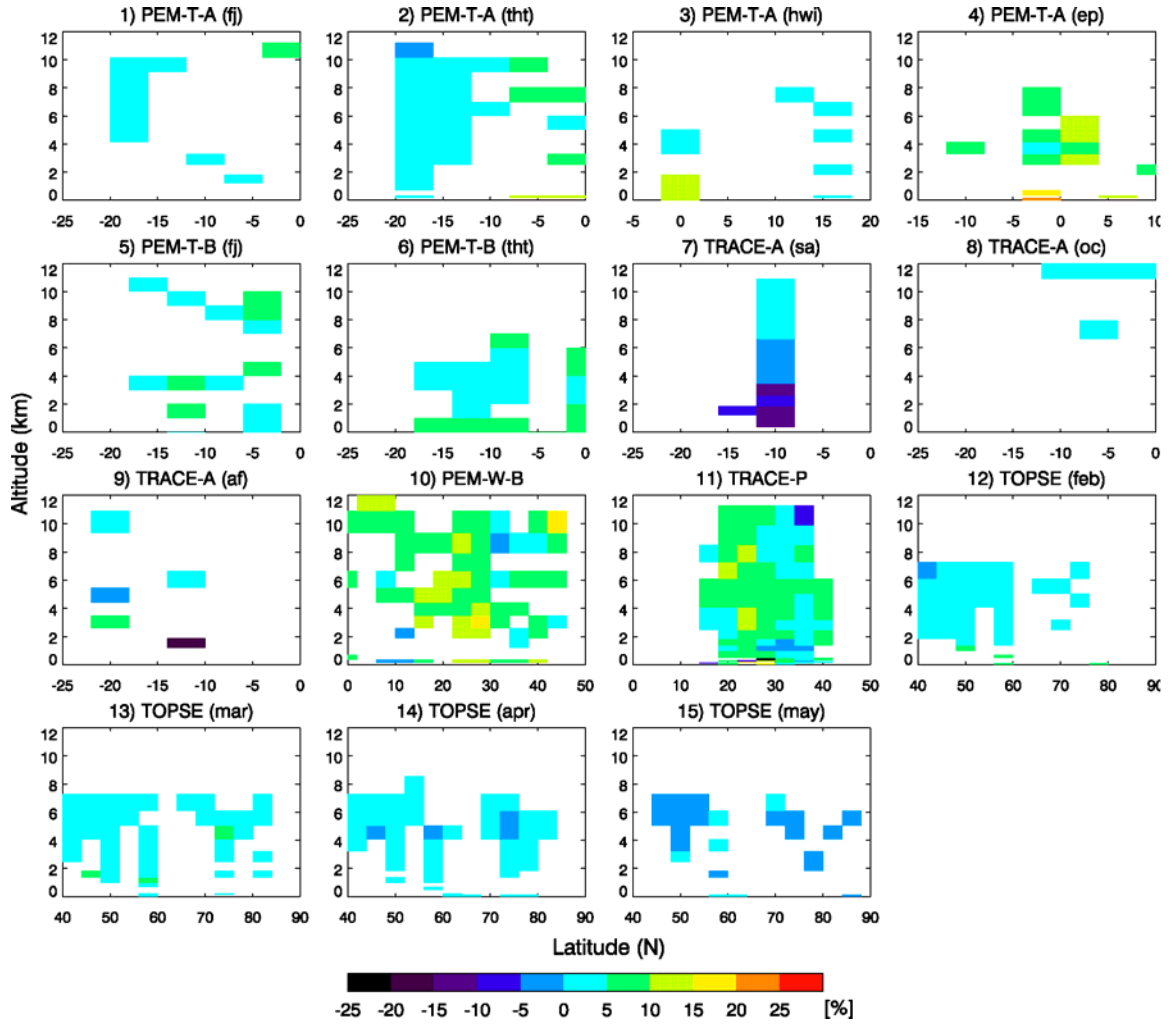


Figure 2.9 Same as Figure 2.8 but for the relative difference computed as (model-observation)/model.

overestimates by 5 to 15% in the northern section (Figures 2.8-2 and 2.9-2). Simulated surface concentrations are too high due to the westward transport of model biogenic and biomass burning CH_3Cl from Central and South America. Unfortunately, there are not enough data points to see the latitudinal variability for the other three PEM-Tropics A regions, though Figures 2.9-2 – 2.9-4 show that the model tends to overestimate the concentrations close to the equator near the surface, resulting mainly from the strong outflow of biogenic CH_3Cl mentioned above.

During PEM-Tropics B, the concentration gradient observed over the Fiji region is opposite of that during PEM-Tropics A (Figure 2.8-5). The model captures the trend although it overestimates the concentrations by ~10% for some locations (Figure 2.9-5). The simulated latitudinal gradient is due to the combination of biomass burning and biogenic CH_3Cl gradients in the model. There are not enough data points to investigate the spatial variability for TRACE-A.

During PEM-West B, the model overestimates the observations by 5 to 20% in most regions (Figure 2.9-10). A few “hot spots” (670–750 pptv) were observed in the lower troposphere around 10°N that could be attributed to biomass burning plumes [Blake *et al.*, 1997]; they are shifted to the northern latitudes in the model results (Figure 2.8-10). After investigating the correlation of CH_3Cl with CO during PEM-West B, Blake *et al.* [1997] concluded that at latitudes north of 25°N, no significant amount of CH_3Cl is emitted from urban/industrial sources or from other high-latitude continental sources and that the enhanced concentrations observed at low latitudes (<25°N) could result from the continental biomass burning outflow. The high concentrations simulated in the model near 25°N are due to biomass burning and biogenic emissions.

Figure 2.8-11 shows a comparison of observed and simulated spatial variability for the TRACE-P experiment. The enhanced concentrations observed in the boundary layer north of 25°N were due to fossil fuel/biofuel combustion effluent from China. During TRACE-P, transport of biomass burning effluents from Southeast Asia was limited to high altitudes south of 35°N [Blake *et al.*, 2003b; Liu *et al.*, 2003]. The model reproduces the general trend, but shows a more distinct latitudinal gradient. The model overestimates the observations at 20°–30°N by 5–15% as a result of strong model transport of biogenic CH₃Cl descending from the upper troposphere (Figure 2.9-11). This strong subsidence persists at the same location, even when the biogenic emissions are restricted to 10°S to 10°N in the model (results not shown), indicating stronger influence of transport from the tropics on mid-latitude CH₃Cl concentrations in the model than is apparent from the observations. Simulated concentrations at 0–2 km north of 30°N are lower by <5% than the observed values. Considering the strong boundary layer Asian outflow at 30°–45°N during TRACE-P [Liu *et al.*, 2003], incineration/industrial and/or biofuel emissions in our model could be underestimated.

Figures 2.9-12 – 2.9-15 show the difference between the observations and model simulations for the TOPSE experiment. The model closely reproduces the observations. Spatial variations and their seasonal evolution of CH₃Cl concentrations are shown in Figures 2.8-12 – 2.8-15. Higher concentrations were observed in the middle troposphere at lower latitudes (<60°N). The latitudinal/altitudinal concentration gradient decreases with season reflecting the reduction of CH₃Cl transport from the tropical regions. The model reproduces the seasonal trend properly. The higher concentrations in the middle

troposphere might be explained by CH₃Cl transport from biomass burning and biogenic sources from the tropics and Southeast Asia.

2.6 Conclusions

We apply a global 3-D chemical transport model, GEOS-Chem, to simulate the global distributions of CH₃Cl. The model simulations are constrained by surface and aircraft observations to define better the characteristics of the required pseudo-biogenic source of atmospheric CH₃Cl that we added to the model and to examine the observational constraints on the other better-known sources. Contributions from the pseudo-biogenic, oceanic, biomass burning, incineration/industrial, salt marsh and wetland sources are quantified through tagged-tracer simulations. Their effects on seasonal variations, latitudinal trends, and regional vertical profiles of CH₃Cl are investigated.

We find that a pseudo-biogenic source of 2.9 Tg yr⁻¹ (66% of the total source) is necessary to explain the observed CH₃Cl concentrations. The large decrease of CH₃Cl from summer to winter at northern mid latitudes implies a negligible biogenic source of CH₃Cl at mid latitudes. We therefore constrain the pseudo-biogenic emissions to 30°S–30°N. Furthermore, we find that scaling the pseudo-biogenic emission to that of isoprene [e.g., *Lee-Taylor et al.*, 2001] leads to an underestimate of the seasonal CH₃Cl variation at northern mid latitudes and tends to concentrate CH₃Cl to a few tropical and subtropical ecosystems resulting in overestimates of aircraft observations downwind from these regions. We assume that tropical and subtropical ecosystems have the same aseasonal

emission rate, which gives better simulations of the observations than scaling the emissions to those of isoprene.

Our model mean annual CH_3Cl oceanic flux over the net emission regions is 510 Gg yr^{-1} , 37% smaller than the RCEI inventory [Khalil *et al.* 1999]. The calculated total oceanic sink over the uptake regions is about 30 Gg yr^{-1} , which is about one fifth of the RCEI inventory [Khalil *et al.*, 1999]. Increasing the oceanic sink over the uptake regions to 150 Gg yr^{-1} , which is the same as in the RCEI inventory, results in the model reproducing well the observed annual-mean latitudinal gradient of CH_3Cl . Our model overestimates the seasonal variation of CH_3Cl at southern mid and high latitudes, implying an underestimate of the seasonal variation of ocean uptake calculated based on SST and wind speed.

Our calculated CH_3Cl emission from the biomass/biofuel burning source using a molar $\text{CH}_3\text{Cl}/\text{CO}$ emission ratio of 5.7×10^{-4} is 610 Gg yr^{-1} , which is about two thirds of that given in RCEI inventory [Lobert *et al.*, 1999]. Our lower biomass burning CH_3Cl emissions yield better agreement with the observed symmetrical annual-mean latitudinal CH_3Cl gradient, while the model results using biomass burning source data from the RCEI inventory show a clear bias towards overestimates in the northern hemisphere.

Our estimated total emission of CH_3Cl from six sources including our 2.9 Tg yr^{-1} pseudo-biogenic source and the other identified sources such as biomass/biofuel burning, ocean, incineration/industry, salt marshes, and wetlands in the model is approximately 4.4 Tg yr^{-1} . The calculated atmospheric burden of CH_3Cl is about 5.0 Tg and the estimated tropospheric lifetime of CH_3Cl against OH oxidation is about 1.2 years. The interhemispheric symmetry in the latitudinal distribution of CH_3Cl and a dominant

tropical/subtropical pseudo-biogenic source imply that the annual hemispheric mean OH ratio is constrained to the range of 0.8–1.3.

A major shortfall in our current understanding of CH₃Cl emissions is the geographical distributions of the biogenic and biomass burning sources. This uncertainty is reflected clearly in the model comparison with aircraft observations. The model simulates generally well vertical profiles of CH₃Cl in most regions especially for high latitudes, where there is little local emission, while the model tends to overestimate or underestimate the observations near biogenic and biomass burning sources, reflecting the uncertainties in those source distributions. The model overestimates the observations over the western Pacific due to the simulated influx of biogenic CH₃Cl associated with the strong subsidence at 20°–30°N. It is noteworthy that the model suggests the dominant source of CH₃Cl in the region is biogenic, while previous studies focused mostly on biomass burning emissions [e.g., *Blake et al.*, 1997; *Liu et al.*, 2003; *Russo et al.*, 2003]. Biomass burning emission sources are likely overestimated in those studies although large uncertainty of the estimated biogenic CH₃Cl source needs to be considered. The comparison over the tropical regions suggests that the model biogenic sources in Central and South America might be overestimated. The estimates of CH₃Cl over India and Southeast Asia suggest that the CH₃Cl/CO molar emission ratio in this region is higher than the value we used in the model. Applying a single CH₃Cl/CO emission ratio to the globe is too simplistic since the CH₃Cl emission rate depends on the fuel type and the burning conditions [*Lobert et al.*, 1999]. The estimated incineration/industrial or biofuel emissions near the coast of China might be underestimated.

CHAPTER III

INVERSE MODELING OF THE GLOBAL METHYL CHLORIDE SOURCES

3.1 Introduction

Methyl chloride (CH_3Cl) is one of the most abundant chlorine-containing gases in the atmosphere and a major contributor to the stratospheric chlorine loading. The global average mixing ratio of CH_3Cl in the troposphere is measured at about 550 ± 30 parts per trillion per volume (pptv); a major concern about this species is the imbalance of its budget, i.e., known sinks are much larger than known sources [e.g., *Montzka et al.*, 2003].

According to the emission data provided in the Reactive Chlorine Emissions Inventory (RCEI) conducted under the International Global Atmospheric Chemistry (IGAC) Global Emissions Inventory Activity (GEIA) project, the estimated emissions from known sources such as biomass burning, oceans, incineration/industrial sources are 910 (650–1120), 650 (40–950), and 162 (30–294) Gg (giga gram = 10^9 gram) yr^{-1} , respectively [*Keene et al.*, 1999; *Khalil et al.*, 1999; *Lobert et al.*, 1999; *McCulloch et al.*, 1999] (the numbers are best estimates with full ranges in the parenthesis). Emission from certain wood-rotting fungi is estimated as 156 (35–385) Gg yr^{-1} , though no global distribution is currently available [*Watling and Harper*, 1998; *Khalil et al.*, 1999; *Lee-Taylor et al.*, 2001]. In addition, *Rhew et al.* [2000] estimated annual global release of 170 (65–440) Gg of CH_3Cl from salt marshes and *Varner et al.* [1999] calculated a global flux of 48 Gg yr^{-1} from wetlands.

The major removal process of CH₃Cl in the atmosphere is due to oxidation by OH radicals, which accounts for a 3.5 (2.8–4.6) Tg (tera gram = 10¹² gram) loss per year [Koppmann *et al.*, 1993]. It is estimated that about 285 Gg of tropospheric CH₃Cl is transported to the stratosphere and lost there by photo dissociation and OH oxidation. Although the ocean is a net source globally, it is a significant net local sink in high-latitude regions. The RCEI estimate for the oceanic sink over the net uptake regions is 150 Gg yr⁻¹ [Moore *et al.*, 1996; Khalil *et al.*, 1999; Keene *et al.*, 1999]. Soil is recognized as an additional sink, and Keene *et al.* [1999] estimated that it could be as much as 256 Gg yr⁻¹, but the uncertainty is quite high [Lee-Taylor *et al.*, 2001; Rhew *et al.* 2001]. The CH₃Cl budget based on the current “best guess” estimates given above leaves a substantial source deficit of ~1.8 Tg yr⁻¹.

There is experimental and modeling evidence that the missing source is biogenic in origin. Enhancements of CH₃Cl that are correlated with a shorted-lived biogenic tracer (α -pinene) were measured by Yokouchi *et al.* [2000]. Yokouchi *et al.* [2002] found strong emissions of CH₃Cl from tropical plants, although the biological processes responsible for the emissions from terrestrial vegetation are unknown [Keene *et al.*, 1999; Yokouchi *et al.*, 2000; Yokouchi *et al.*, 2002].

Khalil and Rasmussen [1999] suggested that 85% of the emission of CH₃Cl comes from tropical and subtropical regions based on their inverse modeling results with simplified box models for tropospheric transport and OH oxidation. Hamilton *et al.* [2003] estimated a global annual CH₃Cl production of 75–2500 Gg between 30°N and 30°S based on their CH₃Cl flux observations from senescent and dead leaves. In a global 3-D model simulation of CH₃Cl, Lee-Taylor *et al.* [2001] found that a biogenic source of

2330–2430 Gg yr⁻¹ is necessary for the model to reproduce surface observations of CH₃Cl.

We also conducted and evaluated global 3-D model simulations of CH₃Cl with aircraft in situ measurements taken in field experiments from 1991 to 2001 as well as surface site measurements [Yoshida *et al.*, 2004]. As in the work by Lee-Taylor *et al.* [2001], we included a large biogenic source of 2900 Gg yr⁻¹ in order to explain the observed CH₃Cl distributions. The source is limited to the region between 30°S–30°N in order to reproduce the observed seasonal and latitudinal variations in the model. We assume that the source is aseasonal because no a priori information is currently available to specify temporal variability of the source in the model. One of the major problems in the model simulations is the overestimate of the seasonal variation of CH₃Cl at southern mid and high latitudes.

We explore in this work a different approach (from Yoshida *et al.* [2004]) to analyze the surface and aircraft observations. The question we pose is to what extent the seasonal and geographical dependence of the biogenic and other sources can be constrained by the available observations. We apply a Bayesian least-squares method to derive the CH₃Cl sources on the basis of the measurements from 7 surface sites and 8 aircraft field experiments. The “bottom-up” inventories by Yoshida *et al.* [2004] are used as a priori. By inspecting the Jacobian matrix and inversion results, we examine the number of emission parameters that can be constrained and compare the constraints by the surface measurements to those by aircraft measurements.

3.2 Methods

3.2.1 Observations

The observations of CH₃Cl from 7 surface stations and 8 aircraft missions are used in this study. Table 3.1 summarizes these measurements. The locations of the surface measurement sites and aircraft observation regions are shown in Figure 3.1. There are two measurement datasets for Alaska, Hawaii, Samoa, Tasmania and Antarctica. Both are used in the inversion. For aircraft observations, the experiment regions are divided into 23 smaller regions [Yoshida *et al.*, 2004]. We calculate monthly mean concentrations for each dataset for model evaluation and inversion calculation. In order to compare the constraints on the CH₃Cl sources by surface measurements with those by aircraft measurements, inverse modeling is conducted using three datasets, (1) data from station observations only, (2) data from aircraft experiments only, and (3) data from both station and aircraft experiments.

3.2.2 Forward Model

3.2.2.1 Model description

The model used in this study is the GEOS-Chem (version 5.02) global 3-D chemical transport model (CTM) of tropospheric chemistry driven by assimilated meteorological fields from the Goddard Earth Observing System (GEOS) of the NASA Global Modeling and Assimilation Office (GMAO) (<http://www-as.harvard.edu/chemistry/trop/geos/>) [Bey *et al.*, 2001]. We use a horizontal resolution of 4° latitude × 5° longitude and 26 vertical levels. We simulate the CH₃Cl distributions

Table 3.1 Atmospheric measurements of CH₃Cl.

| | Region | Time period | Reference |
|--------------------------|---|--|--|
| <i>Surface sites</i> | | | |
| K & R | Alaska (71.2N, 156.5W) Oregon (45.5N, 124W) Hawaii (19.3N, 154.5W) Samoa (14.1S, 170.6W) Tasmania (42S, 145E) Antarctica (90S) | 1981-1997 | <i>Khalil and Rasmussen</i> [1999] |
| NOAA-CMDL | Alaska (71.3N, 156.6W) Hawaii (19.5N, 155.6W) Samoa (14.2S, 170.6W) Antarctica (90.0S, 102.0E) | Jan 1998-Mar 2002 Dec 1999-Feb 2002 Dec 1998-Feb 2003 Jan 2001-Nov 2003 | G. Dutton (personal communication, 2004) |
| AGAGE | Ireland (53.2N, 9.5W) Tasmania (40.4S, 144.4E) | 1998-2001 | <i>Simmonds et al.</i> [2004] |
| <i>Aircraft missions</i> | | | |
| PEM-Tropics A | Tropical Pacific | Aug-Oct 1996 | <i>Blake et al.</i> [1999a] |
| PEM-Tropics B | Tropical Pacific | Mar-Apr 1999 | <i>Blake et al.</i> [2001] |
| ACE 1 | Pacific/Southern Ocean | Nov-Dec 1995 | <i>Blake et al.</i> [1999b] |
| TRACE-A | Tropical Atlantic | Sep-Oct 1992 | <i>Blake et al.</i> [1996] |
| PEM-West A | Western Pacific | Sep-Oct 1991 | <i>Blake et al.</i> [1997] |
| PEM-West B | Western Pacific | Feb-Mar 1994 | <i>Blake et al.</i> [1997] |
| TRACE-P | Western Pacific | Feb-Apr 2001 | <i>Blake et al.</i> [2003b] |
| TOPSE | North America | Feb-May 2000 | <i>Blake et al.</i> [2003a] |

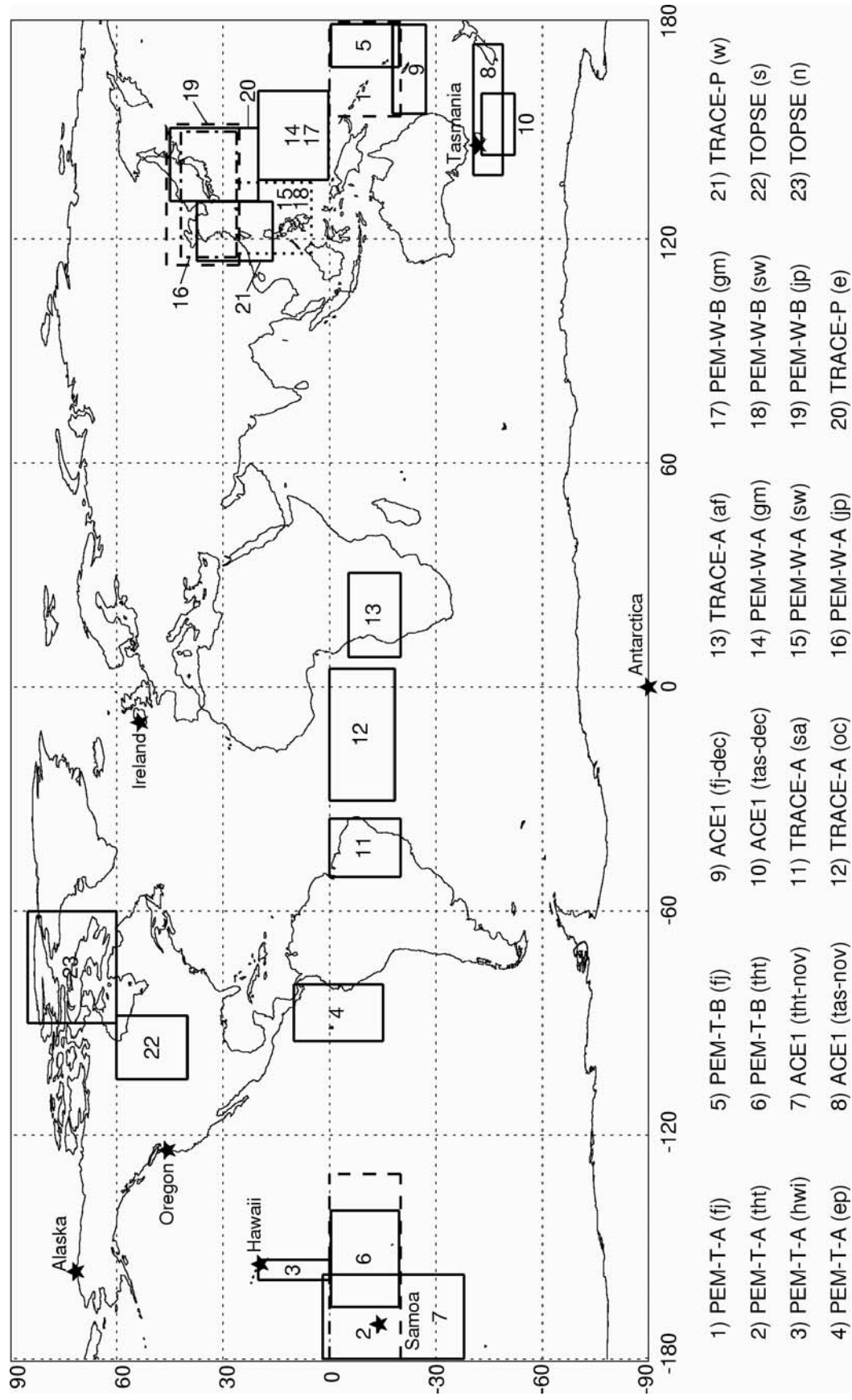


Figure 3.1 Surface measurement sites (indicated by symbols) and aircraft observation regions. The measurements are listed in Table 3.1.

using meteorological fields for August 1996 – September 1997 (GEOS-STRAT). In our previous work [Yoshida *et al.*, 2004], we used the assimilated meteorology for different years and found that the resulting difference in CH₃Cl distributions is relatively small. This uncertainty is now accounted for as part of the model transport error (section 3.2.3.3). CH₃Cl increase (decrease) by a source (sink) is “tagged” by a different tracer. In this manner, the contribution from a source or sink to the spatial and temporal CH₃Cl distributions can be evaluated in the model. The sink by OH oxidation is not treated as a separate tracer; the uncertainties of the OH field and reaction rate constant are taken into account as part of the model error (section 3.2.3.3).

3.2.2.2 Sources and sinks of CH₃Cl

Our a priori sources of CH₃Cl are taken from the best estimates by Yoshida *et al.* [2004]. Table 3.2 summarizes the annual emissions and the sinks. We briefly describe here the sources and sinks. More detailed discussion can be found in the previous work [Yoshida *et al.*, 2004 and references therein].

We distribute the biogenic source of 2900 Gg yr⁻¹ to all vegetated areas between 30°N and 30°S with a flat aseasonal emission rate [Yoshida *et al.*, 2004]. We compute biomass burning CH₃Cl emissions using a CH₃Cl/CO molar emission ratio [Lobert *et al.*, 1999] with the 7-year mean of the GEOS-Chem biomass and biofuel burning CO emissions between 1991 and 2001 [Duncan *et al.*, 2003; Heald *et al.*, 2003]. The resulting annual total biomass burning CH₃Cl emission is about 610 Gg yr⁻¹, which is at the lower limit calculated by Lobert *et al.* [1999].

Table 3.2 (continued).

| | | A priori flux (Gg yr ⁻¹) | Reference | 11 parameters | | |
|-------------------|-----------------------|---|-------------------|---|-----------------------------|---------------------------------|
| | | | | A posteriori flux (Gg yr ⁻¹) | A priori uncertainty (%) | A posteriori uncertainty (%) |
| Biogenic | NH spring | 343 ^a | | 406 | 100 | 38 |
| | NH summer | 343 ^a | | 299 | 100 | 55 |
| | NH fall | 340 ^a | | 401 | 100 | 38 |
| | NH winter | 336 ^a | | 162 | 100 | 40 |
| | <i>NH total</i> | 1362 ^a | | 1268 | | |
| | SH fall | 388 ^a | | 399 | 100 | 32 |
| | SH winter | 388 ^a | | 127 | 100 | 42 |
| Biomass | SH spring | 383 ^a | | 395 | 100 | 32 |
| | SH summer | 379 ^a | | 320 | 100 | 39 |
| | <i>SH total</i> | 1538 ^a | | 1241 | | |
| | <i>Global total</i> | 2900 ^a | 2430 ^b | 2509 | | |
| | NH spring | 141 ^{a,b} | | 119 | 70 | 55 |
| | NH other seasons | 244 ^{a,b} | | 162 | 70 | 61 |
| | SH spring | 98 ^{a,b} | | 116 | 70 | 62 |
| Ocean | SH other seasons | 127 ^{a,b} | | 148 | 70 | 62 |
| | <i>Total</i> | 610 ^{a,b} | 910 ^b | 545 | | |
| | Ocean | 507 ^{a,c} | 805 ^c | 806 | 70 | 51 |
| | Incineration/industry | 162 ^d | 162 ^d | 49 | 100 | 56 |
| | Salt marshes | 170 ^e | 170 ^e | 51 | 100 | 56 |
| | Wetlands | 48 ^f | 48 ^f | 14 | 100 | 56 |
| | <i>Total source</i> | 4397 | 4525 | 3974 | | |
| Soil sink | | | | | | |
| | Ocean sink | 149 ^{a,c} | 150 ^c | 45 | 100 | 56 |
| | Soil sink | 256 ^g | 256 ^g | 77 | 100 | 56 |
| | OH sink | 3992 ^a | 3500 ⁱ | 3852 | | |
| <i>Total sink</i> | | 4397 | 3906 | 3974 | | |

- ^a*Yoshida et al. [2004].*
^b*Lobert et al. [1999].*
^c*Khalil et al. [1999].*
^d*McCulloch et al. [1999].*
^e*Rhew et al. [1999].*
^f*Varner et al. [1999].*
^g*Khalil and Rasmussen [1999] and Keene et al. [1999].*
^h*Lee-Taylor et al. [2001].*
ⁱ*Koppmann et al. [1993].*

The oceanic CH₃Cl emissions and sinks are calculated using the National Oceanic and Atmospheric Administration Climate Monitoring and Diagnostics Laboratory (NOAA-CMDL) empirical relationship between saturation and sea surface temperature (SST) and CH₃Cl saturation anomaly [Khalil *et al.*, 1999] with monthly climatological wind speed distributions. Oceanic sink is scaled so that the net oceanic flux is to be ~350 Gg yr⁻¹ [Yoshida *et al.*, 2004].

The tropospheric OH field is taken from the GEOS-Chem full-chemistry simulation by Martin *et al.* [2003] and the stratospheric OH field is taken from a 2-D stratosphere/mesosphere model [Schneider *et al.*, 2000]. Chemical loss of CH₃Cl via OH oxidation is calculated using reaction rate constant reported by Sander *et al.* [2003]. The a priori total CH₃Cl loss by reaction with OH is about 3990 Gg yr⁻¹. The estimated soil sink of 256 Gg yr⁻¹ [Keene *et al.*, 1999; Khalil and Rasmussen, 1999] is distributed based on the work by Shorter *et al.* [1995] for growing seasons.

3.2.3 Inverse Model

3.2.3.1 Inversion methods

A Bayesian least squares method is applied in order to optimize the a priori source strengths and seasonality using the observed atmospheric CH₃Cl concentrations. The observation vector **y** of CH₃Cl measurements can be explained by the state vector **x** of source/sink model parameters by the following equation:

$$\mathbf{y} = \mathbf{K}\mathbf{x} + \varepsilon_{\Sigma}, \quad (3.1)$$

where **K** is the Jacobian matrix, which relates the source parameters to the concentrations, and ε_{Σ} is the total observational error, which includes measurement error, representation

error, and forward model error. The optimal solution for the state vector ($\hat{\mathbf{x}}$) and the a posteriori error covariance matrix ($\hat{\mathbf{S}}$) are:

$$\hat{\mathbf{x}} = \mathbf{x}_a + \mathbf{S}_a \mathbf{K}^T (\mathbf{K} \mathbf{S}_a \mathbf{K}^T + \mathbf{S}_\Sigma)^{-1} (\mathbf{y} - \mathbf{K} \mathbf{x}_a) \quad (3.2)$$

$$\hat{\mathbf{S}} = (\mathbf{K}^T \mathbf{S}_\Sigma^{-1} \mathbf{K} + \mathbf{S}_a^{-1})^{-1}, \quad (3.3)$$

where \mathbf{x}_a is the a priori parameter state vector, \mathbf{S}_a is the a priori parameter error covariance matrix, and \mathbf{S}_Σ is the observation error covariance matrix [Rodgers, 2000]. Detailed explanation of \mathbf{S}_Σ is in Section 3.2.3.3.

We apply equations (3.2) and (3.3) to the data set that contain both station and aircraft observations described in section 3.2.1. In the sensitivity analysis, we also apply station and aircraft data separately in the inversion.

3.2.3.2 Selection of the state vector

Ideally we wish to constrain the geographical and seasonal distributions of all CH_3Cl sources. However, the available measurements usually provide a limited number of degrees of freedom. The independence of the parameters in our state vector is assessed by inspecting the singular values of the error-normalized Jacobian matrix [Rodgers, 2000]:

$$\tilde{\mathbf{K}} = \mathbf{S}_\Sigma^{-1/2} \mathbf{K} \mathbf{S}_a^{1/2} \quad (3.4)$$

The largest a priori sources are biogenic and biomass burning. The constraints on the biogenic sources are most interesting because of a lack of a priori knowledge. We therefore choose 24 emission parameters for this source representing 4 seasons and 6 continents (north and south Americas, north and south Africa, Asia and Oceania). We specify 8 emission parameters for the biomass burning source in 4 seasons and 2

hemispheres. Adding 7 emission parameters for other source, there are a total of 39 emission parameters (Table 3.3) in our initial inversion analysis. The degree of freedom defined by singular values > 1 of the Jacobian matrix is 10; clearly indicating that current available observations do not provide enough constraints on all estimates of emission parameters.

Following the approach by Heald et al. [2004], we then reduce the number of emissions parameters largely by aggregating the continental biogenic emissions to hemispheric ones. The benefit of the approach is that we obtain physically meaningful results compared to the vector mapping method by Rogers [2000]. However, the approach also makes an implicit assumption that the lumped sources have predetermined distributions. The resulting 16 parameters are listed in Table 3.3. The analysis serves two purposes. First, we will investigate the effect of reducing the number of parameters on the inversion results. Second, we examine the singular vectors of $\tilde{\mathbf{K}}$ (Figure 3.2) in order to combine highly correlated emission parameters together. The final 11 emission parameters are listed in Table 3.3. The degree of freedom in the inversion is 10. In order to check the quality of our inversion results, also examine the averaging kernel matrix [Rodgers, 2000]:

$$\mathbf{A} = \mathbf{G}\mathbf{K} \quad (3.5)$$

where $\mathbf{G} = \mathbf{S}_a \mathbf{K}^T (\mathbf{K} \mathbf{S}_a \mathbf{K}^T + \mathbf{S}_\Sigma)^{-1}$.

3.2.3.3 Error estimation

A priori parameter errors are listed in Table 3.2. We assume that the emission errors are uncorrelated. *Lobert et al.* [1999] suggested an uncertainty of about 30% for

Table 3.3 Model parameters in the state vector.

| | Region | Season (months) | 39 parameters | 16 parameters* | 11 parameters* |
|-------------------------|----------------|-----------------|---------------|----------------|----------------|
| Biogenic | North Americas | Spring (3–5) | 1 | 1 | 1 |
| | | Summer (6–8) | 2 | 2 | 2 |
| | | Fall (9–11) | 3 | 3 | 1 |
| | | Winter (12,1,2) | 4 | 4 | 3 |
| | South America | Fall (3–5) | 5 | 5 | 4 |
| | | Winter (6–8) | 6 | 6 | 5 |
| | | Spring (9–11) | 7 | 7 | 4 |
| | | Summer (12,1,2) | 8 | 8 | 6 |
| | North Africa | Spring (3–5) | 9 | 1 | 1 |
| | | Summer (6–8) | 10 | 2 | 2 |
| | | Fall (9–11) | 11 | 3 | 1 |
| | | Winter (12,1,2) | 12 | 4 | 3 |
| | South Africa | Fall (3–5) | 13 | 5 | 4 |
| | | Winter (6–8) | 14 | 6 | 5 |
| | | Spring (9–11) | 15 | 7 | 4 |
| | | Summer (12,1,2) | 16 | 8 | 6 |
| | Asia | Spring (3–5) | 17 | 1 | 1 |
| | | Summer (6–8) | 18 | 2 | 2 |
| | | Fall (9–11) | 19 | 3 | 1 |
| | | Winter (12,1,2) | 20 | 4 | 3 |
| | Oceania | Fall (3–5) | 21 | 5 | 4 |
| | | Winter (6–8) | 22 | 6 | 5 |
| | | Spring (9–11) | 23 | 7 | 4 |
| | | Summer (12,1,2) | 24 | 8 | 6 |
| Biomass burning | NH | Spring (3–5) | 25 | 9 | 7 |
| | | Summer (6–8) | 26 | 10 | 8 |
| | | Fall (9–11) | 27 | 10 | 8 |
| | | Winter (12,1,2) | 28 | 10 | 8 |
| | SH | Fall (3–5) | 29 | 11 | 9 |
| | | Winter (6–8) | 30 | 11 | 9 |
| | | Spring (9–11) | 31 | 12 | 9 |
| | | Summer (12,1,2) | 32 | 11 | 9 |
| Ocean emission | | | 33 | 13 | 10 |
| Incineration/industrial | | | 34 | 14 | 11 |
| Salt marshes | | | 35 | 14 | 11 |
| Wetlands | | | 36 | 14 | 11 |
| Ocean sink | | | 37 | 15 | 11 |
| NH soil sink | | | 38 | 16 | 11 |
| SH soil sink | | | 39 | 16 | 11 |

* In the 16 and 11 parameter cases, parameters with same number indicate they are lumped as a single parameter.

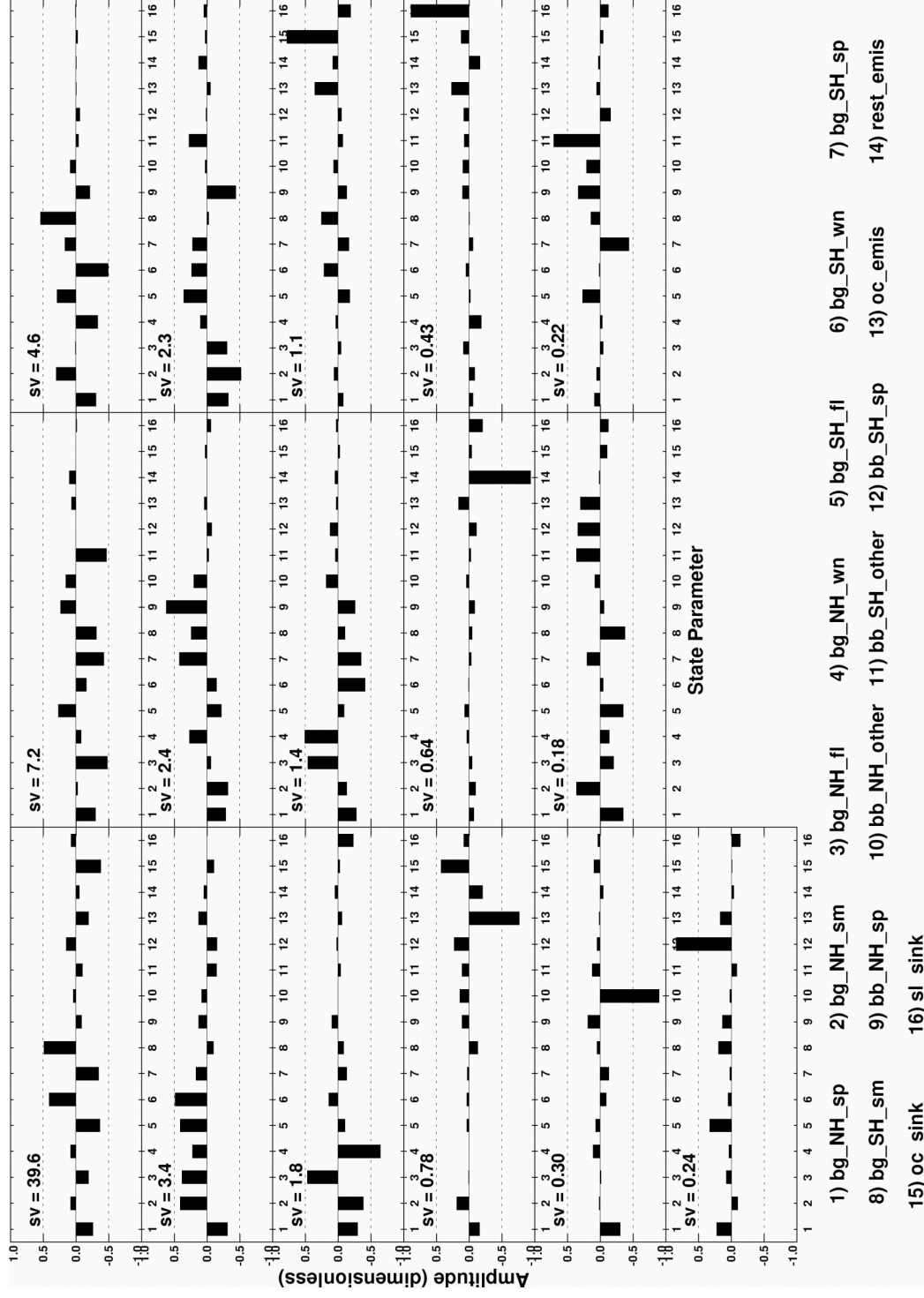


Figure 3.2 Singular vectors of the prewhitened Jacobian matrix $\tilde{\mathbf{K}}$ for the 16 parameter case. “bg”, “bb”, “oc” and “sl” denote biogenic, biomass burning,, ocean and soil, respectively. Spring, summer, fall and winter are denoted by “sp”, “sm”, “fl”, and “wn”, respectively.

biomass burning CH_3Cl emissions. It is relatively low because only the uncertainty in the $\text{CH}_3\text{Cl}/\text{CO}$ molar emission ratio is accounted for. We include the 50% uncertainty for the biomass burning emissions of CO [Palmer *et al.*, 2003] and calculate an uncertainty of 70% for the biomass burning emissions. We assign an uncertainty of 70% to oceanic flux [Khalil *et al.*, 1999]. The uncertainty for incineration/industrial source is about 80% [McCulloch *et al.*, 1999]. We assign 100% of uncertainty to the salt marsh and wetland sources. For the aggregated parameter of the minor sources of incineration/industrial, salt marshes, wetlands and oceanic sink, we use an uncertainty of 100% in the 16 and 11 parameter cases. Direct estimates for the a priori biogenic emissions are unavailable. However, the total source of CH_3Cl is constrained relatively well by its main sink, the OH oxidation. Further considering the uncertainties of other better-known sources, we assign an uncertainty of 100% to the biogenic source.

The observational error covariance \mathbf{S}_Σ in equation (3.2) is the sum of the covariance matrices of individual error types including the measurement errors, the representation error, and the forward model error. These errors are assumed to be uncorrelated. The measurement error is relatively small ($\sim 1\%$). The representation error is calculated as the standard deviation of the observations for each data grid. The forward model error includes the transport error estimated using the relative residual error (RRE) method by Palmer *et al.* [2003], the 7-year interannual variability of modeled CH_3Cl calculated by Yoshida *et al.* [2004], and the errors associated with the OH field (14%) [Prinn *et al.*, 2001] and OH + CH_3Cl kinetics (15%) [Sander *et al.*, 2003]. The total observational error is calculated as the product of square root mean of relative error of

each error types and the observation value of CH_3Cl ; and the mean observational error is about 21%.

3.3 Results

Through inversion, we evaluate the constraints on the estimates of distributions and seasonal variations of CH_3Cl sources and sinks provided by surface and aircraft observations. We first investigate the effects of the state vector size on the inversion results. The state vectors in the three inversion cases (section 3.2.3.2) have 39, 16, and 11 parameters, respectively. The averaging kernels (rows of A in equation (3.5)) show clear peaks at the appropriate level for 16 and 11 parameter cases, indicating those parameters are independent. Parameters lacking with a significant peak such as biomass burning have large a posteriori error in consequence.

3.3.1 Sensitivity to state vector size

3.3.1.1 Monthly flux

The a priori and a posteriori monthly CH_3Cl fluxes are shown in Figure 3.3. The annual total of each source/sink is listed in Table 3.2. The a posteriori fluxes are generally consistent despite the large difference in the state vector size. The more apparent effect of the state vector size is on the uncertainties of the a posteriori emissions. It is particularly large for the biogenic source. The a posteriori uncertainties decrease from 60-90% for 39 parameters, to 35-60% for 16 parameters, and further to 32-40% for 11 parameters. The uncertainty decrease is expected as the number of parameters approaches to the degree of freedom in inversion. The a posteriori uncertainties for the

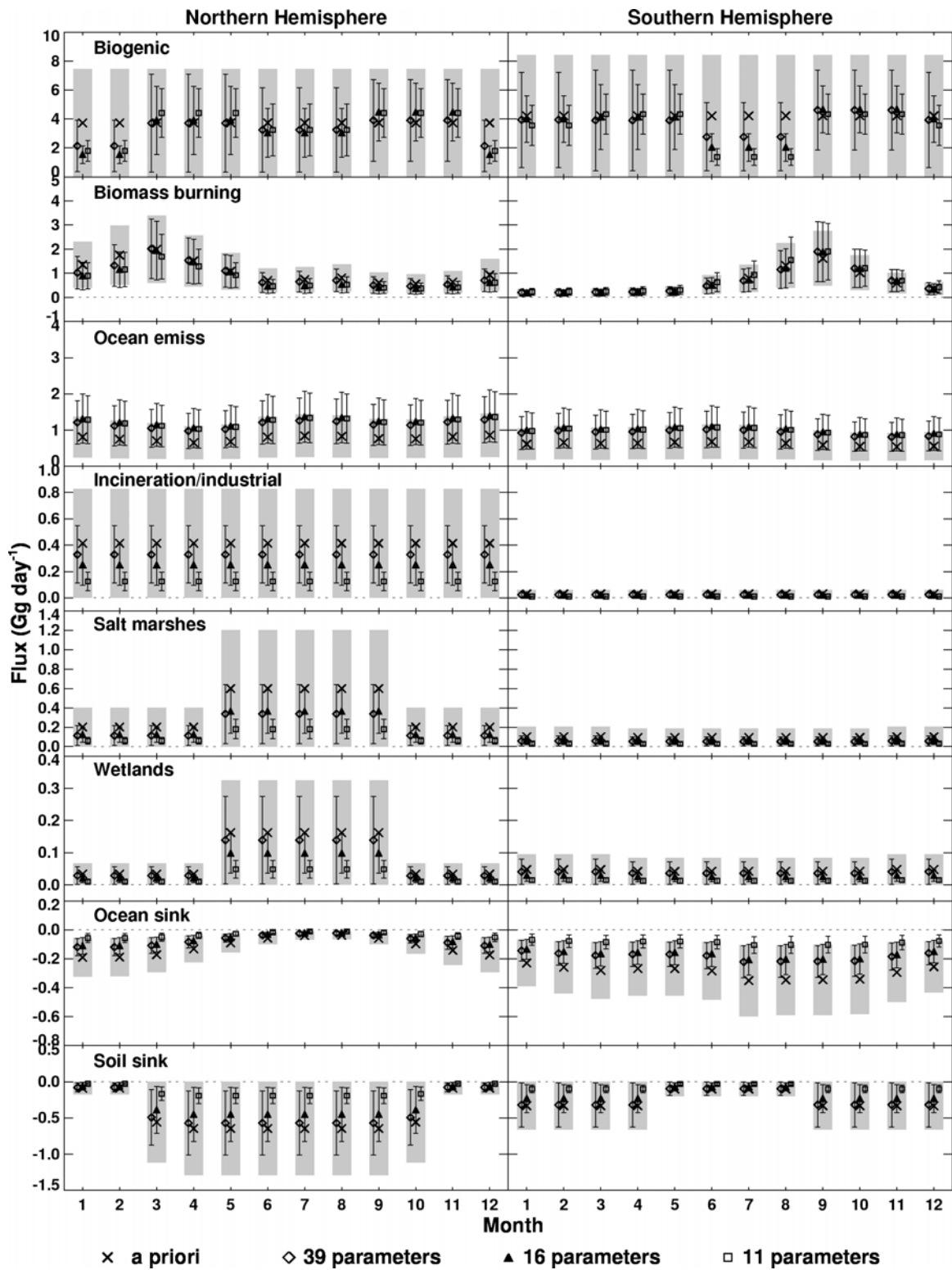


Figure 3.3 A priori and a posteriori monthly sources and sinks for the three cases with different model parameters (Table 3.3).

other sources also decrease with the parameter number but not to the extent of the biogenic sources.

The a posteriori biogenic sources show a clear winter minimum. The northern hemisphere (NH) decrease is 50-60% from spring/fall. The seasonal decrease of 40-70% from spring/fall is more variable in the southern hemisphere. The lower end is estimated with 39 parameters with a relatively large uncertainty. The emissions in summer are also lower by 20-30% than spring/fall. Considering the a posteriori uncertainties of >40%, it is not as statistically significant as the winter minimum.

The a posteriori changes in the biomass burning sources are subtler particularly in light of the a posteriori uncertainties. A general feature emerged from the 3 inversion cases is that the a priori NH biomass burning source in the non-burning seasons (other than spring) is too high by 30%. As a result, the a posteriori biomass burning source is lower and the NH to southern hemisphere (SH) emission ratio decreases from 1.7 to 1.1 (in the 11 parameter case).

The a posteriori oceanic source increases by 60% to $\sim 800 \text{ Tg yr}^{-1}$. The a posteriori error is, however, as large as around 50%, which could be due to limited observations over the tropical/subtropical oceanic emission regions. The observational constraints on the other sources/sinks, which are relatively small in magnitude, are not very good. What is clear is the decreasing trend in the a posteriori results. The largest decrease is found in the 11 parameter case, the a posteriori sources/sinks are $\sim 1/3$ of the a priori values.

In the following sections, we examine the effects of a posteriori sources on the distributions of CH_3Cl . We first compare model simulations with surface measurements

and then with aircraft measurements. The measurement sites and regions are shown in Figure 3.1.

3.3.1.2 Evaluation with surface measurements

Seasonal variations of observed and simulated CH₃Cl at 7 surface sites are shown in Figure 3.4. There is no significant difference among the inversion results with the three different parameter sizes. In the NH, the a priori model overestimates the observations at the middle and high latitudes through the year except in spring. In the a posteriori model, those positive biases are corrected mostly due to the decrease of the biogenic CH₃Cl emissions during winter. The a posteriori results, however, tend to underestimate at the NH sites in spring and early summer. These negative biases appear to be driven in part by the need to correct the a priori (positive) bias in the comparison to aircraft measurements. The a posteriori model improves significantly in the NH winter, reproducing better the observed seasonal minima. In the SH, the a posteriori model corrects the significant a priori positive bias at the three sites from June to November mainly due to the decrease of biogenic emissions during SH winter (June–August). However, the a posteriori model overestimates the seasonal variation at the SH sites.

Figure 3.5 shows the annual and seasonal latitudinal distributions at these sites. The annual-mean latitudinal distribution is symmetric because the major sources of CH₃Cl are located in the tropics. These two features, symmetric distribution and major tropical sources, provide a useful constraint on the ratio of the NH to SH mean OH is within 20% of 1:1 [Yoshida *et al.*, 2004]. The seasonal mean CH₃Cl mixing ratios are high in the NH between December and May, reflecting lower OH concentrations in

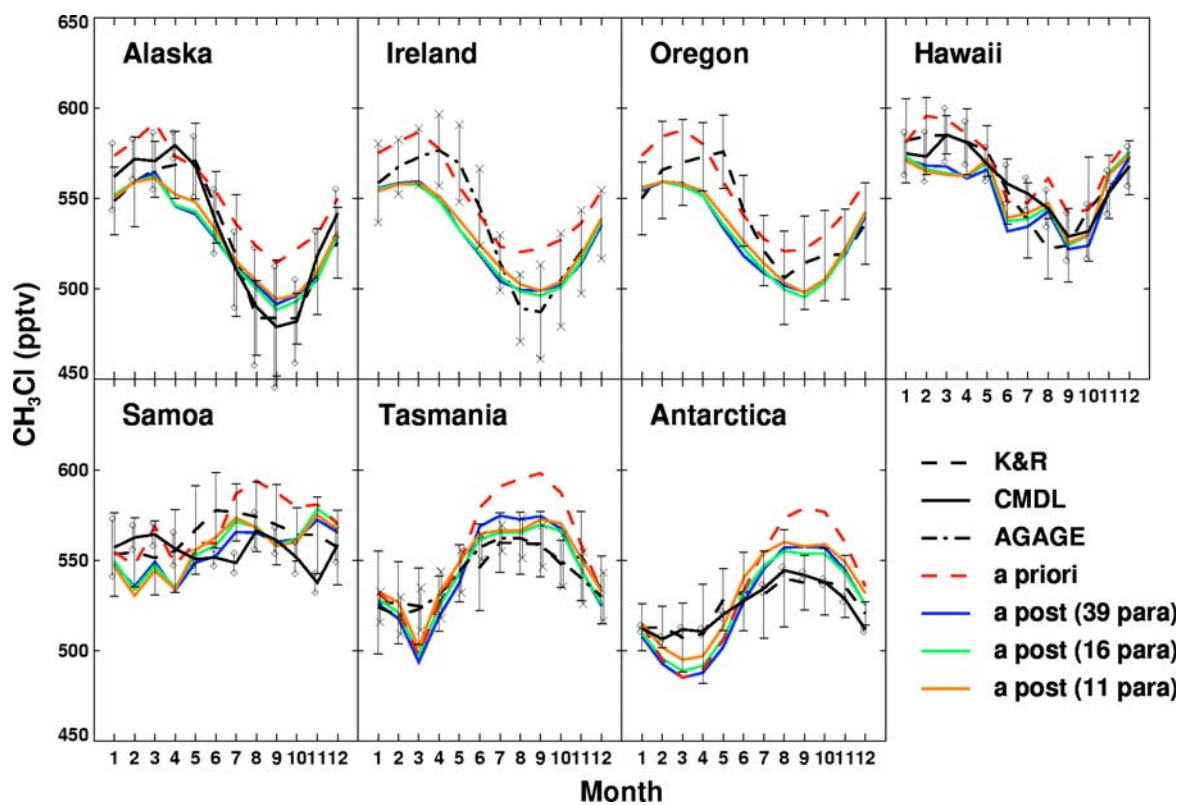


Figure 3.4 Seasonal variations of observed and simulated CH_3Cl at the surface sites. The vertical bars show the standard deviations of the measurements.

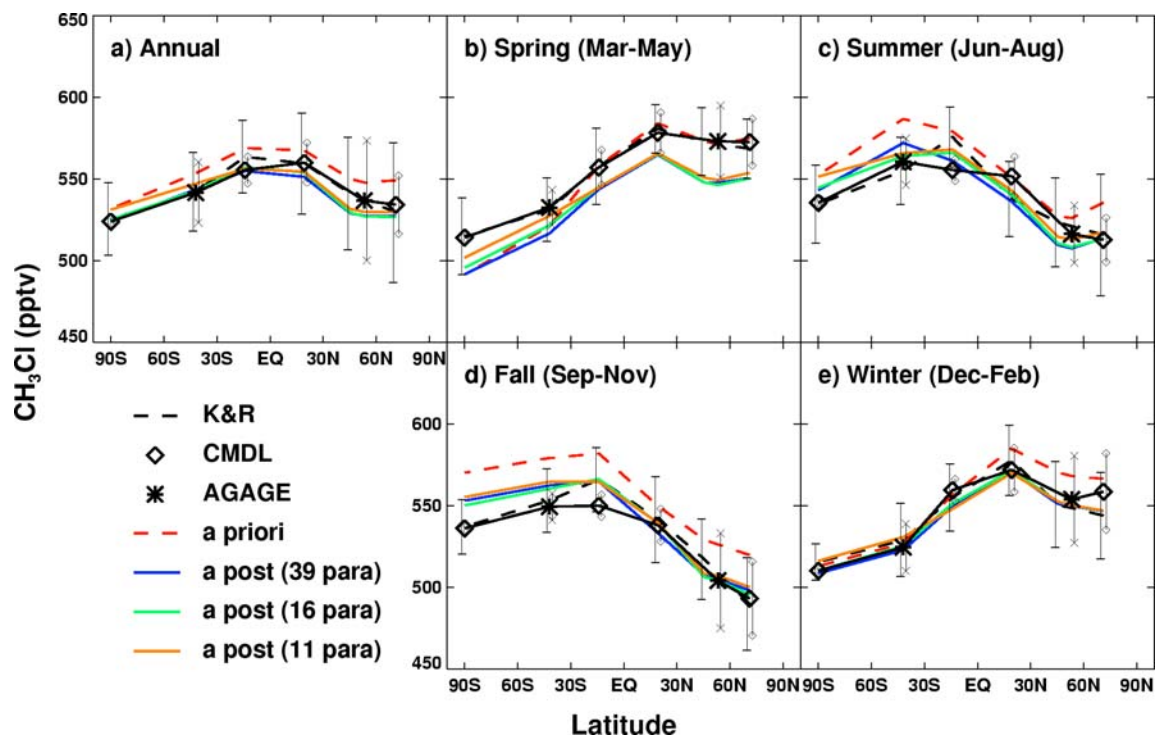


Figure 3.5 Latitudinal distributions of observed and simulated CH_3Cl at the surface sites. The vertical bars show the standard deviations of the measurements.

winter and the relatively long lifetime of > 1 year. The a posteriori model corrects the a priori high biases in June-August in the SH, December-February in the NH, and most significantly in September-November in both hemispheres. However, the a posteriori model has a low bias in March-May over the tropics and the NH.

3.3.1.3 Evaluation with aircraft measurements

As in the comparison with surface measurements, the a posteriori distributions over the aircraft measurement regions are very close in all three cases with different model parameter sizes. We therefore only show the results with 11 parameters in the state vector. Characteristics of CH_3Cl observed in the aircraft experiments have been discussed in detail by *Yoshida et al. [2004]*. We only compare the a priori with a posteriori model biases in the latitude-altitude cross sections here (Figure 3.6). We discuss the comparison by region.

Tropical Pacific (PEM-Tropics A and B)

During PEM-Tropics A, our prior model overestimates the observations by 5 to 20% over the Fiji (fj), Tahiti (tht) and Hawaii (hwi) regions, especially in the northern sections (Figures 3.6-1 – 3.6-3). After the inversion, the biases are reduced to within $\pm 5\%$ over most of the observation points, reflecting the reductions of biogenic and biomass burning CH_3Cl concentrations in our a posteriori model by 7–8% and 17–18% compared to the a priori values, respectively. For the eastern Pacific region (ep), the a priori model overestimates observations by $> 20\%$ due to biogenic and biomass burning emissions and

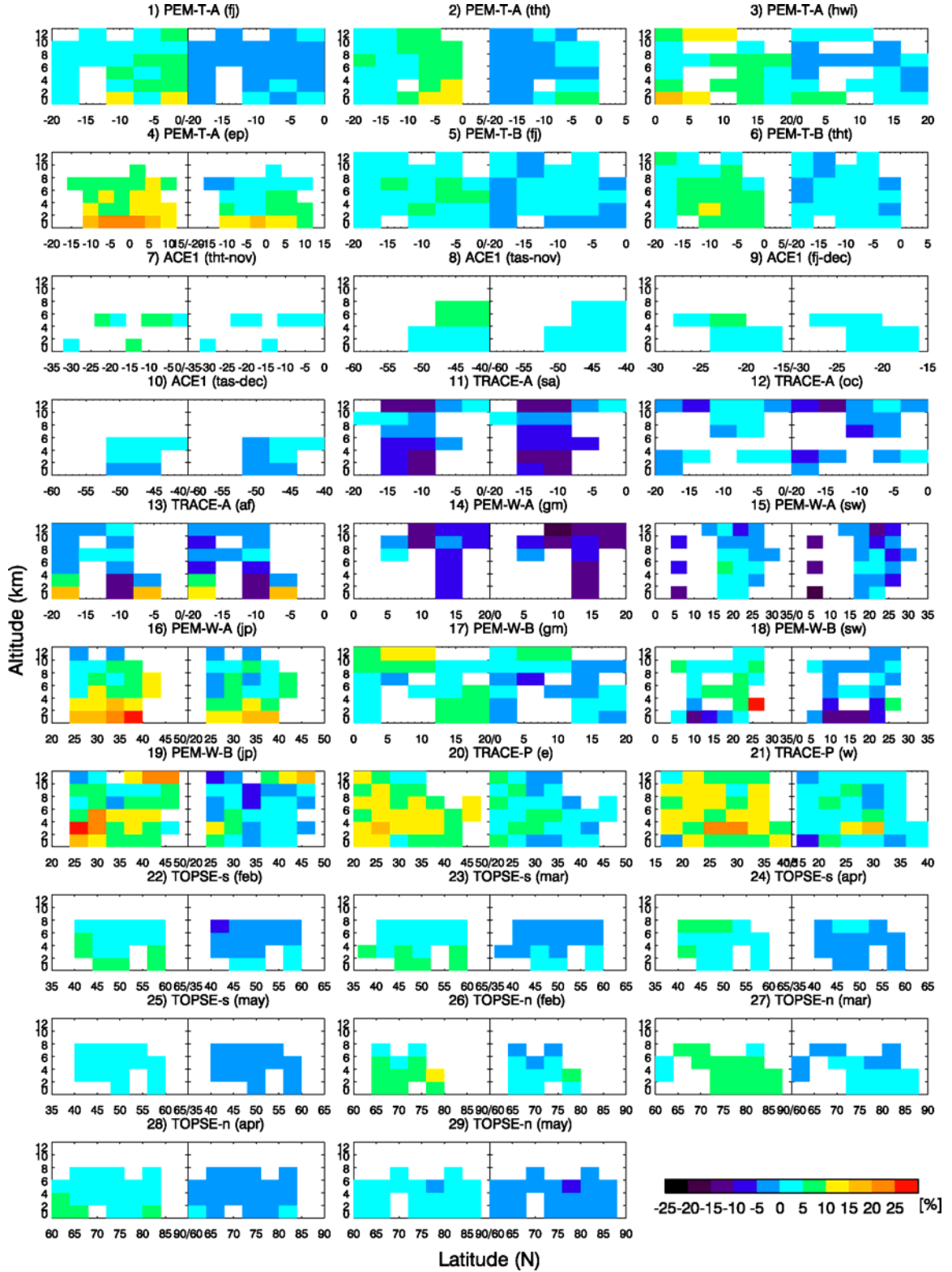


Figure 3.6 A priori and a posteriori relative biases computed as $(\text{model-observation})/\text{observation}$ with respect to aircraft observations as a function of latitude and altitude for regions shown in Figure 3.1.

the positive bias remains after the inversion although the bias is reduced to <15% (Figure 3.6-4).

Figures 3.6-5 and 3.6-6 show the comparisons between the a priori and the a posteriori model biases for the PEM-Tropics B mission. For both Fiji and Tahiti regions, the a posteriori model biases are reduced to within $\pm 5\%$. Significant a priori overestimates near the surface in the Tahiti region between 4° – 12° S are reduced from 22% to 6% after the inversion, mainly reflecting the reduction of biogenic CH_3Cl concentrations.

Tropical Pacific and Southern Ocean (ACE-1)

During the ACE 1 experiment, there are few observation points over the Tahiti-November (tht-nov) region (Figure 3.6-7). Over the Tasmania-November (tas-nov) and Fiji-December (fj-dec) regions, the a priori model overestimates up to 8% especially at higher altitudes (Figures 3.6-8 and 3.6-9). After the inversion, mean concentrations of biogenic CH_3Cl over these two regions are reduced by 50–70 pptv, resulting in a better agreement with the observations. For the Tasmania-December (tas-dec) region, both the a priori and the a posteriori models show small biases (Figure 3.6-10).

Tropical Atlantic (TRACE-A)

The TRACE-A mission was designed to investigate the large effects of biomass burning emissions observed over the South Atlantic, South America, and southern Africa. The a priori model result shows significant large (negative/positive) biases over the South America (sa) and southern Africa (af) regions (Figures 3.6-11 and 3.6-13). In comparison,

the a priori biases are generally within $\pm 5\%$ over the South Atlantic (oc) region (Figure 3.6-12). *Yoshida et al.* [2004] suggested that the large underestimations by the model may be due in part to the biased samplings of biomass burning plumes, which could not be reproduced in the simulated monthly mean concentrations. Consequently, the large biases are not corrected after the inversion. The coexistence of positive and negative biases in the TRACE-A regions also implies problematic spatial distributions of the biogenic and biomass burning sources. However, as we discussed in the previous section (3.3.1.1), available measurements do not provide enough constraints on the continent-dependent CH_3Cl emissions.

Western Pacific (PEM-West A and B, TRACE-P)

Figures 3.6-14 – 3.6-16 show the a priori and a posteriori model biases compared with PEM-West A observations. As discussed by *Yoshida et al.* [2004], during the PEM-West A, enhanced CH_3Cl concentrations were observed at high altitude (above 10 km) reflecting transport of CH_3Cl by typhoons, the effect of which could not be reproduced in our model. Our a priori model tends to underestimate the measurements at lower latitudes ($< \sim 15^\circ$) over the Guam (gm) and southwest (sw) regions. On the other hand, there are large positive biases (up to 26%) over the Japan (jp) region. The a posteriori mean concentrations are lower than the a priori values by $\sim 4\%$ for the all three regions, which result in larger negative biases over the Guam and southwest regions and smaller positive biases over the Japan region. Those lower concentrations are due to a reduction of biogenic CH_3Cl by 10–15% than the prior, as well as a reduction of biomass burning CH_3Cl by 10–16%.

During PEM-West B, the a priori model overestimates observations by 5–27% in most regions except near the surface in the southwest (sw) region (Figures 3.6-17 – 3.6-19). Mean concentrations of the a posteriori results are less than the prior values by 5–7% due to smaller biogenic and biomass burning CH₃Cl. Over the Guam (gm) region, the a posteriori biases are within $\pm 7\%$. Over the southwest region, the a posteriori model shows improvements over much of the region except the underestimation at lower altitudes of up to 15%. The a posteriori biases over Japan region are reduced to within $\pm 5\%$ except in the lower troposphere at $<30^\circ\text{N}$, where high concentrations are simulated in the model due to biogenic and biomass burning CH₃Cl. High positive biases ($<17\%$) above 10 km could be attributed to the relatively large uncertainties in the low mixing ratio measurements [Yoshida *et al.*, 2004].

Figures 3.6-20 and 3.6-21 show the comparisons of a priori and a posteriori biases for the TRACE-P experiment over the eastern (e) and western (w) regions, respectively. There are significant a priori positive biases ($>15\%$) over both regions below 4 km at $20^\circ\text{--}35^\circ\text{N}$. The a posteriori biogenic and biomass burning CH₃Cl mixing ratios are less than the a priori values by ~ 60 and ~ 20 pptv, respectively. Incineration/industrial CH₃Cl mixing ratios also decrease by ~ 25 pptv over these regions. The positive biases are reduced in much of the regions except near 30°N in the western region.

North America (TOPSE)

For the TOPSE experiment, our a priori model biases are relatively small in comparison to other regions. After inversion, the positive biases of 5-10% in some

regions are reduced to <5%. Overall, the posteriori results show very good agreement with the measurements.

3.3.2 Sensitivity to surface and aircraft data sets

We examine here the constraints on CH₃Cl sources placed by surface in comparison to those by aircraft measurements. We apply inverse modeling to three different data sets: surface measurements only, aircraft measurements only, and the combination of surface and aircraft measurements. We use 11 model parameters in the state vector (Table 3.3) in these sensitivity tests.

Figure 3.7 shows the a priori and a posteriori monthly fluxes in the three sensitivity cases. It is apparent that our best source estimates using both surface and aircraft measurements are closer to the results with aircraft measurements only than those with surface measurements only. The latter is closer to the a priori model, suggesting that the aircraft measurements offer better constraints on the CH₃Cl source estimates than surface measurements. For example, the a posteriori biogenic fluxes with surface measurements show almost no seasonal variations in the NH as the a priori model while the solution using aircraft measurements shows the winter minimum although both inversion results show the winter minimum in the SH. The a posterior oceanic source with surface measurements are similar to the a priori model while that with aircraft measurements indicates an increase of the source by 50–60%.

We find 7, 9 and 10 significant singular values in the pre-whitened Jacobian matrices with the measurements from surface, aircraft, and both surface and aircraft, respectively, providing additional evidence of better aircraft constraints. The closer

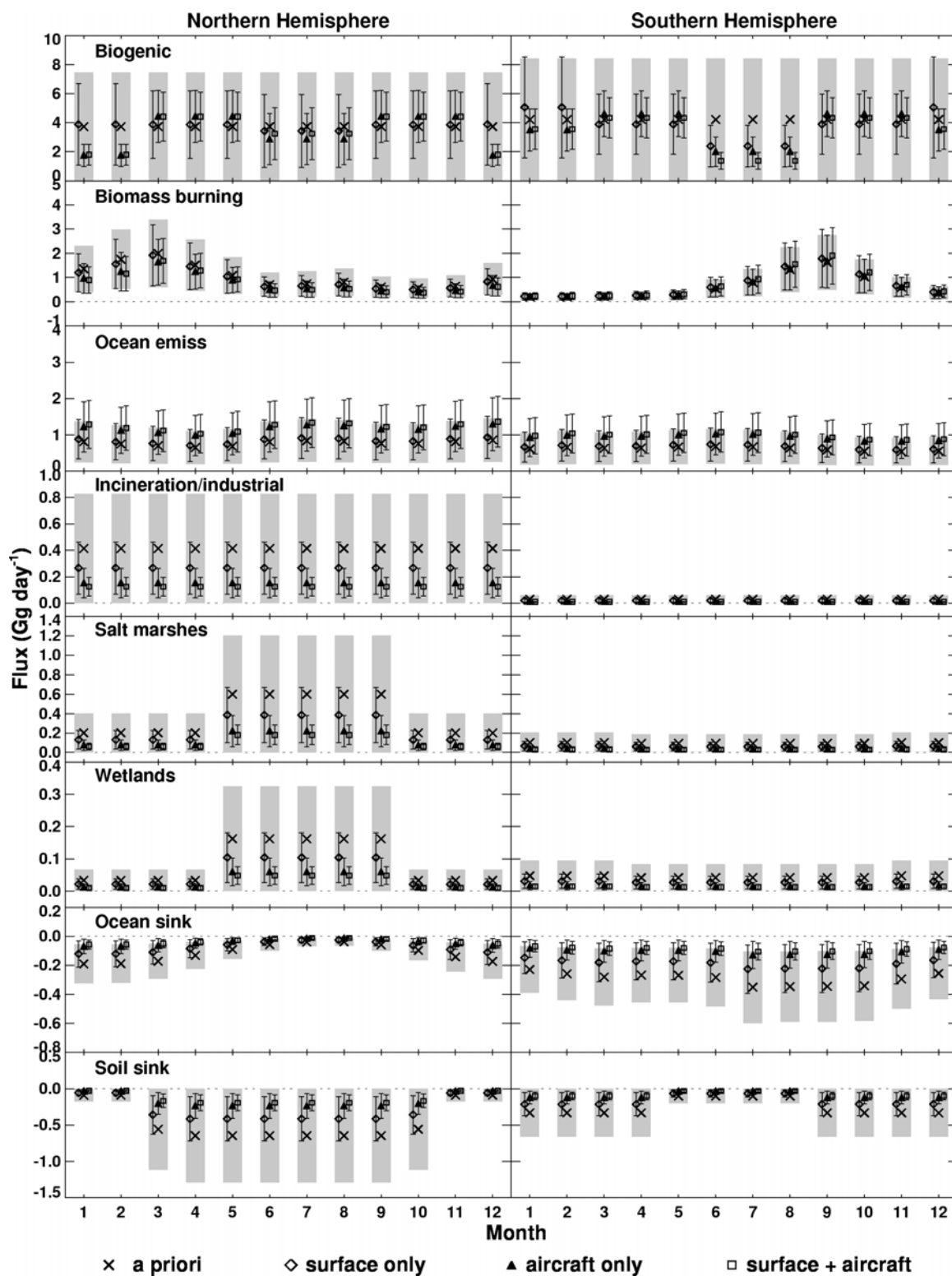


Figure 3.7 A priori and a posteriori monthly sources and sinks using the measurements from surface sites, aircraft, and both.

proximity of aircraft measurements to the source regions appears to entail better constraints on the source estimates. The a priori model also shows larger discrepancies from the measurements. In comparison, the a priori model biases at the remote surface sites tend to be much smaller (particularly when considering the annual means), leading to relatively small changes in the a posteriori emissions.

3.4 Discussion

We compare our a posteriori CH₃Cl sources with the a priori and literature values in this section. As detailed in the previous section, our “best” inversion results are obtained using both surface and aircraft measurements with 11 model parameters. The a posteriori net flux is about 3850 Gg yr⁻¹, only ~4% less than the a priori value of 3990 Gg yr⁻¹, reflecting the relatively small change of the simulated global CH₃Cl concentrations.

The annual total of the a posteriori biogenic CH₃Cl is about 2510 ± 980 Gg yr⁻¹ and about 13% less than the a priori estimate. Although the CH₃Cl emission estimates from tropical plants are still quite uncertain (820–8200 Gg yr⁻¹) [Montzka *et al.*, 2003], our results suggest that the biogenic source contributes to ~60% of the total global source.

The a posteriori biomass burning emission is 545 Gg yr⁻¹, which is about 11% less than the a priori estimate. It is much lower than the source of 910 (650–1120) Gg yr⁻¹ estimated by Lobert *et al.* [1999]. The oceanic CH₃Cl source is estimated at 600 (325–1300) Gg yr⁻¹ by Khalil *et al.* [1999]. Our a priori and a posteriori estimates are 507 and 806 Gg yr⁻¹, respectively. The other emissions and sinks including incineration/industrial, salt marshes and wetland sources, and ocean and soil sinks are smaller in the a posteriori

estimates than the a priori by a factor of 3. However, available measurements do not provide enough information to invert these relatively small sources individually.

3.5 Conclusions

We conduct Bayesian inversion analysis to constrain better CH_3Cl sources and sinks using the observations from 7 surface sites and 8 aircraft field experiments. The GEOS-Chem CTM is used as the forward model. We evaluate the sensitivities of the inversion results to the number of model parameters in the state vector and observation dataset encompassing surface only, aircraft only, or both measurements.

We first compile a “wish-list” of 39 model parameters that among others resolve the continental and seasonal distributions of the biogenic source. However, the degree of freedom in the inversion is 10. We then construct a secondary inversion with 16 parameters by discarding for instance the continental dependence. By examining the structure of the singular vectors of the Jacobian matrix and considering the physical understanding of the source, we reduce the number of parameters to 11 by lumping correlated parameters together. The resulting degree of freedom in the inversion remains to be 10. The three inversion results show largely compatible results. As the number of model parameters gets close to the degree of freedom in the inversion, the a posteriori uncertainties tend to decrease. The best constraint on the biogenic emission estimates is obtained with 11 model parameters.

Additional sensitivities are conducted to examine the constraints placed by surface and aircraft measurements. With only surface measurements, the a posteriori emissions are fairly close to the a priori. With only aircraft measurements, the a posteriori

emissions are much closer to the results when both types of measurements are used, indicating that the a posteriori changes are driven mostly by aircraft measurements. The degree of freedom increases from 7 for surface measurements to 9 for aircraft measurements. To better constrain the temporal and spatial distributions of CH₃Cl emissions, aircraft and surface measurements near the major source regions are essential.

The a posteriori model simulation shows significant improvement in comparison to surface and aircraft observations. The particularly large a priori positive bias at the SH surface sites in June–November is corrected with a posteriori emissions. Discrepancies between the a posteriori model and aircraft observations are generally within $\pm 5\%$ for most regions, except those locations strongly affected by local biogenic and biomass burning CH₃Cl sources.

The a posteriori biogenic source of 2.5 Tg yr⁻¹ shows a clear winter minimum in both hemispheres; the a posteriori uncertainty is generally 30-40%. We find the variations among the other three seasons are smaller than a posteriori uncertainties. Our current knowledge on biogenic CH₃Cl production is insufficient to speculate on specific processes responsible to the winter minimum. The gross a posteriori oceanic emission is 810 Gg yr⁻¹ with an uncertainty of $\sim 50\%$, while the gross a posteriori oceanic sink is only 45 Gg yr⁻¹ with an uncertainty of $\sim 60\%$. Our best estimate of the biomass burning source is ~ 550 Gg yr⁻¹ with an uncertainty of $\sim 60\%$. The most significant change in the a posteriori emissions is the large reduction of NH emissions of 82 Gg yr⁻¹ in seasons other than spring. The a posteriori source decreases by 27% to 281 Gg yr⁻¹ in the NH but increases by 17% to 264 Gg yr⁻¹ in the SH. Our results could either indicate that the CH₃Cl/CO emission ratio is dependent on season and hemisphere or imply that the

NH/SH ratio of biomass burning CO emissions in the GEOS-Chem is overestimated due largely to an overestimate of the NH emissions in seasons other than spring.

CHAPTER IV

UNCERTAINTIES IN USING SATELLITE FIRE COUNTS FOR BIOMASS BURNING EMISSIONS IN THE SOUTHEAST UNITED STATES

4.1 Introduction

Biomass burning is an important emission source of many trace gases and particulates. Although temperate forest fires have significant climatic effects, they have not been studied as extensively as have tropical fires, and their emission characteristics are not well understood [*Kasischke et al.*, 2003; *Li et al.*, 2003]. Though in some regions, information needed to estimate the emissions from biomass burning such as burned area and fire distributions could be provided by fire management agencies, such data are not available for most of the world [*Kasischke and Penner*, 2004]. Satellite remote sensing data have been used to monitor biomass burning, and the fire product data have been used to analyze the global distribution of fires and scale biomass burning emissions [*Scholes et al.*, 1996; *Duncan et al.*, 2003; *Kasischke et al.*, 2003; *van der Werf et al.*, 2003]. An important limitation in using satellite fire products is that a satellite can detect only active fires [*Kasischke and Penner*, 2004]. Assuming that the satellite fire products represent an unbiased sample of total fire activity, *Dwyer et al.* [2000] used a fire product to characterize the spatial and temporal patterns of global fire activities. *Duncan et al.* [2003] and *Schultz* [2002] analyzed spatial and temporal variations of biomass burning emissions using fire count data. However, studies showed that satellite fire count data do not represent an unbiased sample of fire activity [*Scholes et al.*, 1996; *Eva and Lambin*, 1998; *Kasischke et al.*, 2003; *Kasischke and Penner*, 2004].

In this study, we use satellite fire count data from the Moderate Resolution Imaging Spectroradiometer (MODIS) in comparison to a burned area inventory from the Visibility Improvement – State and Tribal Association of the Southeast (VISTAS). We compare seasonal trend of these two data sets and discuss the uncertainties of the satellite fire count data for estimating biomass burning emissions.

4.2 Data and Methods

4.2.1 Burned area inventory

The Visibility Improvement – State and Tribal Association of the Southeast (VISTAS) is an organization comprised of state, local and tribal agencies, and is responsible for technical analyses and planning activities to address regional haze and visibility problems in the southeastern United States. VISTAS developed a 2002 base year emissions inventory based on data provided by the ten VISTAS states: Alabama (AL), Florida (FL), Georgia (GA), Kentucky (KY), Mississippi (MS), North Carolina (NC), South Carolina (SC), Tennessee (TN), Virginia (VA) and West Virginia (WV). These ten states were requested to supply information about fires such as number of acres burned, date of fire, type of material burned, fuel loading and location of fire about four types of burning: wildfires, prescribed (managed) fire, agricultural burning and land clearing of debris. Alabama, Florida, Georgia, and South Carolina provided data on all four fire types and other states only one or two fire type(s) such as prescribed or wildfire (Table 4.1). Data for prescribed fire and wildfire were also provided by Federal agencies such as the U.S. Forest Service, Fish and Wildlife Service, National Park Service, Bureau of Land Management and Bureau of Indian Affairs. If federal data were redundant in

state fire data, state-supplied data were used. After all the state and federal data had been provided, the VISTAS inventory was compiled by MACTEC Engineering and Consulting, Inc [Barnard and Brewer, 2004].

Table 4.1 Fire data provided by state agencies by fire type.

| State | Agriculture | Prescribed/ Silviculture | Land clearing | Wildfire |
|----------------|-------------|-----------------------------|---------------|----------|
| Alabama | √ | √ | √ | √ |
| Florida | √ | √ | √ | √ |
| Georgia | √ | √ | √ | √ |
| Kentucky | | | | √ |
| Mississippi | | √ | | |
| North Carolina | | √ | | √ |
| South Carolina | √ | √ | √ | √ |
| Tennessee | | | | √ |
| Virginia | | | | √ |
| West Virginia | | | | √ |

In the VISTAS 2002 base year emission inventory, we use burned area data calculated for each county in the ten VISTAS states for four types of burning: wildfire, prescribed fire, agricultural burning and land clearing. Figure 4.1 shows monthly total burning areas of the ten VISTAS states and contribution fractions of the four types of burning. Among the four fire types, prescribed burning accounts for 60 – 70% of the total burned area in Alabama, Florida, Georgia, and South Carolina, which are the states that provided data on all four fire types (please also see Figure 4.2). Prescribed burning is widely used in the Southeast for forest resource management. The purposes of prescribed burning are to reduce hazardous fuels, manage competing vegetation, improve wildlife habitat, control insects and diseases, and enhance appearance [Hardy *et al.*, 2001]. The second largest fire component is agricultural burning, which accounts for 25 –30% of

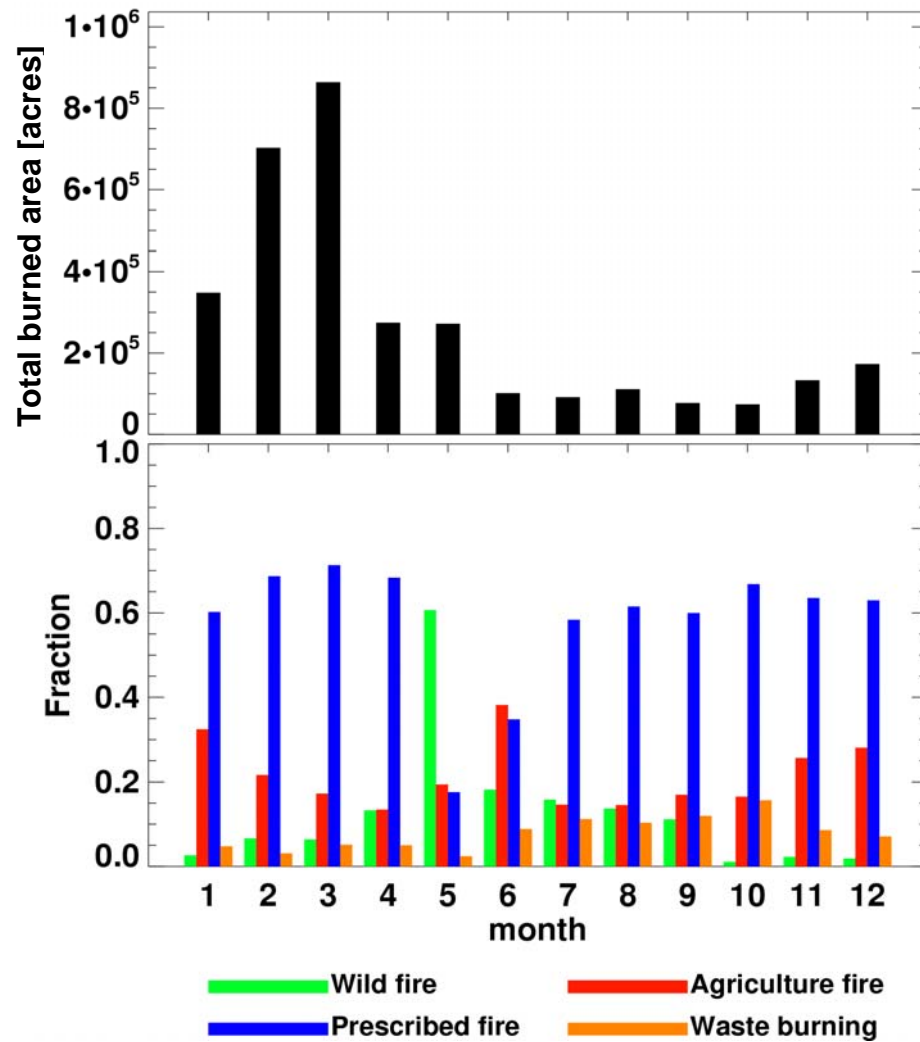


Figure 4.1 Trend of VISTAS fire.

total burned area except in Alabama, where the land clearing fire is the second largest (17%). Wildfire shows relatively small contributions in all states except in May in Georgia.

4.2.2 Fire count data

The MODIS instrument is aboard the Terra satellite launched in February 2000 as part of NASA's Earth Observing System (EOS). The terra MODIS acquires data twice daily (~10:30 am and ~10:30 pm local time). We use the fire count data with 1km resolution observed in January–December 2002. The fire detection algorithm uses brightness temperatures derived from the 4- and 11- μ m channels. MODIS has two 4- μ m channels, one of which saturates at 500 K and the other at 331 K. The 11- μ m channel saturates at approximately 400 K. For cloud masking, the 12- μ m channel is used. MODIS identifies water pixels using the 1-km prelaunch land/sea mask in the geolocation product, though significant errors have been found in the data set and an improved water mask is being developed. After eliminating obvious non-fire pixels such as cloud and water, the algorithm considers only remaining clear land pixels. Examined further with the fire detection algorithm, each pixel of the MODIS swath is ultimately assigned to one of the following classes: missing data, cloud, water, non-fire, fire, or unknown. Pixels lacking valid data are classified as missing data [Giglio *et al.*, 2003].

We use the MODIS/Terra Thermal Anomalies/Fire Daily Level 3 Global 1 km SIN (sinusoidal projection) Grid product (MOD14A1) and compute monthly total fire counts during the year of 2002 for each county in the ten VISTAS states explained in the previous section using a Geographic Information System (GIS) program in order to

investigate the relationships between VISTAS fire inventory burned area data and the satellite's fire observation.

4.2.3 Leaf area index (LAI) data

Leaf area index is defined as one-sided leaf area per unit ground area [Knyazikhin *et al.*, 1999]. We calculate monthly state-level mean LAI for the ten VISTAS states using MOD15_BU data set (<http://cliveg.bu.edu>), which is a monthly 4 km average of MODIS/Terra Leaf Area Index Product. The main MODIS LAI algorithm solves the inversion of a three-dimensional radiative transfer problem using the spectral information of MODIS surface reflectance at up to 7 spectral bands (648, 858, 470, 555, 1240, and 2130 nm, nanometer = 10^{-9} meter). When the main algorithm fails, a backup algorithm estimates LAI based on relations between vegetation indices and LAI [Myneni *et al.*, 2003].

4.2.4 Cloud fraction data

MODIS Cloud Product provides cloud fraction data calculated from the infrared retrieval methods at 5×5 1-km-pixel resolution cloud mask data generated at 1-km and 250-m spatial resolutions. The cloud mask indicates whether the earth surface in a field of view is covered by clouds or by optically thick aerosol. The algorithm includes a series of visible and infrared threshold and consistency tests. If the resulting value of spectral tests approaches a threshold limit, the certainty or confidence is reduced. The confidence level is calculated using a linear interpolation between a low confidence clear threshold (0% confidence of clear) and high confidence clear (100% confidence of clear) threshold

for each spectral test. As a final check, spatial and temporal consistency tests are employed. Basically, pixels with a confidence less than 0.66 are considered cloudy. Cloud fraction of 5×5 pixel area is calculated as the number of cloudy cells in the 25 1-km grids divided by 25 [Ackerman *et al.*, 2002; Menzel *et al.*, 2002]. We use MOD06_L2 data, which are collected from the Terra platform, and compute monthly and daily mean cloud fractions in order to examine the cloud effects on fire detection at state and county levels.

4.3. Results

4.3.1 Correlations between VISTAS burned area and MODIS fire count

Figure 4.2 shows seasonal variations of VISTAS burned area and MODIS fire counts in the ten VISTAS states. Generally, the burned area has maxima in spring for most of the states, whereas fire count in summer to fall except Florida, Georgia, and South Carolina. The annual totals of the burned areas and the fire counts differ from state by state (Table 4.2). For example, the total burned area of Georgia and Florida reported to VISTAS are more than 4000 km², followed by Alabama and South Carolina, which are factors of 2 and 5 smaller than the former, respectively. In other states, partly because are only limited fire type data provided as shown in Table 4.1, the total burned areas are as small as 50 – 200 km². Florida and Georgia have fire counts as large as ~3000 consistent with the large burned area shown in the VISTAS inventory. However, those states that have small burned area reported to the VISTAS such as Mississippi and North Carolina also have high fire counts.

Table 4.2 Annual total of VISTAS burned area and MODIS fire count.

| State | VISTAS burned area | MODIS fire count |
|-------|--------------------|------------------|
| | [km ²] | [counts] |
| AL | 2028 | 1762 |
| FL | 4423 | 3011 |
| GA | 5202 | 2826 |
| KY | 102 | 199 |
| MS | 51 | 1399 |
| NC | 198 | 1455 |
| SC | 823 | 863 |
| TN | 56 | 432 |
| VA | 98 | 687 |
| WV | 59 | 305 |

In order to investigate relationships between the VISTAS burned area and the MODIS fire count data, we calculate correlation coefficient (r values) using monthly total of burned area and fire count for each county in each VISTAS state (Figure 4.3). The results do not indicate any strong correlations between the two data sets. Then we aggregate the county data in each state for each month and compute monthly state-level correlations (Figure 4.4). The correlation coefficients (r) are almost doubled for those states that provide detailed fire type data such as Florida, Georgia, and South Carolina except Alabama. Those states with poor VISTAS data, in which only limited fire type data are provided, show little correlations. These improvements in r values from county- to state-level analysis indicate that there could be spatial biases in MODIS fire observation data.

Figure 4.5 shows the state-level total VISTAS burned area as a function of MODIS fire count in each month. The correlations between the burned area and the fire count data are significantly lower during the months from June to September than those in the rest of the months. The slope of the regression line is also listed in the Figure 4.5.

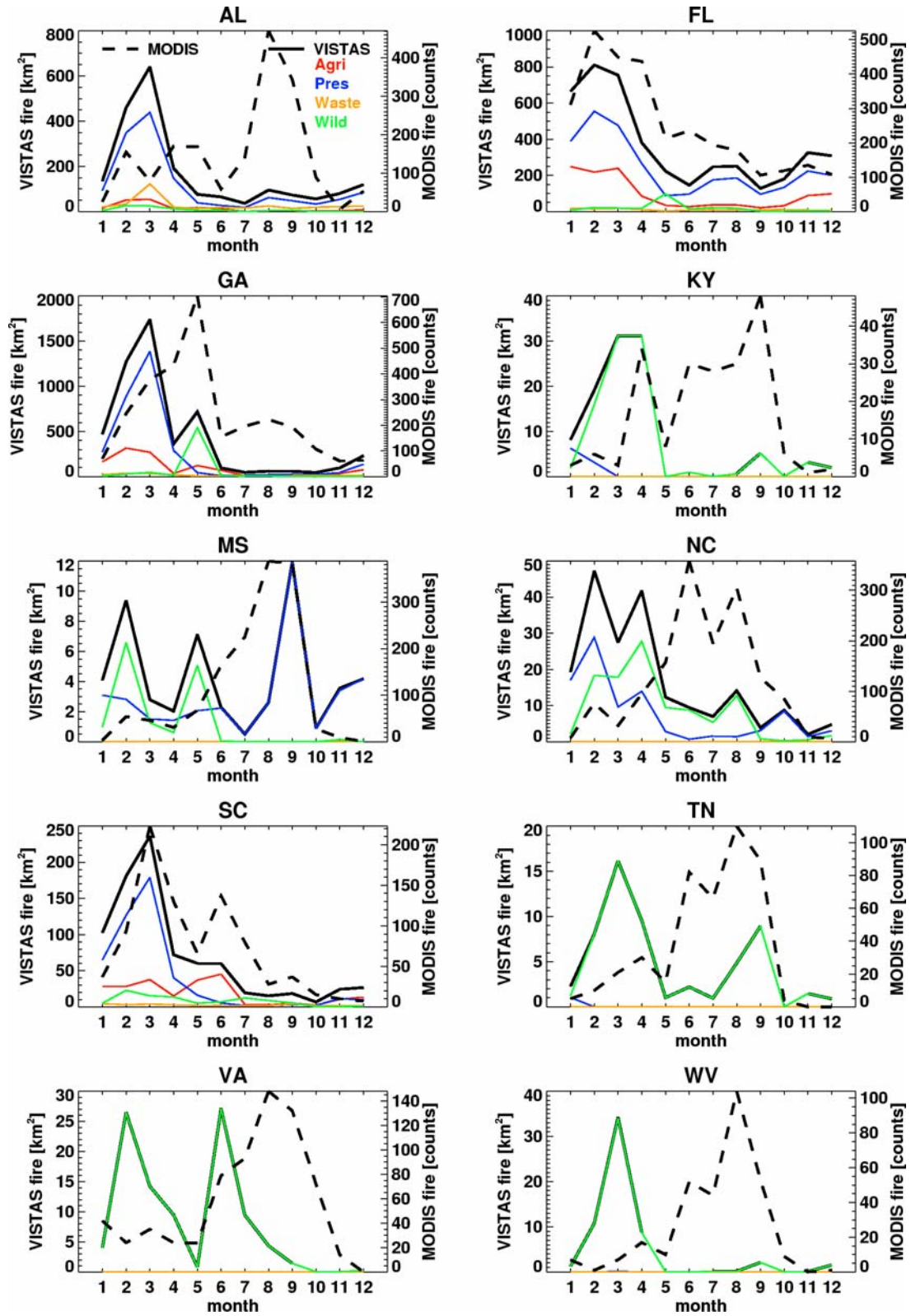


Figure 4.2 Seasonal variations of VISTAS burned areas and MODIS fire counts. Four different fire types in VISTAS are shown in color.

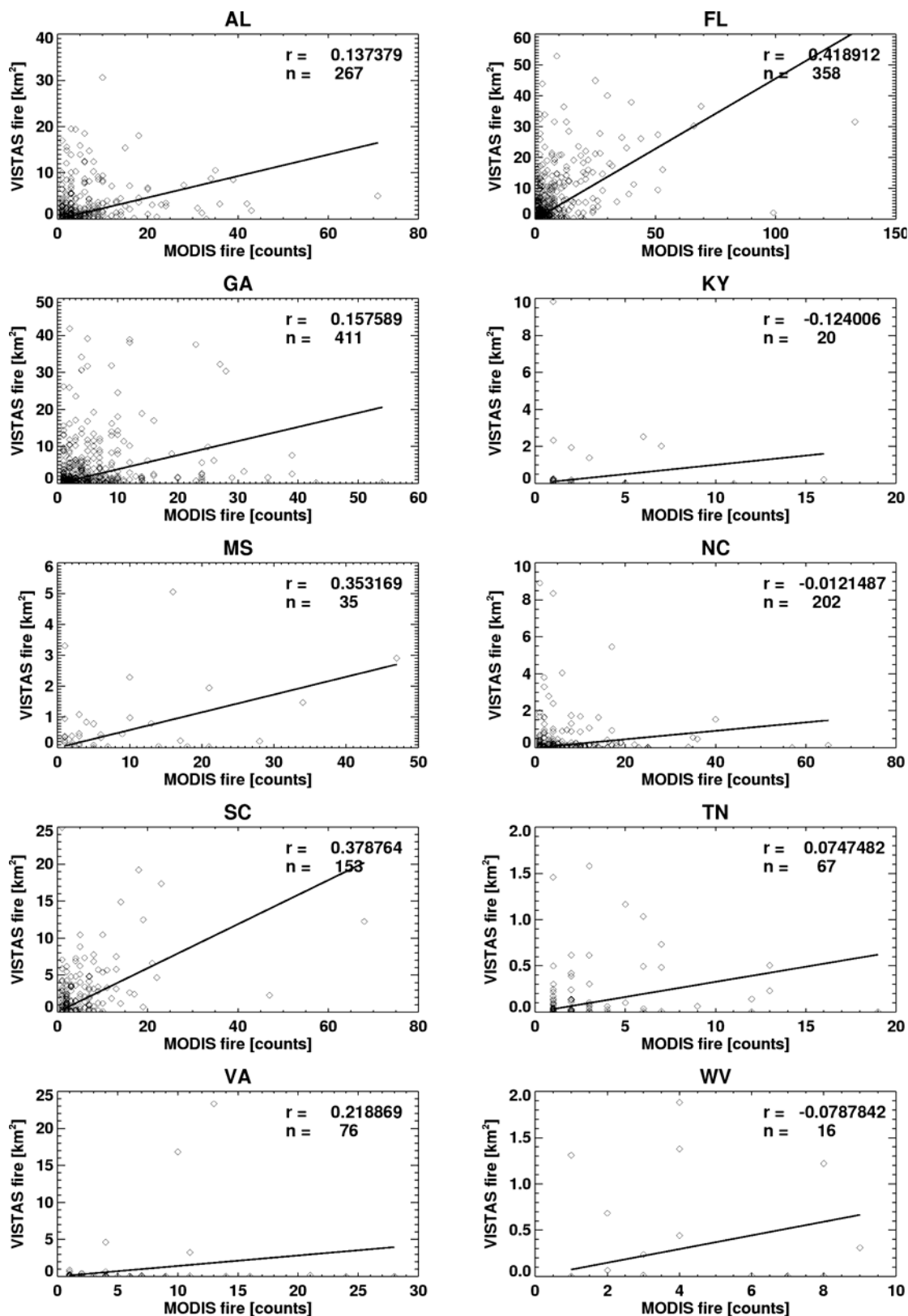


Figure 4.3 County-level monthly total of VISTAS burned area as a function of MODIS fire count.

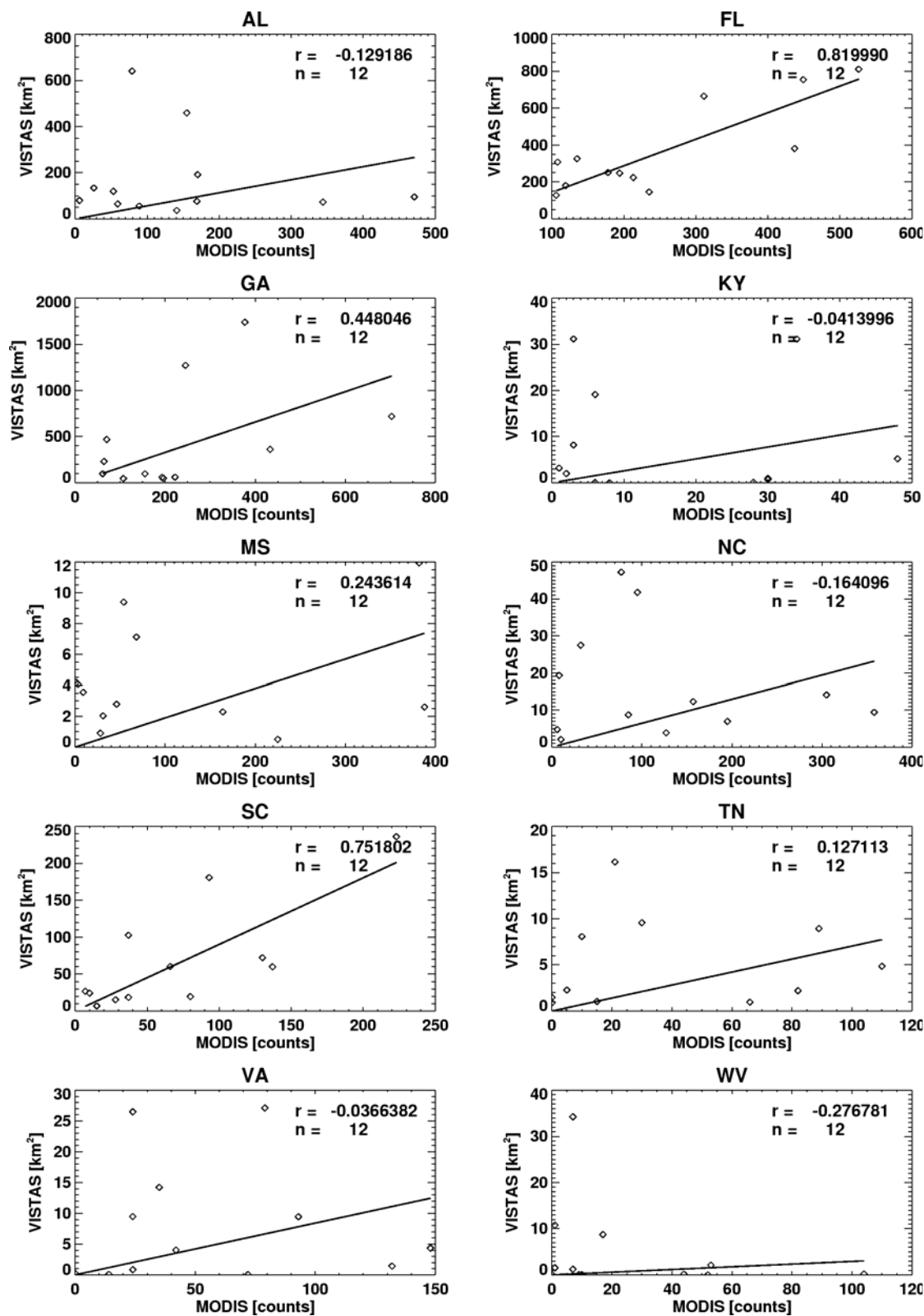


Figure 4.4 State-level monthly total of VISTAS burned area as a function of MODIS fire count.

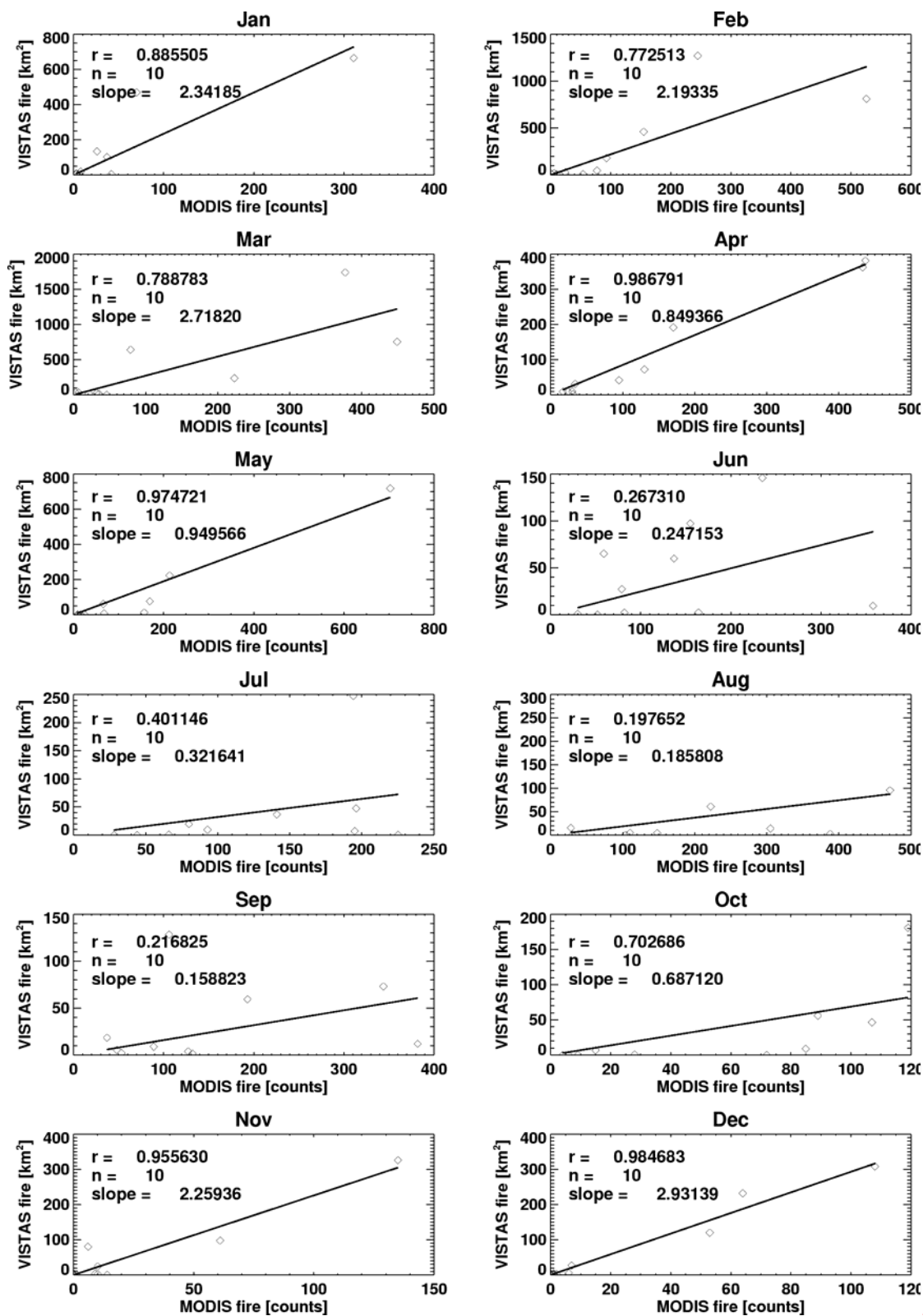


Figure 4.5 State-level total VISTAS burned area as a function of MODIS fire count for each month.

The slopes are as high as 0.7 – 2.9 in those months where the r values are high, but they become significantly lower (< 0.3) where the r values are low. This result could indicate that MODIS overestimates the fire counts or that there are fires that were not reported to VISTAS during summer.

Figure 4.6 shows the state-level monthly total VISTAS burned area as a function of MODIS fire count specified for different VISTAS fire types calculated using the data for the states of Alabama, Florida, Georgia, and South Carolina, which provided data sets of the four fire types. Plots using the total burned area data of all four fire types and the total of all fires without prescribed burning are also shown. Interestingly, the highest correlation coefficient is derived from agricultural burning, whose contributions to the total burned areas are 9 – 30 %. The second highest r value is found with the all VISTAS fires without prescribed burning, which is the largest component among the four fire types in most of the states. Even though the prescribed burning account for about 60 – 70 % of the total fire areas reported, its correlation with MODIS fire counts is not high. The lowest r value is derived with land clearing fire, whose burned areas account for as small as ~4% of the total except for Alabama, where about 17% of the burned area is due to land clearing fire. The correlation between prescribed burning and MODIS are the third lowest, which could suggest prescribed fires are not very well detected by MODIS despite its relatively large burned areas.

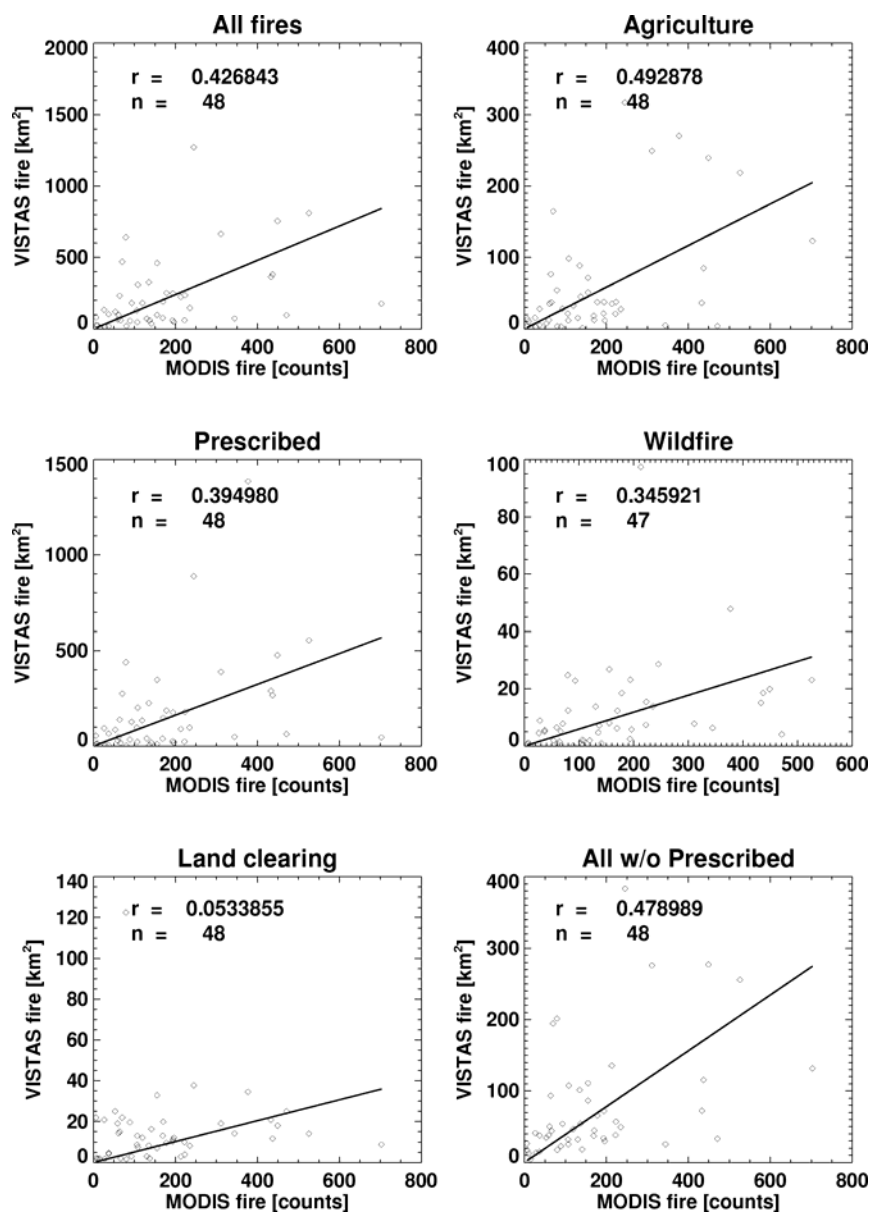


Figure 4.6 State-level monthly total VISTAS burned area as a function of MODIS fire count for different VISTAS fire types.

4.3.2 Effect of cloud cover

Satellite observations are strongly affected by clouds. Studying the boreal forest fires using satellite fire products, *Kasischke et al.* [2003] concluded that the higher rates of detection were associated with lower levels of cloud cover. We calculate correlations between the MODIS fire counts and cloud fractions at daily 5×5 km resolutions (Table 4.3). Only the results for states with daily maximum fire counts ≥ 20 are shown. Generally, states that have low VISTAS burned area, like Kentucky, Tennessee, Virginia, and West Virginia have small numbers of fire counts per day and are dropped from further discussion. In Alabama, there are relatively high negative correlations from July to September. Florida does not show clear correlations except in March, July, and from September to November, but its MODIS fire counts and VISTAS burned areas are highly correlated ($r=0.820$) as shown in Figure 4.4. For Georgia, fire counts are negatively correlated with cloud cover during months of March, April and September. Mississippi gives r values <-0.4 in August and September and North Carolina in June and September. From these results, stronger negative correlations between the fire counts and the cloud cover are observed during spring and summer in Alabama, Florida, and Georgia. Also it is noteworthy that the fire count maxima observed in Alabama, Georgia, and Mississippi are negatively correlated with the cloud fractions.

Table 4.3 Correlations between the MODIS fire counts and cloud fractions at daily basis.

| | AL | FL | GA | MS | NC | SC |
|-----|--------|--------|--------|--------|--------|--------|
| Jan | | -0.354 | | | | |
| Feb | -0.353 | -0.287 | -0.249 | | -0.353 | -0.143 |
| Mar | -0.466 | -0.426 | -0.625 | -0.031 | | -0.390 |
| Apr | -0.461 | -0.135 | -0.533 | | | |
| May | -0.350 | -0.112 | -0.221 | | -0.269 | -0.535 |
| Jun | | -0.357 | -0.374 | -0.110 | -0.508 | -0.274 |
| Jul | -0.626 | -0.527 | -0.340 | -0.129 | -0.242 | |
| Aug | -0.621 | -0.187 | -0.304 | -0.427 | -0.307 | |
| Sep | -0.593 | -0.404 | -0.548 | -0.445 | -0.546 | |
| Oct | -0.038 | -0.425 | | | -0.337 | |
| Nov | | -0.521 | | | | |
| Dec | -0.203 | -0.331 | -0.271 | | | |

4.3.3 Effect of LAI

As discussed in the previous sections, prescribed fire accounts for a major part of fire reported to VISTAS. Because prescribed fires generally occur inside tree canopy, we investigate, in this section, correlations between the detection rate and LAI. Figure 4.7 shows the correlation coefficients (r) between the MODIS fire counts and LAI. Monthly mean LAI and monthly total fire count data are used in the calculation. We anticipate seeing some negative correlations because prescribed fires are mostly under-story burning and heavy canopy cover could block those fires from satellite detection. However, the results suggest strong positive correlations for most of the states. For Georgia and South Carolina, there are no significant relationships. Only Florida shows a negative correlation, but the monthly LAI variation in Florida is much smaller (from ~ 1.7 to ~ 2.7) than other states (from ~ 1 to $4\text{--}6$). These results reflect that the MODIS detects more fires during summer months, though no such burning is captured by the VISTAS inventory.

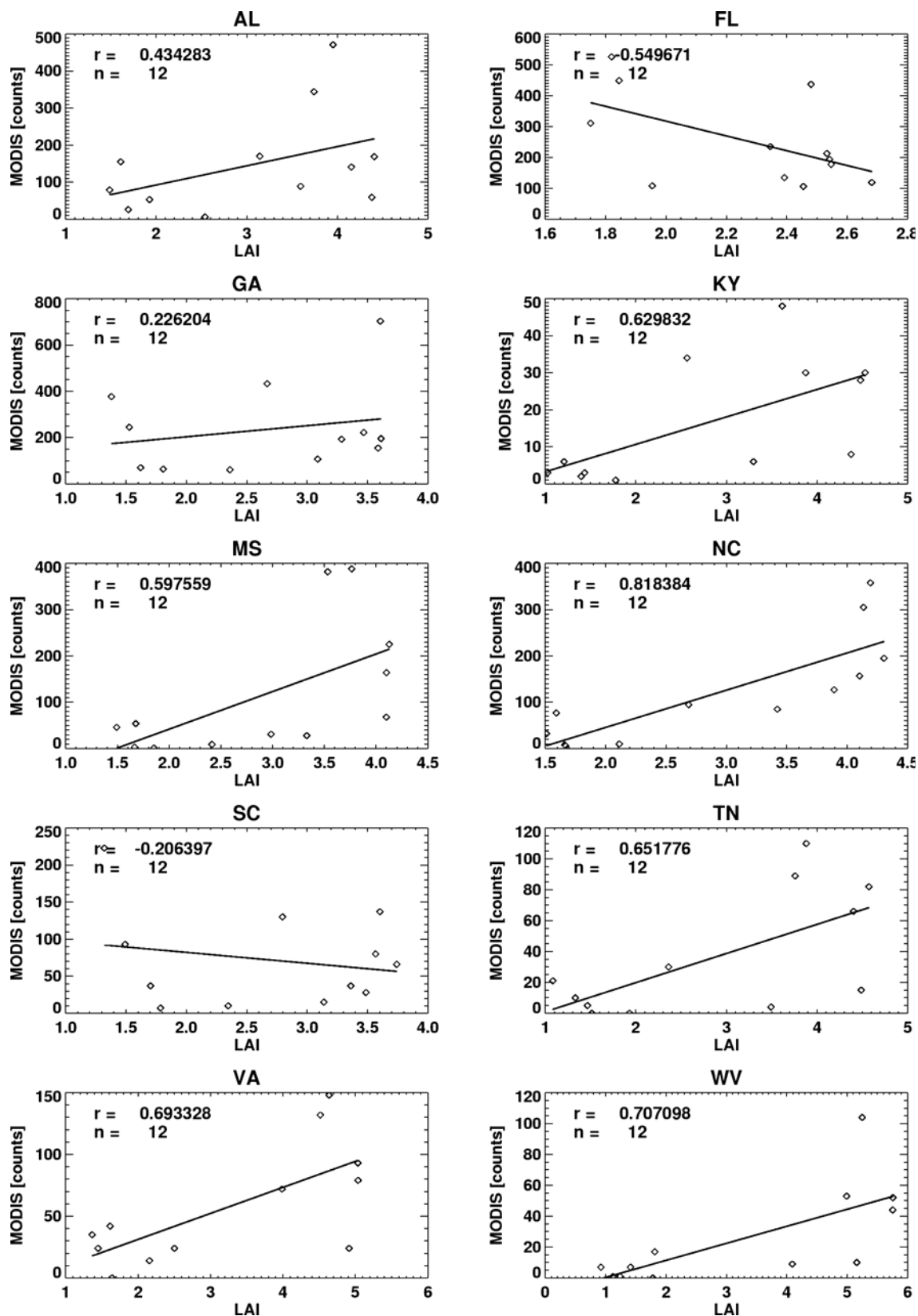


Figure 4.7 State-level monthly total MODIS fire counts as a function of monthly mean LAI.

4.4 Discussion

The results discussed in the previous sections pose a few questions regarding the mismatch in the seasonality between the VISTAS burned area and the MODIS fire count data; a) is the spring peak shown by the VISTAS real?, b) if the answer for the question a) is yes, why does the MODIS not capture those fires?, and c) is the summer peak of MODIS fire count real?

In order to answer the first question, we use a model to investigate the effects of emissions from the prescribed burning, which has a maximum in spring in Alabama, Florida, Georgia, and South Carolina. Zeng *et al.*, [2006] simulated atmospheric aerosol and trace gases over southeastern U.S. with the version 4.4 EPA Models-3 Community Multiscale Air Quality (CMAQ) modeling system [EPA, 1999] using the VISTAS inventory as fire emission input data. The model results are evaluated using observations from two networks, the Southeastern Aerosol Research and Characterization project (SEARCH) [Hansen *et al.*, 2003] and Interagency Monitoring of Protected Visual Environments (IMPROVE) [Malm and Day, 2000; Malm *et al.*, 2000] (Figure 4.8). Figures 4.9 and 4.10 show the model results compared with surface observations for organic carbon (OC), and elemental carbon (EC), respectively, at four sites of Centreville (AL), Cohutta (GA), Gulfport (MS) and Mammoth Cave (KY) in March 2002. The model results with prescribed burning emissions show better agreement with the observations for both OC and EC. These model results indicate that the prescribed fires in VISTAS is “real,” and thus there might be some reasons for MODIS not to detect those fires.

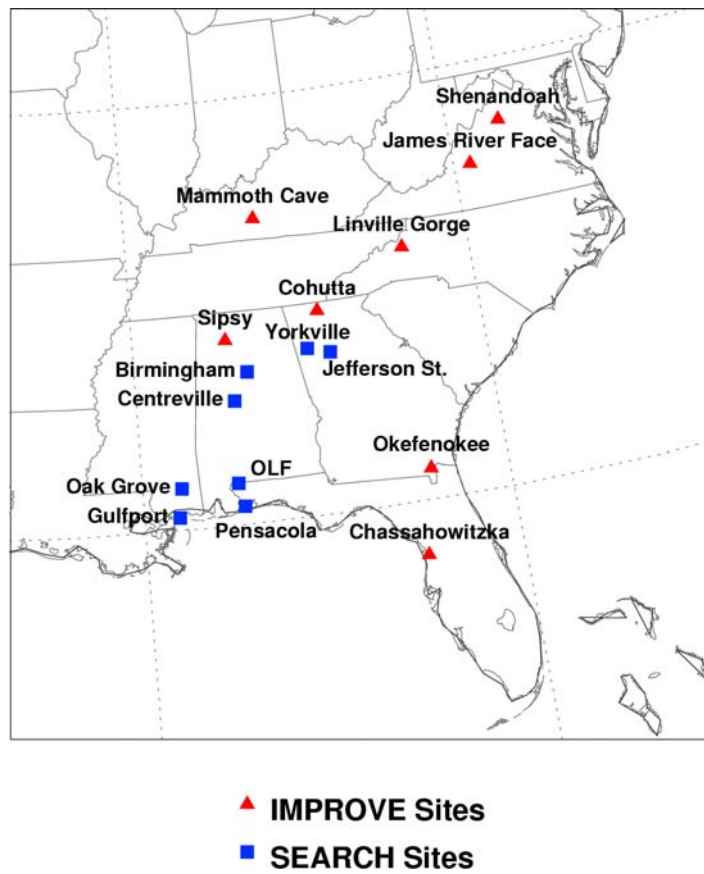


Figure 4.8 Surface observation sites used in the CMAQ simulation evaluation [Zeng *et al.*, 2006].

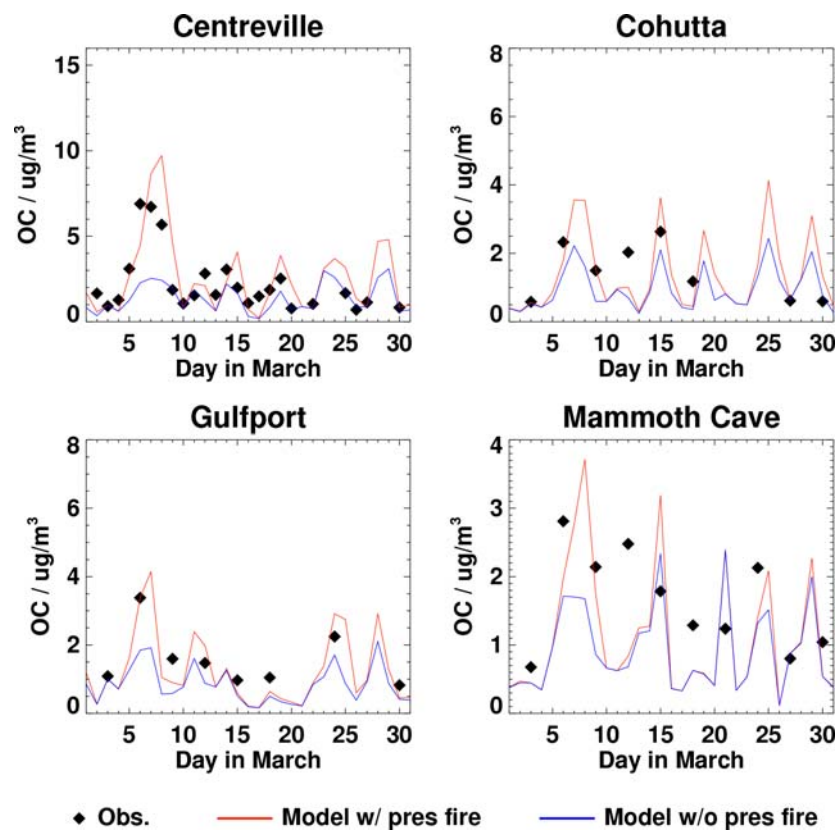


Figure 4.9 CMAQ simulation results compared with observations for OC [Zeng *et al.*, 2006].

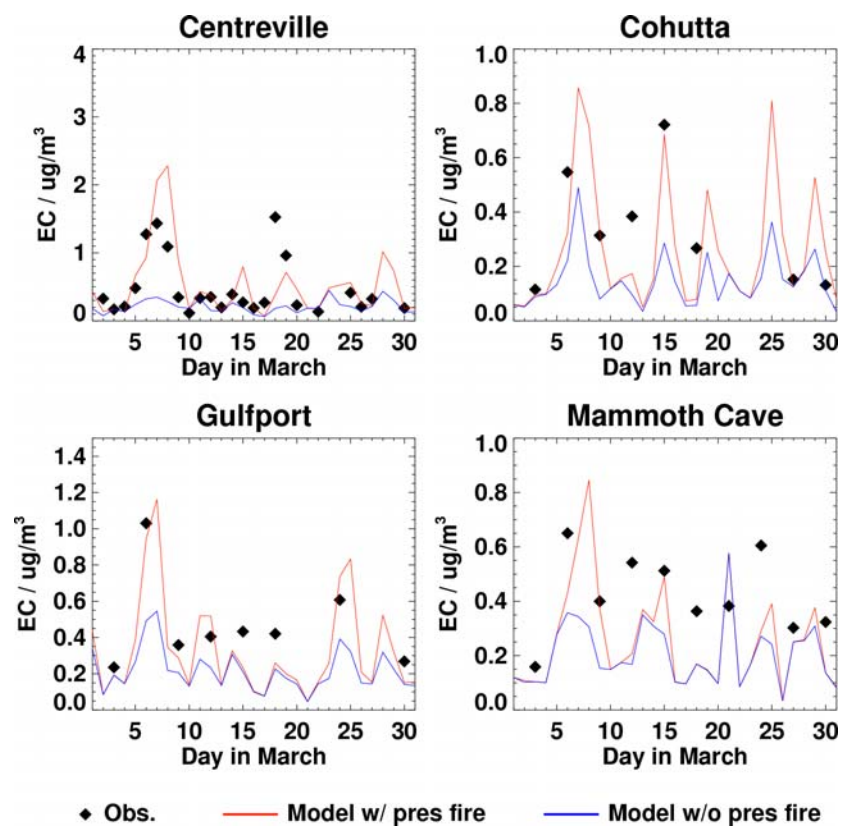


Figure 4.10 CMAQ simulation results compared with observations for EC [Zeng *et al.*, 2006].

Next, in answer to the second question, we investigate the relationships between the characteristics of fire and detection probability of MODIS. Figure 4.11 shows the probability of fire detection of MODIS [Giglio *et al.*, 2003]. The probability of detection is strongly dependent on the temperature and area of fire. The size of the smallest flaming fire with a 50% of detection probability under ideal conditions (which means that the fire is observed at or near nadir on a fairly homogeneous surface, there are no fires in the background window, and the scene is free of clouds, heavy smoke, and sun glint) is about 100 m^2 [Giglio *et al.*, 2003]. Giglio *et al.* [2003] mentioned that purely smoldering fires had to be 10–20 times larger than flaming fires to achieve a similar probability of detection. Figure 4.11 does not show the probability for fires $< 500 \text{ K}$, but the probability could be very low (L. Giglio, personal communication, 2006). The mean maximum temperature of nine prescribed burns measured at a longleaf pine forest in the southeastern U.S. is about 440 K (range of $310 - 770 \text{ K}$) [Kennard, *et al.*, 2005]. The small number of MODIS fire counts relative to the reported burned areas in February and March observed in Alabama and Georgia (Figure 4.2) could be due to omission errors derived from the combined effects of the fire and the meteorological conditions.

In order to answer the third question, we examine a burning trend in summer in the southeastern U.S. According to the source apportionment study of $\text{PM}_{2.5}$ collected from four urban and four rural/suburban sites in Alabama, Florida, Georgia, and Mississippi from April 1999 to January 2000 conducted by Zheng *et al.* [2002], wood combustion factor does not show maxima during summer but in fall. The trend of this factor might be similar for the other year (M. Zheng, personal communication, 2006). It is hard to believe that there is such a huge number of burning activities during summer as

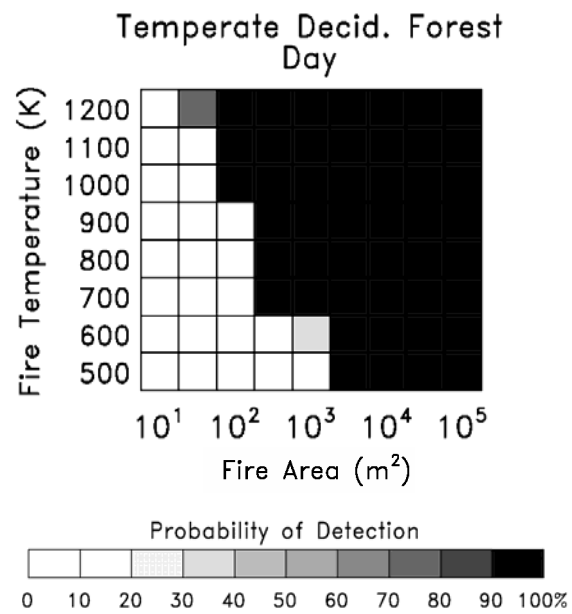


Figure 4.11 Probability of fire detection of MODIS for temperate deciduous forest in daytime [Giglio *et al.*, 2003].

the MODIS fire count data show especially in Alabama and Georgia. *Giglio et al.* [2003] mentioned that MODIS could exhibit large commission errors over a surface that is hot and dry. *Ichoku et al.* [2003] conducted a fire accuracy assessment study using MODIS and other algorithms for fires in Canada during 1995, and reported that most commission errors in all the algorithms occurred in non-forest agricultural areas with very high surface temperatures. We found that most of fire counts reported by MODIS in Alabama, which has the fire counts as large as ~500 during August 2002 are located over forest areas and a few on cropland/grassland.

4.5 Conclusions

We conducted a study of the relationships between the MODIS fire count data and the VISTAS burned area inventory. Among the four types of fire reported to VISTAS, prescribed burning is the most significant, and its effects on air quality are shown in 3-D air quality model simulations. In the ten VISTAS states in the southeastern U.S., only Florida shows clear correlations between the fire counts and burned area data. For Alabama and Georgia, there are significant discrepancies between the two data sets; spring peaks in the VISTAS inventory and summer peaks in the MODIS fire count data. Those states that did not provide precise fire data such as Kentucky, Mississippi, North Carolina, Virginia, and West Virginia are not considered as important in this analysis. MODIS fire detections could be affected by cloud over in some states in some months. There is no clear evidence found that shows LAI affects the fire detections. One possible reason for the discrepancy in early spring in Alabama and Georgia is that the temperature of prescribed burning could be too low to be detected by MODIS. The summer

discrepancy could be due to the false detections of MODIS, which tend to occur on hot and dry surfaces.

Our results indicate that it is difficult to use the satellite fire count data to calculate quantitatively prescribed burning in the Southeast. Due to known issues with satellite detection such as the limitation to “active” fires, fire stage, cloud, and surface characteristics and temperature, we do not expect to find a linear proportionality between fire count and burned area data. The systematic seasonal difference between the two datasets and observations of PM_{2.5} in the Southeast indicate that MODIS fire counts underestimate prescribed fires in spring (likely to due to low fire temperatures) but overestimate prescribed fires in summer due to false positives. The reasons for large summer false positives are not clear.

REFERENCES

- Ackerman, S., K. Strabala, P. Menzel, R. Frey, C. Moeller, L. Gumley, B. Baum, S. W. Seeman, and H. Zhang, Discriminating clear-sky from cloud with MODIS, Algorithm Theoretical Basis Document, 2002.
- Asplund, G., A. Grimvall, and C. Pettersson, Naturally produced adsorbable organic halogens (AOX) in humic substances from soil and water, *Sci. Tot. Environ.* 81/82, 239 – 248.
- Barnard, W. R., and P. Brewer, Development of managed burning and wildland fire emission estimates for VISTAS, presentation at the International Emission Inventory Conference, “Working for Clean Air in Clearwater,” Clearwater, Florida, June 7 - 10, 2004.
- Bey, I., D. J. Jacob, R. M. Yantosca, J. A. Logan, B. Field, A. M. Fiore, Q. Li, H. Liu, L. J. Mickley, and M. Schultz, Global modeling of tropospheric chemistry with assimilated meteorology: Model description and evaluation, *J. Geophys. Res.*, 106, 23,073 – 23,096, 2001.
- Blake, N.J., D. R. Blake, O., B. C. Sive, T-Y. Chen, F. S. Rowland, J. E. Collins Jr., G. W. Sachse, and B. E. Anderson, Biomass burning emissions and vertical distribution of atmospheric methyl halides and other reduced carbon gases in the South Atlantic region, *J. Geophys. Res.*, 101, 24,151 – 24,164, 1996.
- Blake, N.J., D. R. Blake, O., T-Y. Chen, J. E. Collins Jr., G. W. Sachse, B. E. Anderson, and F. S. Rowland, Distribution and seasonality of selected hydrocarbons and halocarbons over the western Pacific basin during PEM-West A and PEM West B, *J. Geophys. Res.*, 102, 28,315 – 38,331, 1997.
- Blake, N.J., D. R. Blake, O. W. Wingenter, B. C. Sive, L. M. McKenzie, J. P. Lopez, I. J. Simpson, H. E. Fuelberg, G. W. Sachse, B. E. Anderson, G. L. Gregory, M. A. Carroll, G. M. Albercook, and F. S. Rowland, Influence of southern hemispheric biomass burning on midtropospheric distributions of nonmethane hydrocarbons and selected halocarbons over the remote South Pacific, *J. Geophys. Res.*, 104, 16,213 – 16,232, 1999a.
- Blake, N.J., D. R. Blake, O., O. W. Wingenter, B. C. Sive, C. H. Kang, D. C. Thornton, A. R. Bandy, E. Atlas, F. Flocke, J. M. Harris, and F. S. Rowland, Aircraft measurements of the latitudinal, vertical, and seasonal variations of NMHCs, methyl nitrate, methyl halides, and DMS during the First Aerosol Characterization Experiment (ACE 1), *J. Geophys. Res.*, 104, 21,803 – 21,817, 1999b.

- Blake, N.J., D. R. Blake, I. J. Simpson, J. P. Lopez, N. A. Johnston, A. L. Swanson, A. S. Katzenstein, S. Meinardi, B. C. Sive, J. J. Colman, E. Atlas, F. Flocke, S. A. Vay, M. A. Avery, and F. S. Rowland, Large-scale latitudinal and vertical distributions of NMHCs and selected halocarbons in the troposphere over the Pacific Ocean during the March-April 1999 Pacific Exploratory Mission (PEM-Tropics B), *J. Geophys. Res.*, 106, 32,627 – 32,644, 2001.
- Blake, N.J., D. R. Blake, B. C. Sive, A. S. Katzenstein, S. Meinardi, O. W. Wingenter, E. L. Atlas, F. Flocke, B. A. Ridley, and F. S. Rowland, The seasonal evolution of NMHCs and light alkyl nitrates at middle to high northern latitudes during TOPSE, *J. Geophys. Res.*, 108, 8359, doi:10.1029/2001JD001467, 2003a.
- Blake, N.J., D. R. Blake, I. J. Simpson, S. Meinardi, A. L. Swanson, J. P. Lopez, A. S. Katzenstein, B. Barletta, T. Shirai, E. Atlas, G. Sachse, M. Avery, S. Vay, H. E. Fuelberg, C. M. Kiley, K. Kita, and F. S. Rowland, NMHCs and halocarbons in Asian continental outflow during the Transport and Chemical Evolution over the Pacific (TRACE-P) field campaign: Comparison with PEM-West B, *J. Geophys. Res.*, 108, 8806, doi:10.1029/2002JD003367, 2003b.
- daSilva, A., A. C. Young, and S. Levitus, Atlas of Surface Marine Data 1994, Volume 1: Algorithms and Procedures, Tech. Rep. 6, U.S. Department of Commerce, NOAA, NESDIS,, 1994.
- DeFries, R. S. and J. R. G. Townshend, NDVI-derived land cover classification at global scales, *Int. J. Remote Sensing*, 15, 3567 – 3586, 1994.
- DeMore, W. B., S. P. Sander, D. M. Golden, R. F. Hampson, M. J. Kurylo, C. J. Howard, A. R. Ravishankara, C. E. Kolb, and M. J. Molina, Chemical kinetics and photochemical data for use in stratospheric modeling, JPL Publ. 97-4, Eval.,12, Jet Propul. Lab., Pasadena, Calif., 1997.
- Duncan, B. N., R. V. Marti, A. C. Staudt, R. Yevich, and J. A. Logan, Interannual and seasonal variability of biomass burning emissions constrained by satellite observations, *J. Geophys. Res.*, 108, 4100, doi: 10.1029/2002JD002378, 2003.
- Dwyer, E. S. Pinnock, J.-M. Gregoire, and J. M. C. Pereira, Global spatial and temporal distribution of vegetation fire as determined from satellite observations, *Int. J. Remote Sens.*, 21, 1289 – 1302, 2002.
- Environmental Protection Agency (EPA), Science Algorithms of the EPA Models-3 Community Multiscale Air Quality (CMAQ) Modeling System; U.S., Research Triangle Park, NC, EPA/600/R-99/030, 1999.
- Eva, H. and E. F. Lambin, Remote sensing of biomass burning in tropical regions: sampling issues and multisensor approach, *Remote Sens. Environ.*, 64, 292 – 315, 1998.

- Giglio, L., J. Descloitres, C. O. Justice, Y. J. Kaufman, An enhanced contextual fire detection algorithm for MODIS, *Remote Sensing of Environment*, 87, 273 – 282, 2003.
- Graedel, T. E. and W. C. Keene, Tropospheric budget of reactive chlorine, *Global Biogeochem. Cycles*, 9, 47 – 77, 1995.
- Graedel, T. E. and W. C. Keene, The budget and cycle of Earth's natural chlorine, *Pure and Applied. Chem.*, 68, 1689 – 1697, 1996.
- Gribble, G. W., Naturally-occurring organohalogen compounds- a survey, *J. of Natural Products*, 55, 1353 – 1395, 1992.
- Gribble G. W., Naturally-occurring organohalogen compounds – a comprehensive survey, In: *Progress in the chemistry of organic natural products* (ed. Hera W. et al.), 68, Springer, Berlin Heidelberg New York, 1996.
- Hall, F. G., B. Meeson, S. Los, L. Steyaert, E. Brown de Colstoun, and D. Landis, eds. ISLSCP Initiative II. NASA. DVD/CD-ROM. NASA, 2003.
- Hamilton, J. T. G., W. C. McRoberts, F. Keppler, R. M. Kalin and D. B. Harper, Chloride methylation by plant pectin: an efficient environmentally significant process, *Science*, 301, 206 – 209, 2003.
- Hansen, D. A., Edgerton, E. S., Hartsell, B. E., Jansen, J. J., Kandasamy, N., Hidy, G. M., Blanchard, C. L., The Southeastern aerosol research and characterization study: Part 1—overview, *J. Air Waste Manage. Assoc.*, 53, 1460 – 1471, 2003.
- Hardy, C. C., S. M. Hermann, and R. E. Mutch, Overview, *Smoke Management Guide for Prescribed and Wildland Fire*; Hardy, C. C. et al., Eds.; NFES 1279, National Wildfire Coordination Group: Boise, ID, 2001.
- Heald, C. L., D. J. Jacob, P. I. Palmer, M. J. Evans, G. W. Sachse, H. B. Singh, and D. R. Blake, Biomass burning emission inventory with daily resolution: application to aircraft observation of Asian outflow, *J. Geophys. Res.*, 108, 8368, doi: 10.1029/2002JD002732, 2003.
- Heald, C. L., D. J. Jacob, D. B. A. Jones, P. I. Palmer, J. A. Logan, D. G. Streets, G. W. Sachse, J. C. Gille, R. N. Hoffman, and T. Nehr Korn, Comprehensive inverse analysis of satellite (MOPITT) and aircraft (TRACE-P) observations to estimate Asian sources of carbon monoxide, *J. Geophys. Res.*, 109, D23306, doi:10.1029/2004JD005185, 2004.
- Houghton, R.A., Changes in storage of terrestrial carbon since 1850, In: *Advances in Soil Science: Soils and Global Change*, (ed. R. Lal, J. Kimble, E. Levine, and B. A. Stewart), Boca Raton: CRC Press., 45 – 65, 1995.

- Ichoku, C., Y. J. Kaufman, L. Giglio, A. Li, R. H. Fraser, J.-Z. Jin, and W. M. Park, Comparative analysis of daytime fire detection algorithms using ABHRR data for the 1995 fire season in Canada: perspective for MODIS, *Int. J. Remote Sensing*, 24, 1669 – 1690, 2003.
- Jacob, D. J., J. H. Crawford, M. M. Kleb, V. S. Connors, R. J. Bendura, J. L. Raper, G. W. Sachse, J. C. Gille, L. Emmons, and C. L. Heald, Transport and chemical evolution over the Pacific (TRACE-P) aircraft mission: design, execution, and first results, *J. Geophys. Res.*, 108, 9000, doi:10.1029/2002JD003276, 2003.
- Kasischke, E. S., J. H. Hewson, B. Stocks, G. van der Werf, and J. Randerson, The use of ATSR active fire counts for estimating relative patterns of biomass burning – a study from the boreal forest region, *Geophys. Res. Lett.*, 30, 1969, doi: 10.1029/2003GL017859, 2003.
- Kasischke, E. S. and J. E. Penner, Improving global estimates of atmospheric emissions from biomass burning, *J. Geophys. Res.*, 109, D14S01, doi:10.1029/2004JD004972, 2004.
- Keene, W. C., M. A. K. Khalil, D. J. Erickson III, A. McCulloch, T. E. Graedel, J. M. Lobert, M. L. Aucott, S. L. Gong, D. B. Harper, G. Kleiman, P. Midgley, R. M. Moore, C. Seuzaret, W. T. Sturges, C. M. Benkovitz, V. Koropalov, L. A. Barrie, and Y. F. Li, Composite global emissions of reactive chlorine from anthropogenic and natural sources: Reactive Chlorine Emissions Inventory, *J. Geophys. Res.*, 104, 8429 – 8440, 1999.
- Kennard, D. K., K. W. Outcalt, D. Jones, and J. J. O'Brien, Comparing techniques for estimating flame temperature of prescribed fires, *Fire Ecology*, 1, 75 – 84, 2005.
- Khalil, M. A. K., R. M. Moore, D. B. Harper, J. M. Lobert, D. J. Erickson, V. Koropalov, W. T. Sturges, and W. C. Keene, Natural emissions of chlorine-containing gases: Reactive Chlorine Emissions Inventory, *J. Geophys. Res.*, 104, 8333 – 8346, 1999.
- Khalil, M. A. K., and R. A. Rasmussen, Atmospheric methyl chloride, *Atmos. Environ.*, 33, 1305 – 1321, 1999.
- Knyazikhin, Y., J. Glassy, J. L. Privette, Y. Tian, A. Lotsch, Y. Zhang, Y. Wang, J. T. Morisette, P. Votava, R. B. Myneni, R. R. Nemani, and S. W. Running, MODIS leaf area index (LAI) and fraction of photosynthetically active radiation absorbed by vegetation (FPAR) product (MOD15) algorithm theoretical basis document, <http://eosps0.gsfc.nasa.gov/abtd/modistables.html>, 1999 (Aug., 2005).
- Kondo, Y., M. Koike, S. Kawakami, H. B. Singh, H. Nakajima, G. L. Gregory, D. R. Blake, G. W. Sachse, J. T. Merrill, and R. E. Newell, Profiles and partitioning of reactive nitrogen over the Pacific Ocean in winter and early spring, *J. Geophys. Res.*, 102, 28,405 – 28,424, 1997.

- Koppmann, R., F. J. Johnen, D. Plass-Dülmer, and J. Rudolph, Distribution of methyl chloride, dichloromethane, trichloroethene and tetrachloroethene over the North and South Atlantic, *J. Geophys. Res.*, 98, 20,517 – 20,526, 1993.
- Krol, M., and J. Lelieveld, Can the variability in tropospheric OH be deduced from measurements of 1,1,1-trichloroethane (methyl chloroform)?, *J. Geophys. Res.*, 108, 4125, doi:10.1029/2002JD002423, 2003.
- Lee-Taylor, J. M., G. P. Brasseur, and Y. Yokouchi, A preliminary three-dimensional global model study of atmospheric methyl chloride distributions, *J. Geophys. Res.*, 106, 34,221 – 34,233, 2001.
- Li, A., R. Fraser, J. Jin, A.A. Abuelgasim, I. Csiszar, P. Gong, R. Pu, and W. Hao, Evaluation of algorithms for fire detection and mapping across North America from satellite, *J. Geophys. Res.*, 108, 4076, doi: 10.1029/2001JD001377, 2003.
- Liu, H., D. J. Jacob, I. Bey, R. M. Yantosca, B. N. Duncan, and G. W. Sachse, Transport pathways for Asian pollution outflow over the Pacific: Interannual and seasonal variations, *J. Geophys. Res.*, 108, 8786, doi:10.1029/2002JD003102, 2003.
- Lobert, J. M., W. C. Keene, J. A. Logan and R. Yevich, Global chlorine emissions from biomass burning: Reactive Chlorine Emissions Inventory, *J. Geophys. Res.*, 104, 8373 – 8389, 1999.
- Malm, W. C. and D. E. Day, Optical properties of aerosols at Grand Canyon National Park, *Atmos. Environ.*, 34, 3373 – 3391, 2000.
- Malm, W. C., et al., Spatial and seasonal pattern and temporal variability of haze and its constituents in the United States, Report III, ISSN: 0737-5352-47, <http://vista.cira.colostate.edu/improve/Default.htm>, 2000 (May, 2006).
- Martin, R. V., D. J. Jacob, R. M. Yantosca, M. Chin, and P. Ginoux, Global and regional decreases in tropospheric oxidants from photochemical effects of aerosols, *J. Geophys. Res.*, 108, 4097, doi: 10.1029/2002JD002622, 2003.
- McCulloch, A., M. L. Aucott, C. M. Benkovitz, T. E. Graedel, G. Kleiman, P. M. Midgley, and Y. Li, Global emissions of hydrogen chloride and chloromethane from coal combustion, incineration and industrial activities: Reactive Chlorine Emissions Inventory, *J. Geophys. Res.*, 104, 8391 – 8403, 1999a.
- McCulloch, A., M. L. Aucott, T. E. Graedel, G. Kleiman, P. M. Midgley, and Y. Li, Industrial emissions of trichloroethene, tetrachloroethene, and dichloromethane: Reactive Chlorine Emissions Inventory, *J. Geophys. Res.*, 104, 8417 – 8427, 1999b.
- Menzel, W. P., B. A. Baum, K. I. Strabala, and R. A. Frey, Cloud top properties and cloud phase, Algorithm Theoretical Basis Document, 2002.

- Montzka, S. A., P. J. Fraser (lead authors), J. H. Butler, P. S. Connell, D. M. Cunnold, J. S. Daniel, R. G. Derwent, S. Lal, A. McCulloch, D. E. Oram, C. E. Reeves, E. Sanhueza, L. P. Steele, G. J. M. Velders, R. F. Weiss, R. J. Zander, Controlled substances and other source gases, Chapter 1 in Scientific Assessment of Ozone Depletion: 2002, Global Ozone Research and Monitoring Project—Report No. 47, World Meteorological Organization, Geneva, 2003.
- Moore, R. M., W. Groszko, and S. J. Niven, Ocean-atmosphere exchange of methyl chloride: Results from NW Atlantic and Pacific Ocean studies, *J. Geophys. Res.*, 101, 28,529 – 28,538, 1996.
- Moore, R. M., The solubility of a suite of low molecular weight organochlorine compounds in seawater and implications for estimating the marine source of methyl chloride to the atmosphere, *Chemosphere: Global Change Science*, 2, 95 – 99, 2000.
- Myneni, R., Y. Knyazikhin, J. Glassy, P. Votava, and N. Shabanov, User's guide, FPAR, LAI (ESDT: MOD15A2) 8-day composite NASA MODIS land algorithm, <http://cybele.bu.edu/modismisr/products/modis/userguide.pdf>, 2003 (Feb., 2006).
- Newell, R. E., W. Hu, Z-X. Wu, Y. Zu, H. Akimoto, B. E. Anderson, E. V. Browell, G. L. Gregory, G. W. Sachse, M. C. Shipham, A. S. Bachmeier, A. R. Bandy, D. C. Thornton, D. R. Blake, F. S. Rowland, J. D. Bradshaw, J. H. Crawford, D. D. Davis, S. T. Sandholm, W. Brockett, L. DeGreef, D. Lewis, D. McCormick, E. Monitz, J. E. Collins Jr., B. G. Heikes, J. T. Merrill, K. K. Kelly, S. C. Liu, Y. Kondo, M. Koike, C.-M. Liu, F. Sakamaki, H. B. Singh, J. E. Dibb, and R. W. Talbot, Atmospheric sampling of Supertyphoon Mireille with NASA DC-8 aircraft on September 27, 1991, during PEM-West A, *J. Geophys. Res.*, 101, 1853 – 1871, 1996.
- Öberg, G., The natural chlorine cycle – fitting the scattered pieces, requisitioned review, *Applied and Environmental Microbiology*, 58, 565 – 581, doi:10.1007/s00253-001-0895-2, 2002.
- Öberg, G., The biogeochemistry of chlorine in soil, In: *The handbook of environmental chemistry Vol. 3, part P., the natural production of organohalogen compounds* (ed. Gribble, G.), Springer-Verlag, 43 – 62, 2003.
- Page A.L. (ed.). *Methods of soil analysis, Part 2: Chemical and microbiological properties*, American Society of Agronomy, Soil Science Society of America, Madison, WI, US., 1982.
- Palmer, P. I., D. J. Jacob, D. B. A. Jones, C. L. Heald, R. M. Yantosca, J. A. Logan, G. W. Sachse, and D. G. Streets, Inverting for emissions of carbon monoxide from Asia using aircraft observations over the western Pacific, *J. Geophys. Res.*, 108, 8828, doi:10.1029/2003JD003397, 2003.

- Prinn, R. G., J. Huang, R. F. Weiss, D. M. Cunnold, P. J. Fraser, P. G. Simmonds, A. McCulloch, C. Harth, P. Salameh, S. O'Doherty, R. H. J. Wang, L. Porter, B. R. Miller, Evidence for substantial variations of atmospheric hydroxyl radicals in the past two decades, *Science*, 292, 1882 – 1888, 2001.
- Rhew, R. C., B. R. Miller, and R. F. Weiss, Natural methyl bromide and methyl chloride emissions from coastal salt marshes, *Nature*, 403, 292 – 295, 2000.
- Rhew, R. C., B. R. Miller, M. K. Vollmer, and R. F. Weiss, Shrubland fluxes of methyl bromide and methyl chloride, *J. Geophys. Res.*, 106, 20,875 – 20,882, 2001.
- Rodgers, C. D., *Inverse Methods for Atmospheric Sounding*, World Sci., Tokyo, 2000.
- Russo, R. S., R. W. Talbot, J. E. Dibb, E. Scheuer, G. Seid, D. E. Jordan, H. E. Fuelberg, G. W. Sachse, M. A. Avery, S. A. Vay, D. R. Blake, N. J. Blake, E. Atlas, A. Fried, S. T. Sandholm, D. Tan, H. B. Singh, J. Snow, and B. G. Heikes, *J. Geophys. Res.*, 108, 8804, doi:10.1029/2002JD003184, 2003.
- Sander, S. P., A. R. Ravishankara, D. M. Golden, C. E. Kolb, M. J. Kurylo, M.J. Molina, G. K. Moortgat, and B. J. Finlayson-Pitts, Chemical kinetics and photochemical data for use in stratospheric modeling, *JPL Publ. 02-25, Eval.*, 14, Jet Propul. Lab., Pasadena, Calif., 2003.
- Scheeren, H. A., J. Lelieveld, J. A. de Gouw, C. van der Veen, and H. Fischer, Methyl chloride and other chlorocarbons in polluted air during INDOEX, *J. Geophys. Res.*, 107, 8015, doi:10.1029/2001JD001121, 2002.
- Schneider, H. R., D. B. A. Jones, M. B. McElroy, and G.-Y. Shi, Analysis of residual mean transport in the stratosphere: 1. Model description and comparison with satellite data, *J. Geophys. Res.*, 105, 19,991 – 20,011, 2000.
- Scholes, R. J., J. Kendall, and C. O. Justice, The quantity of biomass burned in southern Africa, *J. Geophys. Res.*, 101, 23,667 – 23,676, 1996.
- Schultz, M. G., On the use of ATSR fire count data to estimated the seasonal and interannual variability of vegetation fire emissions, *Amos. Chem. Phys.*, 2, 387 – 395, 2002.
- Sellers, P. J., B. W. Meeson, F. G. Hall, G. Asrar, R. E. Murphy, R. A. Schiffer, F. P. Bretherton, R. E. Dickinson, R. G. Ellingson, C. B. Field, K. F. Huemmrich, C. O. Justice, J. M. Melack, N. T. Roulet, D. S. Schimel, and P. D. Try, Remote sensing of the land surface for studies of global change: Models - algorithms – experiments, *Remote Sens. Environ.*, 51(1), 3 – 26, 1995.

- Shorter, J. H., C. E. Kolb, P. M. Crill, R. A. Kerwin, R. W. Talbot, M. E. Hines, and R. C. Harriss, Rapid degradation of atmospheric methyl bromide in soils, *Nature*, 377, 717 – 719, 1995.
- Simmonds, P. G., S. O'Doherty, R. G. Derwent, A. J. Manning, D. B. Ryall, P. Fraser, L. Porter, P. Krummel, R. Weiss, B. Miller, P. Salameh, D. Cunnold, R. Wang, and R. Prinn, In-situ AGAGE observations by GC-MS of methyl bromide and methyl chloride at the Mace Head, Ireland and Cape Grim, Tasmania (1998-2001) and their interpretation, submitted to *J. Atmos. Chem.*, 2004.
- Smith, T. M. and R. W. Reynolds, Extended reconstruction of global sea surface temperature based on COADS data (1854-1997), *Journal of Climate*, 16, 1495 – 1510, 2003.
- Spivakovsky, C. M., J. A. Logan., S. A. Montzka, Y. J. Balkanski, M. Foreman-Fowler, D. B. A. Jones, L. W. Horowitz, A. C. Fusco, C. A. M. Brenninkmeijer, M. J. Prather, S. C. Wofsy, and M. B. McElroy, Three-dimensional climatological distribution of tropospheric OH: Update and evaluation, *J. Geophys. Res.*, 105, 8391 – 8980, 2000.
- Symonds, R. B., W. L. Rose, and M. H. Reed, Contribution of Cl⁻ and F⁻ bearing gases to the atmosphere by volcanoes, *Nature*, 334, 415 – 418, 1988.
- Talbot, R. W., J. D. Bradshaw, S. T. Sandholm, S. Smyth, D. R. Blake, N. R. Blake, G. W. Sachse, J. E. Collins, B. G. Heikes, B. E. Anderson, G. L. Gregory, H. B. Singh, B. L. Lefer, and A. S. Bachmeier, Chemical characteristics of continental outflow over the tropical South Atlantic Ocean from Brasil and Africa, *J. Geophys. Res.*, 101, 24,187 – 24,202, 1996.
- Tokarczyk, R., K. D. Goodwin, and E. S. Saltzman, Methyl chloride and methyl bromide degradation in the Southern Ocean, *Geophys. Res. Lett.*, 30, 1808, doi:10.1029/2003GL017459, 2003.
- Varner, R. K., P. M. Crill, and R. W. Talbot, Wetlands: a potentially significant source of atmospheric methyl bromide and methyl chloride, *Geophys. Res. Lett.*, 26, 2433 – 2436, 1999.
- Wanninkhof, R., Relationship between wind speed and gas exchange over the ocean, *J. Geophys. Res.*, 97, 7373 – 7382, 1992.
- Watling, R., and D. B. Harper, Chloromethane production by wood-rotting fungi and an estimate of the global flux to the atmosphere, *Mycol. Res.*, 102, 769 – 787, 1998.
- Winterton, N., Chlorine: the only green element – towards a wider acceptance of its role in natural cycles, *Green Chemistry*, 173 – 225, doi: 10.1039/b003394o, 2000.

- Yokouchi, Y., M. Ikeda, Y. Inuzuka, and T. Yukawa, Strong emission of methyl chloride from tropical plants, *Nature*, 416, 163 – 165, 2002.
- Yokouchi, Y., Y. Noijiri, L. A. Barrie, D. Toom-Sauntry, T. Machida, Y. Inuzuka, H. Akimoto, H.-J. Li, Y. Fujinuma, and S. Aoki, A strong source of methyl chloride to the atmosphere from tropical coastal land, *Nature*, 403, 295 – 298, 2000.
- Yoshida, Y., Y. Wang, T. Zeng, and R. Yantosca, A three-dimensional global model study of atmospheric methyl chloride budget and distributions, *J. Geophys. Res.*, 109, D24309, doi:10.1029/2004JD004951, 2004.
- Yoshida, Y., Y. Wang, C. Shim, D. Cunnold, D. R. Blake, and G. S. Dutton, Inverse modeling of the global methyl chloride sources, *J. Geophys. Res.*, inpress, 2006.
- Zander, R., E. Mahieu, M. R. Gunson, M. C. Abrams, A. Y. Chang, M. Abbas, C. Aellig, A. Goldman, F. W. Irion, N. Kampfer, H. A. Michelsen, M. J. Newchurch, C. P. Rinsland, R. J. Salawitch, G. P. Stiller, and G. C. Toon, The 1994 northern midlatitude budget of stratospheric chlorine derived from ATMOS/ATLAS-3 observations, *Geophys. Res. Let.*, 23, 2357 – 2360, 1996.
- Zeng, T. et al., Prescribed fire emission and the impact on air quality over the southeastern US in spring, (to be submitted, 2006).
- Zheng, M., G. R. Cass, J. J. Schauer, and E. S. Edgerton, Source apportionment of PM_{2.5} in the southeastern United States using solvent-extractable organic compounds as tracers, *Environ. Sci. Technol.* 36, 2361 – 2371, 2002.